NON-BOOLEAN CHARACTERIZATION OF HOMER1A INTRANUCLEAR TRANSCRIPTION FOCI

WING KAR LI WITHARANA

Bachelor of Science, University of Alberta, 2009

A Thesis
submitted to the School of Graduate Studies
of the University of Lethbridge
in Partial Fulfilment of the
Requirements for the Degree

MASTER OF SCIENCE

Department of Neuroscience

University of Lethbridge

LETHBRIDGE, ALBERTA, CANADA

NON-BOOLEAN CHARACTERIZATION OF HOMER1A INTRANUCLEAR TRANSCRIPTION FOCI

Abstract

Activity-induced immediate-early gene (IEG) transcription foci can be labelled with fluorescent probes, permitting high temporal and spatial resolution in mapping neuronal circuits. Previous quantification approaches have assumed a Boolean function of transcription foci, assuming that cells are either active or inactive. Due to multiple amplification steps in the *in situ* hybridization process, it was thought that information relating to magnitudes of firing rates was lost. However, the current data suggest that transcription foci actually exhibit non-Boolean intensity and size values which vary according to behavioural condition. Systematic characterization of transcription foci intensity and size revealed incremental variations such that: home-cage < one-environment exposure < five-environment exposure < maximal electroconvulsive shock. Visual differences in transcription foci may result from a quantifiable relationship between spiking patterns and transcription rates. The exact stoichiometry between neuronal spiking and transcription is not yet clear, but these results suggest that Boolean applications of IEG imaging may neglect accurate neuronal activation properties.

ACKNOWLEDGEMENTS

The author would like to acknowledge the following individuals for providing technical support: Valérie Lapointe, Lucy Lu, Mariam Alaverdashvili, Ben Clark, Zaneta Navratilova, and Jeannie Xie. Special thanks also to the author's thesis supervisory committee, Dr. Bruce McNaughton, Dr. Robert Sutherland, and Dr. Robert McDonald. In addition, the author would like to acknowledge the continual support from Dr. Dinesh Witharana in this endeavour.

Table of Contents

LIST OF TABLES

LIST OF TABLES (continued)

LIST OF FIGURES

LIST OF FIGURES (continued)

LIST OF FIGURES (continued)

LIST OF ABBREVIATIONS

1E: one-environment exposure
5E: five-environments exposure
CatFISH: cellular compartment analysis of temporal activity by fluorescent *in situ* hybridization
CD: cue-deprived transport
CR/CA: cue-rich or cue-available transport
DAPI: 4',6-diamidino-2-phenylindole
DG: dentate gyrus
DS: dorsal subiculum
DNA: deoxyribonucleic acid
EC: entorhinal cortex
FISH: fluorescent or fluorescence *in situ* hybridization
FITC: fluorescein isothiocyanate
HPC: hippocampus
HC: home-cage control
$\mathbf{I_{avg}}$: average intranuclear foci pixel intensity (green channel)
$\mathbf{I_{b:}}$ average blue intensity (of intranuclear foci pixels)
$\mathbf{I_{max:}}$ peak intranuclear foci pixel intensity (green channel)
IEG: immediate-early gene
IHC: immunohistochemistry
INF: intranuclear foci
LTP: long-term potentiation
MEC: medial entorhinal cortex
MECS: maximal electroconvulsive shock
mGluRs: metabotropic glutamate receptors
PPC: posterior parietal cortex
RNA: ribonucleic acid
ROI: region of interest
$\mathbf{S_{avg}}$: average INF size expressed as number of pixels
TSA: tyramide signal amplification system
UTR: untranslated region

NON-BOOLEAN CHARACTERIZATION OF HOMER1A INTRANUCLEAR TRANSCRIPTION FOCI

FULL ABSTRACT

Immediate-early gene (IEG) activation analyses using fluorescent *in situ* hybridization has become a powerful tool in the study of neuronal population dynamics. In particular, the appearance of IEG transcription locales as bright, intranuclear foci (INF) lends well to automated analysis. Because of the signal amplification steps during *in situ* hybridization procedure, however, it has been assumed that information about the magnitude of expression within a cell is not available, and that all INF are more or less equivalent. Consequently, the standard analysis approach has been Boolean, and the resulting dependent measure is the proportion of positively labelled cells. However, it is clear that these estimates may vary substantially depending on image characteristics and arbitrary threshold selection. This may lead to more serious errors if there is intrinsic variation in the INF characteristics depending on firing characteristics between regions or neuronal types. The present studies demonstrate that intranuclear transcription foci characteristics indeed vary in size and intensity in a manner suggesting that these parameters vary systematically with net spiking activity. Four groups of rats were studied: home cage (HC); one-environment exposure (1E); five-environments exposure (5E) or maximal electroconvulsive shock (MECS), which presumably activates expression of IEGs maximally in all cells capable of expressing the IEG. Using

automated analysis software, we quantified the size and intensity of fluorescent *Homer1a* INFs from dorsal subiculum, CA1, CA3 and dentate gyrus. INF intensity and size were highly correlated in all conditions and increased monotonically across conditions (HC < 1E < 5E < MECS). Sizes and intensities did not differ appreciably across hippocampal sub-regions. The stoichiometry between spiking and initiation of transcription events is not yet clear, but the present data suggest that there is substantially more information available about firing rate distributions within populations of active neurons than given by the standard Boolean analysis. Based on what is currently known about the dynamic relationship between transcription and electrophysiological activation, it is plausible that these variations in INF intensity and size depend on the intensity or duration of neural activation. The current data may therefore open up a new quantitative dimension in the use of IEG imaging to decode neuronal circuits.

INTRODUCTION

Immediate-early gene transcription is induced by a range of stimuli

Immediate-early genes (IEGs) in the brain refer to genes that are rapidly and transiently induced in response to a wide range of stimuli (Greenberg, Thompson, & Sheng, 1992). In particular, many IEGs are dynamically transcribed at the onset of synaptic or electrical activation; that is, when a neuron fires an action potential, or a train of action potentials (Morgan, Cohen, Hempstead, & Curran, 1987; Cole, Saffen, Baraban, & Worley, 1989). It has been demonstrated that IEGs play a pivotal role in long-lasting regulation of neuronal responses (Flavell & Greenberg, 2008).

The IEG *Homer1a* is important for synaptic plasticity processes

Immediate-early genes (IEGs) may encode transcription factors, effector proteins, or signalling molecules which participate in an array of molecular cascades implicated in long-term memory processes. *Homer1a* is a short-splice isoform belonging to the scaffold protein family Homer. *Homer1a* is distinct from other Homer variants because is it the only isoform whose transcription is dynamically induced by neuronal activation (Bottai, Guzowski, Schwarz, Kang, Xiao, Lanahan et al., 2002). It has also been shown that *Homer1a* is selectively expressed in principal neurons across brain regions (Vazdarjanova, McNaughton, Barnes, Worley, & Guzowski, 2002; Vazdarjanova et al., 2006), and as such has become a useful marker of recent principal neuronal activity (Imamura, Nonaka, Yamamoto, Matsuki, & Nomura, 2011).

Homer proteins bind to inositol-1,4,5- triphsophate receptors (IP3Rs) (Tu et al., 1998), metabotropic glutamate receptors (mGluRs) (Brakeman et al., 1997), and also indirectly to NMDA receptors through Shank (Sheng & Kim, 2000). Homer1a acts as an endogenous dominant negative regulator that competes with constitutively expressed Homer family members (Xiao, Tu, & Worley, 2000; Kato, Ozawa, Saitoh, Fukazawa, Sugiyama, & Inokuchi, 1998) and aids in the trafficking of receptors by signalling intracellular reserves of calcium (Naisbitt et al., 1999). In other cases, Homer1a regulates synaptogenesis and increases calcium influx induced by action potentials in neocortical pyramidal neurons (Yamamoto, Sakagami, Sugiura, Inokuchi, Shimohama, & Kato, 2005). The involvement of its effector protein products in downstream metaplasticity events enables the use of *Homer1a* in marking cellular activity during behavioural episodes which investigate coding properties underlying memory and learning processes. *Homer1a* is unique among IEGs because of its uncharacteristically long introns, resulting in a complete primary transcript length of ~45kb (Bottai et al., 2002) and thus providing a relatively long window of post-activation transcription.

In addition to *Homer1a*, a number of other immediate-early genes are also involved in cellular plasticity mechanisms. Many IEGs have been linked to plasticity mechanisms wherein their protein products bind to downstream protein complexes that are involved in the regulation of synaptogenesis, receptor trafficking, calcium signaling, and targeting of receptor units (Tully, 1997). For example, the protein products of the IEG *Arc* (or *Arg 3.1*) are exported to dendrites where they associate with cytoskeletal protein complexes (Lyford et al., 1995). This association is important for maintaining long-term potentiation and the stabilization of spatial memories (Guzowski et al., 2000).

Other examples of IEGs implicated in synaptic plasticity include *Zif268* (Cole, Saffen, Baraban, & Worley, 1989), and *C-fos* (Morgan, Cohen, Hempstead, & Curran, 1987).

Use of immediate-early genes as neuronal markers of activation

In the past two decades, analyses of regional population activity patterns have capitalized on the use of immediate-early gene (IEG) transcript labeling techniques to identify, with considerable temporal and spatial resolution, specific cells activated in a particular behavioural epoch in time (Guzowski, McNaughton, Barnes, & Worley, 2001; Guzowski, Timlin, Roysam, McNaughton, Worley, & Barnes, 2005). Typically, research subjects are exposed to a certain spatial, cognitive, or behavioural task, and then sacrificed at a time point that coincides with the peak transcription timeline of the IEG of choice. The selective and immediate induction of IEGs in excitatory and inhibitory principal cells across brain regions (Bottai et al., 2002; Imamura et al., 2011; Vazdarjanova, Ramirez-Amaya, Insel, Plummer, Rosi, Chowdhury et al., 2006) during pertinent behavioural epochs permits identification of functional circuits involved in specific cognitive tasks. Fluorescent *in situ* hybridization (FISH) involves tagging sequences of primary IEG RNA transcripts (intranuclear foci or INF) with a variety of fluorochromes. The appearance of IEG transcripts within neuronal nuclei serves as an activity label, and thus individual neurons activated in a particular behavioural epoch may be detected from a fluorescent image. Effectively, IEGs may be used to generate a whole-brain snapshot of activation.

Several effecting IEG imaging techniques have evolved as methods have become more sensitive in capturing multiple transcription time-points. Initially, single-IEG catFISH, or cellular compartment analysis of temporal activity by using fluorescent *in*

situ hybridization (Chawla et al., 2005), involved both intranuclear and cytoplasmic compartment quantification of transcription foci of a single IEG, such as *Arc* (Burke, Chawla, Penner, Barnes, & McNaughton, 2005). *Arc* CatFISH permitted the analysis of two distinct neuronal populations, each activated by one of two behavioural epochs separated by 20 minutes of rest. The intranuclear foci (INF)-tagged population would represent neurons activated ~5-8 minutes before sacrifice, while the cytoplasmic mRNA-tagged neurons would have been activated in the epoch ~20 – 25 minutes prior to sacrifice (Chawla et al., 2005).

Later on, dual-IEG imaging techniques were subsequently developed which expanded on the testing timelines originally employed in catFISH (5 min test, 20 min rest, 5 min test). *Homer1a* has frequently been combined with the IEG *Arc* in learning and memory studies as a popular example of dual-IEG imaging. It has also been shown that both these effector IEGS are co-expressed in the same population of cells and are induced by similar stimuli, such as novel context experiences (Vazdarjanova et al., 2002). *Homer1a* generates a relatively long primary transcript (~45kb), whereas *Arc* generates a much shorter primary transcript (~3.5kb) (Bottai et al., 2002). This size disparity between the mRNA transcripts of these two IEGs permits the transcription of the target sequences for *Homer1a* (3'UTR) to occur rough 25- 30 minutes after behaviourally-induced activation, and full-length *Arc* (introns) to occur between 5-8 minutes post-activation. This temporal difference in transcription (Guzowski, Timlin, Roysam, McNaughton, Worley, & Barnes, 2005, p.601) permit the combined use of *Homer1a* and *Arc* in dual-label studies where two neuronal populations can be identified in two behavioural epochs (5 min each) separated by 20 minutes of rest. Later adaptations have also combined dual-

IEG imaging (*H1a/Arc*) with catFISH (*Arc/Arc*) to include a third activation time-point (Marrone, Schaner, McNaughton, Worley, & Barnes, 2008).

IEG imaging complements other population analysis methods because of its capacity to convert neuronal activity into a time-stamped image that is readily visualized and quantified. Using IEGs, large brain regions can be visualized and the resolution of single neuron activation can be achieved in on a population-scale. As a result of these properties, IEG activation imaging has been implemented to map discrete populations activated in spatial navigation (Kubik, Miyashita, & Guzowski, 2007; Miyashita, Kubik, Haghighi, Steward & Guzowski, 2009; Vazdarjanova & Guzowski, 2004; Burke et al., 2005; Marrone, Schaner, McNaughton, Worley, & Barnes, 2008), operant learning (Kelly & Deadwyler, 2003), and emotional conditioning (Inoue, Nakao, Migishima, Hino, Matsui, Hayashi et al., 2009).

Boolean assumptions of IEG transcription foci may be overly simplistic

Previous quantification protocols in IEG studies generally assumed a Boolean (all-or-nothing) nature of intranuclear foci (INFs). Quantification was based on whether cells were IEG-positive (signal present) or IEG-negative (signal absent) (Guzowski et al., 2005; Vazdarjanova & Guzowski, 2004; Burke et al., 2005; Chawla et al., 2005; Marrone, Schaner, McNaughton, Worley, & Barnes, 2008). It was also previously assumed that due to the amplification steps required in FISH, information regarding the magnitudes of transcription or neuronal activity (i.e. firing rate) was lost. Thus, previous Boolean approaches to IEG quantification (Vazdarjanova & Guzowski, 2004; Guzowski et al., 1999; Chawla et al., 2005) treated the appearance of transcription foci as an all-or-nothing marker of absolute cellular activity, without consideration of possible variations

in foci characteristics as a result of varying activation intensities or rates. Moreover, most IEG studies to date have neglected the possibility that IEG images may provide information regarding a window of neural coding if one considers the actual temporal dynamics of electro-transcriptional coupling. Since the onset of IEG transcription is activity-regulated, it is plausible that not all INF transcription foci are uniform in size and intensity if different neurons were activated later in the behavioural epoch, or more strongly than other cells. The consistent use of laser confocal microscropy in IEG detection also necessitated the implementation of arbitrary intensity thresholds, which would presumably alter INF characteristics as perceived by the human eye. If INF intensity and size values within a single brain are intrinsically variable, then confocal thresholding would eliminate the lower portions of these parameter distributions by default.

One of the first indications that Boolean IEG quantification may neglect activation magnitude information was presented by Miyashita and colleagues who studied the effects of extended experience on neuronal recruitment. Miyashita et al. (2009) trained rats to run a rectangular track either one lap on a single day, four laps a day, one lap for 4 days or four laps for four days, and reported *Arc* foci intensity differences as a result of increased training. Despite the rigour of thresholding in confocal microscopy and possible elimination of faint and small INFs, Miyashita et al. (2009) were still able to observe differences in *Arc*-INF pixel intensities within CA1 a result of increased training in track-running. Later on, Penner et al., (2011) also observed significant variations in integrated intensity levels in *Arc* transcription between groups of young and aged rats who were tested in spatial exploration tasks. Furthermore, both

Miyashita et al., (2009) and Penner et al., (2011) provided direct PCR quantification data of *Arc* mRNA levels to measure effects of overtraining or aging on IEG expression in hippocampal sub-regions. Specifically, Penner et al. (2011) reported significant decreases in behaviourally-induced *Arc* mRNA levels as a result of aging, which corresponded to decreased mean integrated intensities of behaviourally-induced *Arc*-INFs in CA1 and dentate gyrus. Both of these studies provide support for the current hypothesis that the approach of simply classifying cells as either INF+ or INF- in a binary (all-or-nothing) fashion (Chawla et al., 2005; Guzowski, Setlow, Wagner, & McGaugh, 2001; Guzowski, et al., 2005) may be an overly simplistic approach for accurate characterization of population activity dynamics. The plausibility that these incremental variations exist is based on the following biomolecular mechanisms.

Dynamic relationship of electro-transcriptional coupling may be directly proportional

While the stoichiometry of electro-transcriptional coupling remains largely unexplored, there is convincing biomolecular evidence that firing rates may proportionally influence cycles of IEG transcription (Atar, Backx, Appel, Gao, & Marban, 1995; Fields, Eshete, Stevens, & Itoh, 1997).

It is widely accepted that the transient and immediate transcription of synaptic-plasticity related IEGs is an important component of long-last memory in numerous brain circuits (Bliss & Collingridge, 1993; Flavell & Greenberg, 2008; Kandel, 2001). The frequency and intensity of neuronal electrical activation has been shown to directly affect the induction of long-lasting enhancement or potentiation (McNaughton, 1982; Barnes, Jung, McNaughton, Korol, Andreasson, & Worley, 1994), and late-phase LTP depends

on gene transcription and subsequent protein synthesis (Kandel, 2001). *Homer1a*, *Arc*, and other IEGs, respond to activity-dependent NMDA receptor-mediated calcium ion influx, and the mitogen-activated protein kinase molecular cascade regulates transcription (Sato, Suzuki, & Nakanishi, 2001). Immediate-early gene transcription depends largely on calcium regulation of the transcription factor CREB (cyclic AMP response element-binding protein) and evidence shows that high frequency neuronal activation may involve a corresponding increase in calcium influx (Hardingham, Chawla, Johnson, & Bading, 1997), followed by upregulated CREB-related transcription activity of IEGs (Fields, Eshete, Stevens, & Itoh, 1997). A related study in cultured cells (Greenberg, Thompson, & Sheng, 1992) characterized a model in which voltage-gated calcium ion channels were activated by depolarizing stimulation, which led to the activation of CaM kinase, and then to CREB phosphorylation which activated the transcription of the IEG *c-fos*. This specific pathway may be implicated for other IEGs (Nguyen, Kobierski, Comb, & Hyman, 1990) although there are other complex transcription factors and kinases involved, depending on the specific neurotransmitter and IEG (Xia, Dudek, Miranti, & Greenberg, 1996). The most convincing evidence for this general mechanism of IEG activation arises from studies which show IEGs are most responsive to depolarizing factors containing many cAMP responding-elements in their regulatory areas (Sheng & Greenberg, 1990).

These mechanistic considerations provide a basis for the plausibility that there is a quantifiable proportionality between activation intensity levels and transcription rates, specifically for IEGs like *Homer1a* and *Arc*. For example, it is likely that increased spiking also leads to increased influxes of calcium ions, which in turn signal and amplify

the CREB recruitment within the nuclear transcription domain. In this regard, an electrical event is converted into a chemical signal that becomes a genetic transcriptional signal and amplification is possibly at each conversion because of the tight biomolecular coupling between membrane depolarization and transcription initiation. Indirect evidence supporting this proportional relationship was reported in vitro by Fields, Eshete, Stevens, and Itoh (1997). Mouse dorsal root ganglion (DRG) cells were electrically stimulated with 540 action potentials administered in four variable patterns for 30 minutes. Transient intracellular calcium levels were measured via fluorescent imaging with Ca^2+-indicators while *c-fos* expression was measured with semiquantitative PCR (polymerase chain reaction). Immunocytochemical staining was also used to quantify CREB phosphorylation (based on quantifying intensities within cell nuclei). The authors observed that specific temporal features of action potentials directly influenced Ca^2+ influx patterns which also correlated with increases in *c-fos* expression and CREB phosphorylation levels. These findings suggest that temporal dynamics of neuronal activation or membrane depolarization lead to corresponding peaks in calcium ion influx, which transiently coordinate the transcription rates of immediate early genes via specific signal cascades with variable kinetics.

Non-Boolean variations in INF size and intensity can be maintained during FISH amplification

Despite the underlying proportional relationship in electro-transcriptional coupling, another reason for Boolean quantification of IEG images has been the assumption that gross FISH amplification steps are not sensitive enough to detect minute differences in the local density of target RNA molecules. In the FISH protocol that has

been widely adopted for IEG processing, a hapten-labeled antisense, single-stranded RNA oligonucleotide probe is hybridized to the primary RNA transcript of the target IEG. The hapten molecules, usually small ligands or dye molecules (e.g. fluorescein, or DIG) are much too small to be detected by standard microscopy so amplification steps usually involve the binding of primary antibodies to the hapten ligands within the RNA probe. An antibody that binds the hapten is then conjugated to an HRP (horseradish peroxidase) enzyme that catalyzes and forms bonds with a signal amplifying dye (such as tyramide). This amplification exponentially increases the detectable signal generated by aggregates of RNA transcripts by recruiting a compound volume of fluorescent dye molecules to surround each hapten molecule (see Figure 1), and it is this aggregate of fluorochromes which produces the visible fluorescent foci. However, if the factor of amplification across behavioural conditions is monotonic, then even this exponential amplification ratio may still produce detectable differences in the intensity and size of transcription foci, granted image acquisitions are consistent for behavioural conditions as in the Miyashita et al. (2009) study. Thus, if the current FISH protocol is carried out uniformly across behavioural conditions (such as combining test groups on a single microscope slide to homogenize tissue processing), then INF variations in intensity and size may still potentially be quantified on the resulting images, although the linearity of the amplification function would need to be quantified experimentally. Such quantification can potentially be accomplished using populations of neurons whose physiological response function to given stimuli are already known, for example, visual cortical responses to variably repeated oriented bar stimuli, or, in the case of the hippocampus, variably repeated traversals of a fixed region of space.

Intranuclear foci correspond to locations of stable transcription factories

It has been shown that DNA containing immediate-early gene sequences are mobilized and recruited to stable transcription factories when transcription is initiated (Osborne, Chakalova, Mitchell, Horton, Wood, Bolland et al., 2007). In fact, the two punctate intranuclear foci that are targeted by RNA-probes in FISH actually correspond to the intranuclear locations of these transcription complexes where nascent primary RNA transcripts are generated and accumulate during parallel transcription (Jackson, Hassan, Errington, & Cook, 1993; Wansink, Schul, van der Kraan, Steensel, van Driel, & de Jong, 1993). Transcription factories are independent intranuclear compartments composed of aggregates of RNA polymerase II (RNAPII) enzymes, and possibly other transcription factors and holoenzymes (Jackson et al., 1993; Grande, van der Kraan, de Jong, & van Driel, 1997). Electron microscopy suggests these intranuclear factories are between 45-100nm in diameter (Martin and Pombo, 2003; Iborra, Pombo, Jackson, & Cook, 1996), and are present in consistent numbers within similar cell types (Iborra et al., 1996). These factories are maintained in the absence of transcription (Mitchell and Fraser, 2008) and also after removal of chromatin (Jackson et al., 1993). Several studies also provide evidence for co-localization of genetic transcription activity (initiation and elongation) across multiple genes such that several activated genes have been shown to share the same transcription factories (Mitchell and Fraser, 2008; Osborne, Chakalova, Brown, Carter, Horton, Debrand et al., 2004). The discovery of transcription factories contradicted the standard textbook model of transcription whereby RNA polymerases are recruited to promoters of genes upon activation, suggesting that transcription sites are generated de novo on the actual specific genes (Jackson et al., 1993). In actuality, FISH

shows discrete and stable transcription complexes corresponding to distinct locations of transcription factories (Mitchell & Fraser, 2007), instead of diffuse and scattered dispersal of novel RNA transcripts as proposed by the outdated model.

The densely packed RNAPII enzymes anchored within transcription factories enable the generation of multiple primary mRNA transcripts in response to a specific level of neuronal activation (Sutherland & Bickmore, 2009). DNA is looped by stationary polymerase enzymes during transcription, and the production of nascent RNA strands from the same gene is restricted to a small area (about 50nm) corresponding to the location of the transcription factories (see Figure 2, adapted from Martin & Pombo, 2003). It is plausible, because of this stable and direct mechanism, that transcription foci may increase in intensity and size in response to increasing neuronal stimulation (cumulative action potentials). As well, the IEG intranuclear foci may expand as the bulk of transcripts expand, spread, and prepare for shuttling to the cytoplasm for translation into amino acid sequences. In effect, INFs may expand and dissipate (grow in size but diminish in intensity) at successive time-points after activation because of the accumulation of newly synthesized RNA and their gradual translocation to the cytoplasm. As a result, the timing of IEG protocols may have a larger effect on foci characteristics than previously thought. By considering these biomolecular dynamics of IEG transcription, it is likely that transcription foci encode a more detailed neural coding time window than provided by a Boolean approach.

The idea that static IEG images could convey both the identity of activated neurons and magnitudes of neuronal activation (i.e. firing rates) has important implications for the field of brain imaging. Based on previous reports (Miyashita et al.,

2009) and the underlying biomolecular properties of electro-transcriptional coupling, we hypthothesized that there are actual non-Boolean variations in the intensity and size of IEG INFs. Thus, the objective of the current study was to systematically characterize the intensity and size of *Homer1a* transcription foci to determine whether a true non-Boolean function of these parameters exists. As well, the current experiment investigated the correlation between increasing intensity and size as a function of cumulative environmental experience. Our initial studies were aimed at replicating previous activation proportions across hippocampal sub-regions as discussed extensively in preceding literature (Vazdarjanova & Guzowski, 2004). The original goal was to extend and further previous environmental exposure tasks but pilot endeavours showed home-cage counts that were much higher than expected, among other discrepancies in activation proportions contradictory to the literature. Past studies typically cite that home-cage controls exhibit the lowest level of activity, as evidenced by low activation proportions in the range of 2-10% (Chawla et al., 2005; Vazdarjanova, McNaughton, Barnes, Worley, & Guzowski, 2002) while MECS robustly drove all eligible cells to express IEGs maximally (Cole, Abu-Shakra, Saffen, Baraban, & Worley, 1990). Specifically, our initial observations failed to produce cumulative increases in cellular recruitment in added environmental exposures. As well, assays prior to the current experiment failed to replicate a low home-cage activation proportion but yielded a large volume of faint, small INFs present across home-cage conditions. Thus the current study was established in order to perform a systematic assay of *Homer1a* transcription intensity and size across behavioural conditions.

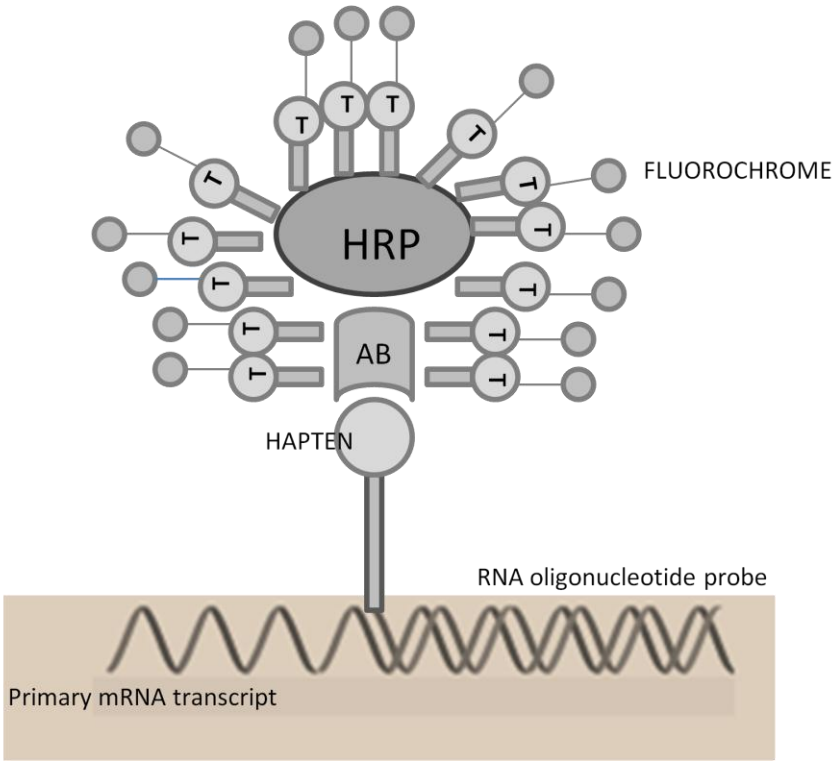

Figure 1. General model of one-step signal amplification used in FISH. Hapten-labeled oligonucleotide RNA probe is hybridized to its antisense nascent primary mRNA target within the nucleus. The hapten label (usually DIG or FITC) is immuno-bound to an antibody conjugated to HRP (horse-radish peroxidase). HRP catalyzes reaction with signal amplification molecules, (T, usually tyramide signal amplification system) which is bound to a fluorochrome molecule. This compound amplification of dye molecules conjugated to antibody-HRP results in exponential signal enhancement generated from a single RNA primary transcript. HRP=horseradish peroxidase; AB=antibody against hapten ligand; hapten= small ligand (typically a dye or small substrate) integrated in single-strand RNA probe; T= tyramide or other HRP-catalyzed signal amplification reagent.

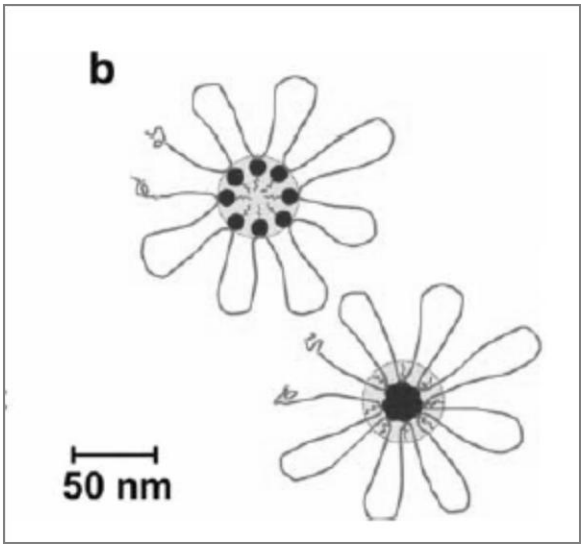

Figure 2. Theoretical model of the structure of transcription factories as discrete foci of gene transcription within the nucleus. Dark round structures correspond to stationary RNAPII molecules through which mobile DNA sequences are strung and transcribed. It is not yet known whether several RNAPII molecules expel nascent RNA transcripts into the centre of each factory, or a concentrated packet of RNAPII extrudes transcripts to the periphery of the factory. Both schemes would produce an aggregate collection of primary IEG transcripts concentrated at discrete sites within the nucleus. (Illustration from Martin & Pombo, 2003, p.467)

METHODS

Refer to Appendix I Supplementary Material: Methods and Procedures for additional details.

Behaviour

Adult male Long-Evans (n=43) & Brown Norway (n=6) rats between 3-7 months old were divided into two test groups: one-environment exposure (1E), or five-environment (5E) exposure; and two control groups: home-cage (HC) or MECS. All animal handling adhered to regulations according to the Canadian Council on Animal Care. Experimental procedures were approved by the University of Lethbridge Animal Welfare Committee.

Note: Initially, the complete data set was comprised of two separate cohorts. Both cohorts received identical manipulations except that one cohort (cue-deprived transport) was transferred between locations in a covered transport cage. Meanwhile, the other cohort (cue-available transport) was transferred in a transparent cage and also received 3 days of minor transport habituation. However, analyses showed no significant differences between the two transport methods and thus, data from both cohorts were combined and treated uniformly in the Results. For specific details and methods pertaining to each of the two cohorts, refer to Appendix I.

On test day, all rats rested in an undisturbed, darkened antechamber in their home-cages for a minimum of one hour to ensure quiescence and minimal IEG expression. Rats in the 1E condition were introduced to a triangular enclosure in a novel test room, allowed to explore freely for 5 minutes, and returned to the darkened

antechamber to rest for 25 minute before immediate sacrifice. Rats in the 5E condition were exposed to 5 consecutive environments with each exposure lasting 2 minutes, and then returned to the darkened antechamber to rest for 25 minutes before immediate sacrifice. Each of the 5E environmental exposures consisted of a uniquely-shaped enclosure situated in separate testing rooms. During all unrestrained exploration, the experimenter ensured that the subject traversed all parts of the enclosure as indicated by grid markings on the floor of each enclosure. In summary, the total time that elapsed from the first removal from the darkened antechamber till sacrifice was ~32 minutes for 1E rats and ~38 minutes for 1E rats. Home-cage (HC) controls were removed from the darkened antechamber for immediate sacrifice after their quiescent period. MECS subjects received a brief pulse of electroconvulsive stimulation via two ear clips connected to a research-grade ECT (electroconvulsive therapy) machine (Ugo Basile). It has been previously shown that MECS treatment induced the maximal level of transcription within all neurons capable of IEG expression, and thus served as an effective positive control (Bottai et al., 2002; Cole, Abu-Shakra, Saffen, Baraban, & Worley, 1990). After environmental exposures or MECS, all test rats rested for 25 minutes, the duration required to transcribe the 3'UTR of the *Homer1a* primary transcript (Bottai et al., 2002).

Sacrifice

Subjects were placed in a tightly-sealed 5% isoflurane chamber for a minimum of 40 seconds until fully anaesthetized. Between 0.4-0.8mL of sodium pentobarbital (Euthansol) was injected intracardially to arrest cardiac activity and subjects were then decapitated with a rat guillotine. Following rapid brain extraction and skull removal,

brains were submerged for 2 minutes in a metal container of -50^{o}C liquid 2-methylbutane surrounded by a slurry of dry ice in 70% ethanol (quick-freeze method). Frozen brains were then wrapped in aluminum foil, labeled and stored in a Falcon tube at -80^{o}C until cryosectioned.

Cryosectioning

Brains were removed from -80^{o}C storage, and hemispheres were separated with a razor after removing the cerebellum. Cryosectioning was performed on a LEICA Microsystems Cryostat (model CM1900). SuperFrost slides (FisherScientific) were used to capture 3-4 20μm serial coronal hemi-sections belonging to two different behavioural groups (e.g. HC & 1E; 1E & 5E; 5E & MECS, etc). Pairings were counterbalanced to ensure every possible match was represented across slides, and to ensure equal samples of left or right sections from each test condition. These arrangements controlled for slight processing variations that occurred between batches during tissue collection and subsequent FISH. Slides were allowed to dry at room temperature for a maximum of 30 minutes, frozen at -20^{o}C for two hours, and then transferred to storage in -80^{o}C.

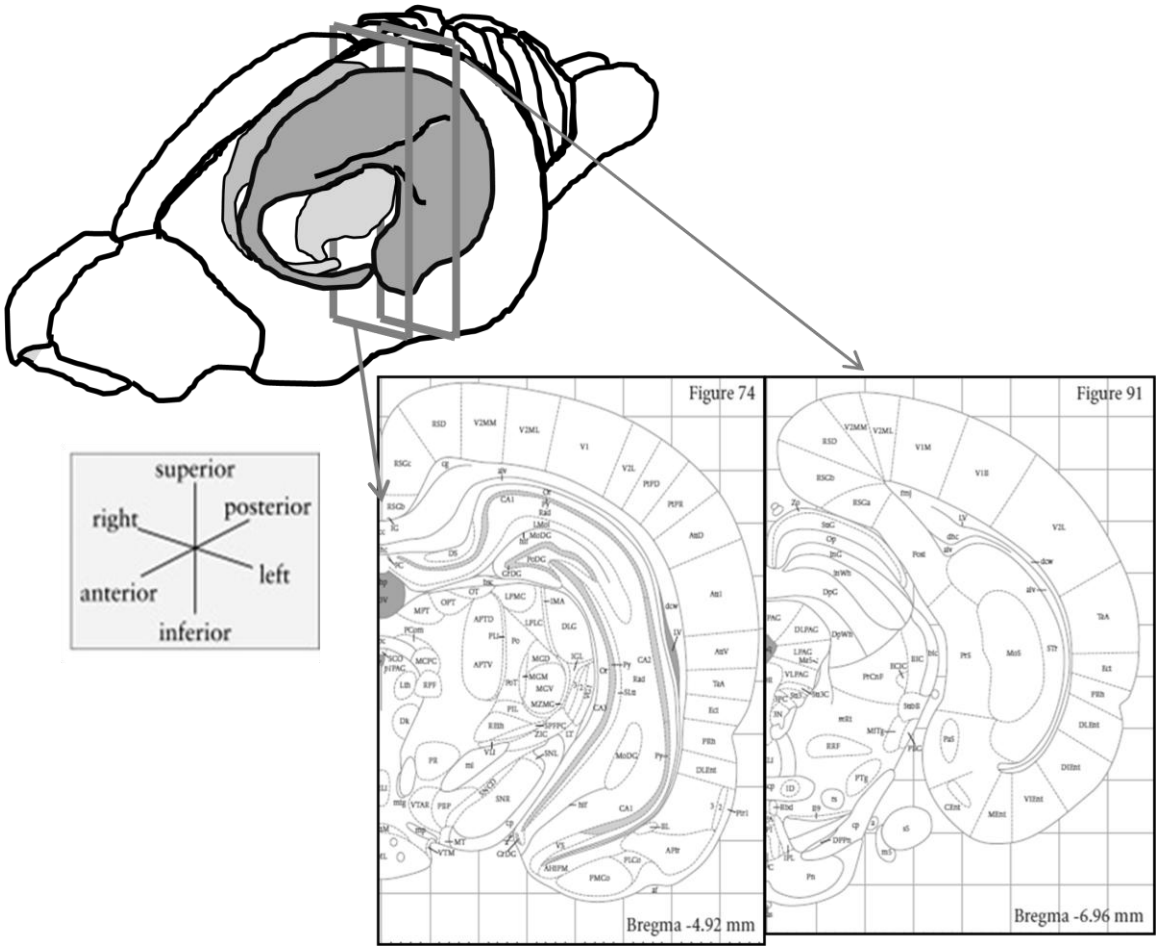

Figure 3. Diagram of anterior-posterior position of coronal sections analyzed containing dentate gyrus, CA1, CA3, and dorsal subiculum from -4.92mm to -6.96mm from bregma. Only dorsal portions of hippocampal sub-regions were included in *Homer1a* INF characterization. Atlas images adapted from Paxinos and Watson, 2007, Figures 74 and Figure 91.

Fluorescent *in situ* hybridization (FISH)

Alternating 20μm coronal sections located -4.92mm to -6.96mm from bregma were selected from all experimental subjects (see Figure 3). Standard fluorescent *in situ* hybridization was administered in order to detect *Homer1a* intranuclear transcription

foci. Detailed methods of the FISH employed here have been previously described (Vazdarjanova & Guzowski, 2004; Guzowski et al., 1999) with the exception that in this case, *Homer1a* was detected by a TSA (tyramide signal amplification), or fluorescein-tyramide labeling kit via HRP (horseradish peroxidase) conjugation (see Figure 1, Introduction).

Antisense oligonucleotide riboprobe targeting the 3'UTR of the *Homer1a* primary transcript were synthesized from *Homer1a* DNA template (provided in-house) with the use of a Maxscript RNA Synthesis Kit (Ambion). During RNA probe synthesis, each uracil base of the riboprobe was conjugated to a fluorescein molecule, which served as the hapten substrate for antibody amplification (see Figure 1, Introduction). All solutions and buffers were prepared with distilled water filtered through a Nanopure system (Barnstead) set at 18.2mOhms to ensure the removal of DNAses and RNAses. Slides were removed from -80^{o}C storage, thawed for 30 minutes at room temperature (~21^{o}C), and then fixed in 4% paraformaldehyde for 7 minutes at 4^{o}C. Following a 2X saline sodium citrate buffer (SSC) wash, slides were then treated with acetic anhydride in triethanolamine buffer for 10 minutes to lower background signal by binding to polar groups that bind to the probe, followed by a 5 minute 1:1 acetone-methanol treatment (to perforate nuclear envelope to enable probe penetration). Sections were then pre-hybridized with hybridization buffer for a minimum of 1 hour to prevent background staining, and then incubated overnight (16 hours) in the hybridization oven with prepared riboprobes. Slides were then cooled for 15 minutes, incubated with RNAse A for 30 minutes to digest single-stranded RNA that has not bound to the probe and then washed in a succession of buffers in increasing stringency. To quench the endogenous

peroxidases that would bind to the antibody, slides were washed in 2% hydrogen peroxide for 15 minutes, and washed in buffered solution. TSA blocking buffer with 5% normal sheep serum was pipetted onto each slide to block all non-specific binding sites for anti-FITC to reduce the background and incubated for 40 minutes at room temperature. The antibody anti-fluorescein (JacksonImmuno Research) was added to the slides which were then incubated at 4^{o}C for 18 hours. Following three more washes in buffered solution, slides were then incubated with 1:100 fluorescein-tyramide (PerkinElmer) for 30 minutes, washed in buffer, and counter-stained with DAPI (Sigma), and coverslipped with VectaShield Mounting Media for Fluorescence (Vector Labs).

Image Acquisition

Single 2μm median z-planes of all processed slides were scanned with a 40X objective digital Nanozoomer micro-scanner (Olympus). Image acquisition saturation was set at consistent 4:4:4 RGB (Red:Green:Blue) intensities for all scanning sessions. All regions of interest on each section (dorsal subiculum, CA3, CA1, and dentate gyrus) were manually cropped into sub-images by outlining with NDPToolkit (Hamamatsu), in reference to the Rat Brain Atlas (Paxinos & Watson, 2007). Acquired images were originally saved in the Olympus proprietary format, .NDPI, so images were then converted into bitmap (.BMP) images with NDPConvert (in-house development by V. Trivedi) and renamed numerically to prepare for automated intranuclear foci (INF) detection. ROI cropping yielded a total of 28014 image files as a result of mass sampling from alternating serial sections throughout posterior hippocampus. Also, sub-images

were cropped to relatively small sizes (<900MB) to prevent exceeding computer processing limitations.

Automated INF quantification and characterization

Bitmap sub-images were processed in large batches by using an automated intranuclear foci quantification program (GreenDot.exe) created in-house (by V. Trivedi) with Visual Basic code (Microsoft). Threshold parameters were maintained for all batches to maintain cross-condition consistency such that minimum INF green intensity = 20; minimum green-blue differential =15; minimum INF size = 6 pixels. Prior to quantification, sub-images were pre-processed to minimize blue-green channel bleedthrough since the emission spectra of fluorescein (green, peak at 520nm, PerkinElmer) and DAPI (blue, peak at 461nm, Sigma) overlap. INFs were detected according to strict scanning algorithms based on circularity, adherence to 2D Gaussian spread in intensity, and intensity levels above background "noise" thresholds. To distinguish putative INFs from noise, the detection algorithm required that the brightest peaks (most intense pixels) were situated at the centre of the INF (i.e. origin), and surrounding pixels must gradually decrease in intensity in a step-wise function. For each processed image, a corresponding Excel (Microsoft) file was generated, which listed the location of each detected INF according to the *x*- and *y*- coordinates of the INF origin. In addition, for each identified INF, a string of data was outputted, with values pertaining to 1) the INF's maximum intensity value (I_{max}, or intensity of the origin); 2) the total size of the INF (sum of pixels included in the area of the INF, S_{avg}); 3) the total value of all pixel intensities within the INF (which provided the average intensity of all INF pixels when

divided by the sum of INF pixels, I_{avg}); 4) the total value of all blue intensity levels within all INF pixels (to determine average blue channel penetration from DAPI stain, I_b); and 5) the total number of blue pixels belonging to the pre-determined range of estimated "neuronal" intensity values (refer to Appendix III for systematic derivation of neuronal intensity range). Activation proportions, or the number of INFs expressed in each sub-region, were derived by dividing total INF counts by the estimated total neurons. Total neuronal nuclei counts were estimated by dividing the total number of blue pixels by the average area of hippocampal principal neuron nucleus, or 3013.58 (refer to Appendix III for details on how this estimate of nuclear area was determined, and also how glial cells were eliminated from detection).

RESULTS

One 1E and two 5E rats were rejected from analysis due to poor tissue quality. Three MECS treatments were unsuccessful and thus also eliminated from analyses. There were no significant differences between the two original cohorts (i.e. no significant effect of covered or uncovered transportation, see Appendix II for statistical tests) so subject data from both cohorts were pooled. Final subject numbers included in the analysis were: HC n= 10; 1E n=13; 5E n=13; and MECS n=7.

Non-Boolean variation in INF intensity and size

Four main INF characteristics were analyzed: 1) maximum INF intensity (I_{max}, average intensity of each INF "Origin"); 2) average INF size (S_{avg}, area in pixels); 3) I_{avg}, average INF green intensity; and 4) average INF blue intensity (I_b). Correlations were also examined between: 1) maximum INF intensity and INF size; 2) average INF intensity and INF size; 3) maximum INF intensity and average INF green intensity and average blue intensity. Only data reflecting I_{max}, S_{avg}, I_{avg}, and correlation between S_{avg} and I_{max} are presented here. Refer to Appendix II for supplementary results showing I_b (average blue penetration intensities), additional correlations, and post-hoc ANOVA statistical analyses between testing conditions.

Overall, there were monotonic increases in peak INF intensity (I_{max}), average INF intensity (I_{avg}), and INF size (S_{avg}, expressed as number of pixels), as experimental exposures also increased. In general, MECS treatments generated the highest values in all three parameters in all regions, greater than 5E, 1E, and HC. There was a significant

effect of cumulative environment exposure on peak INF intensity (I_{max}) in DS[1], CA1[2], CA3[3], and DG[4] (Figure 4). There was also significant effect of cumulative environmental exposure on average INF intensity (I_{avg}) in DS[5], CA1[6], CA3[7], and DG[8] (Figure 6). Average INF sizes were significantly affected by environmental exposure in DS[9], CA1[10], and CA3[11] but not quite significant in DG[12] unless MECS values were disregarded[13] (Figure 5). Finally, significant differences in average blue INF-pixel intensities (I_b) within sub-regions were not observed in both cohorts[14] as environmental exposures increased.

The least amount of variation in INF intensity and size was observed in CA3 across behavioural conditions although not consistently significant across all test conditions[15] (Refer to Appendix II, sections 1d, 2d, and 3d for cohort-specific statistical analyses of sub-regional differences).

A strong correlation between peak INF intensity and average INF size was reported by a Pearson correlation test ($r=0.88$, $r^2=0.78$) of pooled means from both cohorts in HC, 1E, and 5E conditions across all regions (Figure 7). For detailed

[1] DS INFs increased in I_{max} across conditions: [$F(42)=509.4$, $p<0.001$]
[2] CA1 INFs increased in I_{max} across conditions: [$F(42)=389.43$, $p<0.001$]
[3] CA3 INFs increased in I_{max} across conditions: [$F(42)=1411.77$, $p<0.001$]
[4] DG INFs increased in I_{max} across conditions: [$F(42)=435.91$, $p<0.001$]
[5] DS INFs increased in Iavg across conditions: [$F(42)=387.85$, $p<0.001$]
[6] CA1 INFs increased in Iavg across conditions: [$F(42)=1048.18$, $p<0.001$]
[7] CA3 INFs increased in Iavg across conditions: [$F(42)=2405.66$, $p<0.001$]
[8] DG INFs increased in Iavg across conditions: [$F(42)=560.54$, $p<0.001$]
[9] DS INFs increased in size (S_{avg}) across conditions: [$F(42)=10.15$, $p<0.001$]
[10] CA1 INFs increased in size (S_{avg}) across conditions: [$F(42)=13.44$, $p<0.001$]
[11] CA3 INFs increased in size (S_{avg}) across conditions: [$F(42)=12.28$, $p<0.001$]
[12] DG INFs did not increase in size (S_{avg}) across conditions: [$F(42)=2.78$, $p=0.05$]
[13] DG INFs increased in size (S_{avg}) across conditions without MECS [$F(35)=12.23$, $p<0.001$]
[14] See Appendix II: 4a and Appendix II:4b for I_b statistical results.

[15]See Appendix II, 1d, 2d, and 3d for cohort-specific analyses of regional effects on INF parameters.

correlations between average INF intensity versus average INF size, including MECS groups, refer to Appendix II.

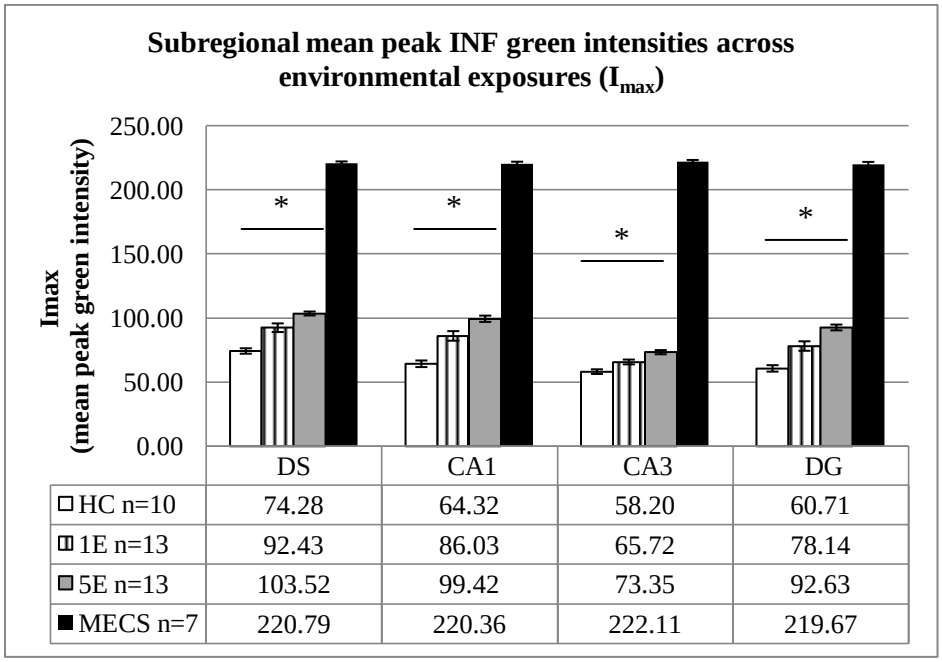

	DS	CA1	CA3	DG
HC n=10	74.28	64.32	58.20	60.71
1E n=13	92.43	86.03	65.72	78.14
5E n=13	103.52	99.42	73.35	92.63
MECS n=7	220.79	220.36	222.11	219.67

Figure 4. Mean peak intensities (I_{max}) in combined cohort data across regions and conditions. All regions showed effect of cumulative exposure increasing peak INF intensities. Highest intensities observed in MECS conditions.

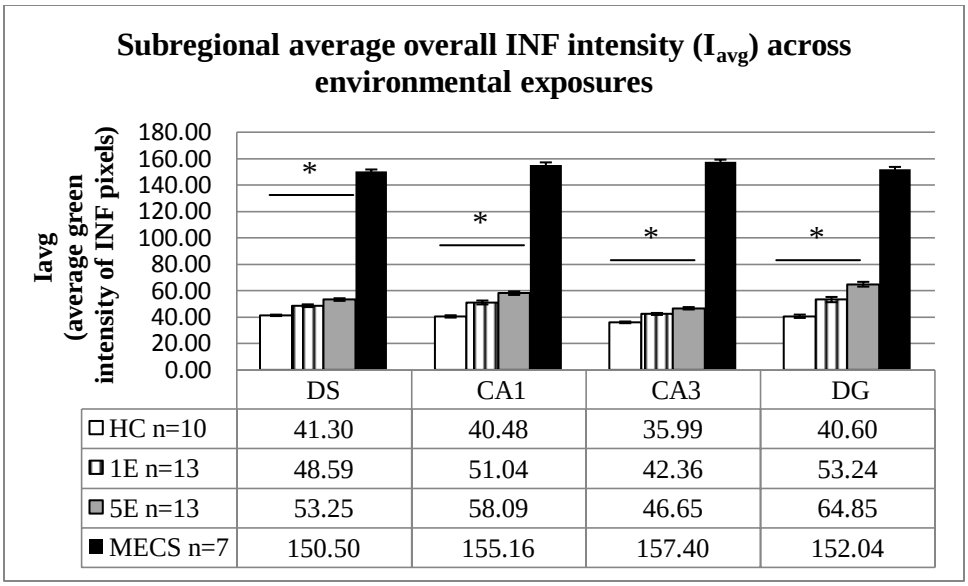

	DS	CA1	CA3	DG
HC n=10	41.30	40.48	35.99	40.60
1E n=13	48.59	51.04	42.36	53.24
5E n=13	53.25	58.09	46.65	64.85
MECS n=7	150.50	155.16	157.40	152.04

Figure 5. Average intensity of within-INF pixels (I_{avg}) in combined cohort data. All regions showed significant effect of cumulative environmental exposure on increasing I_{avg} values. Highest average intensities observed in MECS conditions.

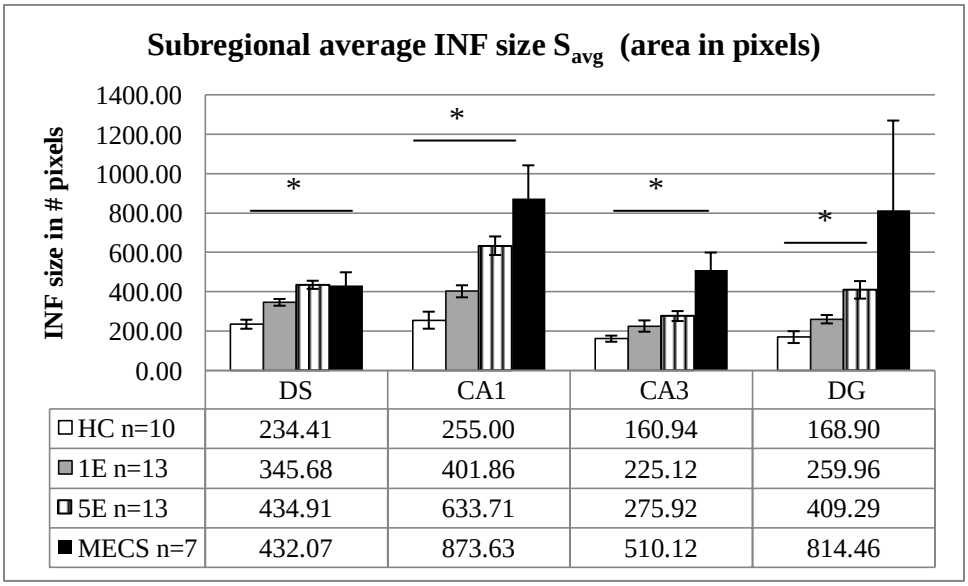

	DS	CA1	CA3	DG
HC n=10	234.41	255.00	160.94	168.90
1E n=13	345.68	401.86	225.12	259.96
5E n=13	434.91	633.71	275.92	409.29
MECS n=7	432.07	873.63	510.12	814.46

Figure 6. Average INF size (S_{avg}, measured in number of pixels) across all conditions, with both cohorts' data combined. All regions showed significant increases in INF size as

a result of cumulative environmental exposure. Largest INF sizes observed in MECS conditions, except in DS.

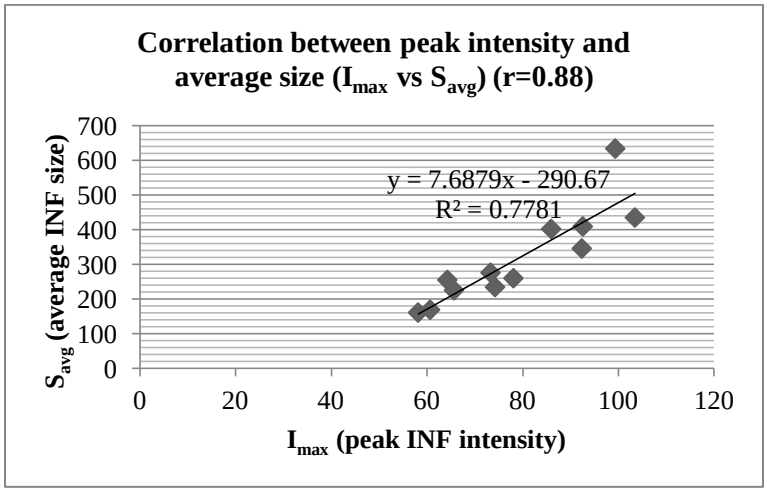

Figure 7. Strong correlation (r=0.88, r^2=0.78) between I_{max} (peak INF intensity) and S_{avg} (average INF size). All HC, 1E and 5E averages across sub-regions, within both CR and CD cohorts pooled.

Frequency distributions of average overall intensity (I_{avg}) and size of INFs across conditions and sub-regions

1. **Iavg (Average INF pixel intensities) Histograms**

a) **Dorsal subiculum Average INF Intensity**

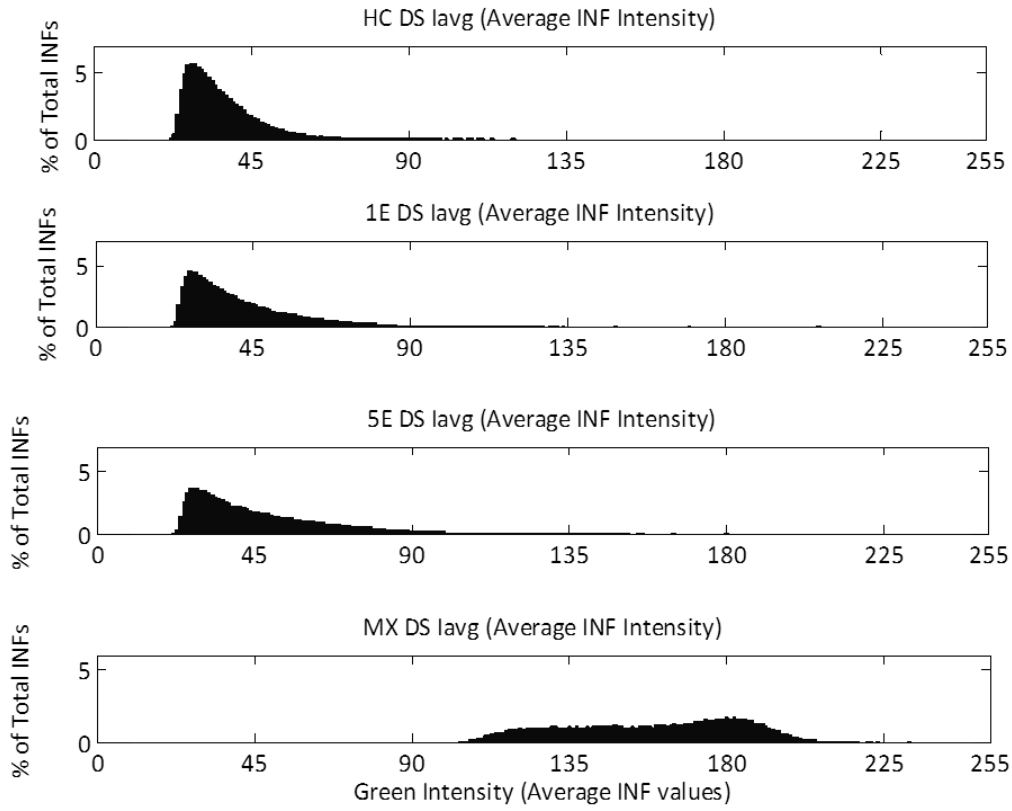

Figure 8. Percentage distributions of all INFs according to average INF-pixel intensity in dorsal subiculum.

b) CA1 Average INF Intensity

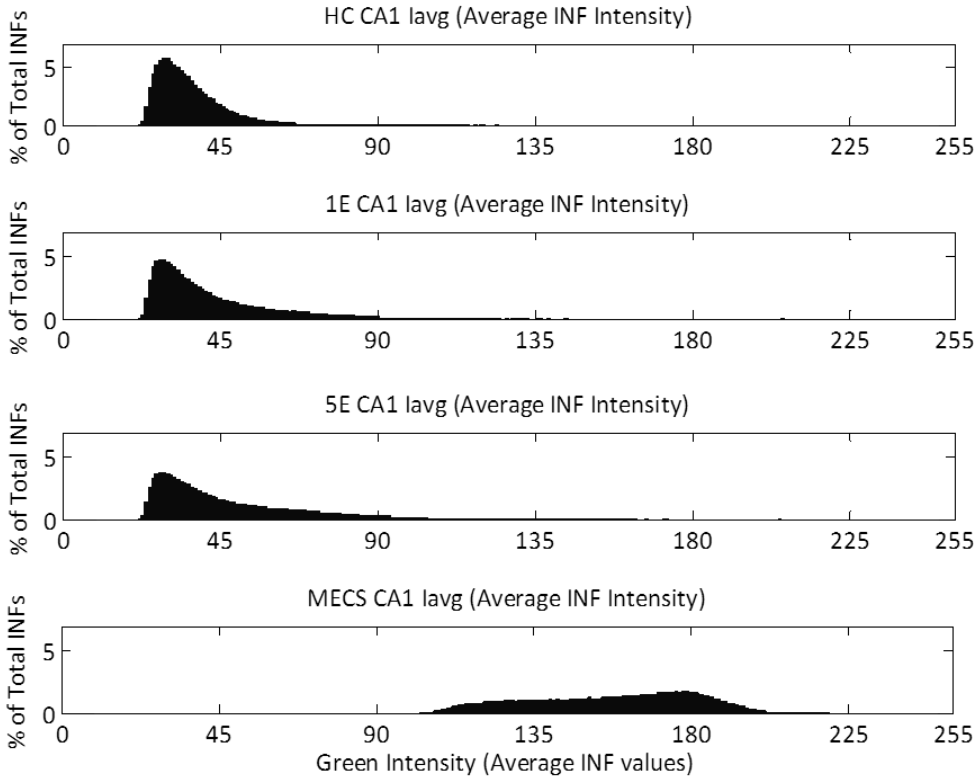

Figure 9. Percentage distributions of all INFs according to average INF-pixel intensity in CA1.

c) CA3 Average INF Intensity

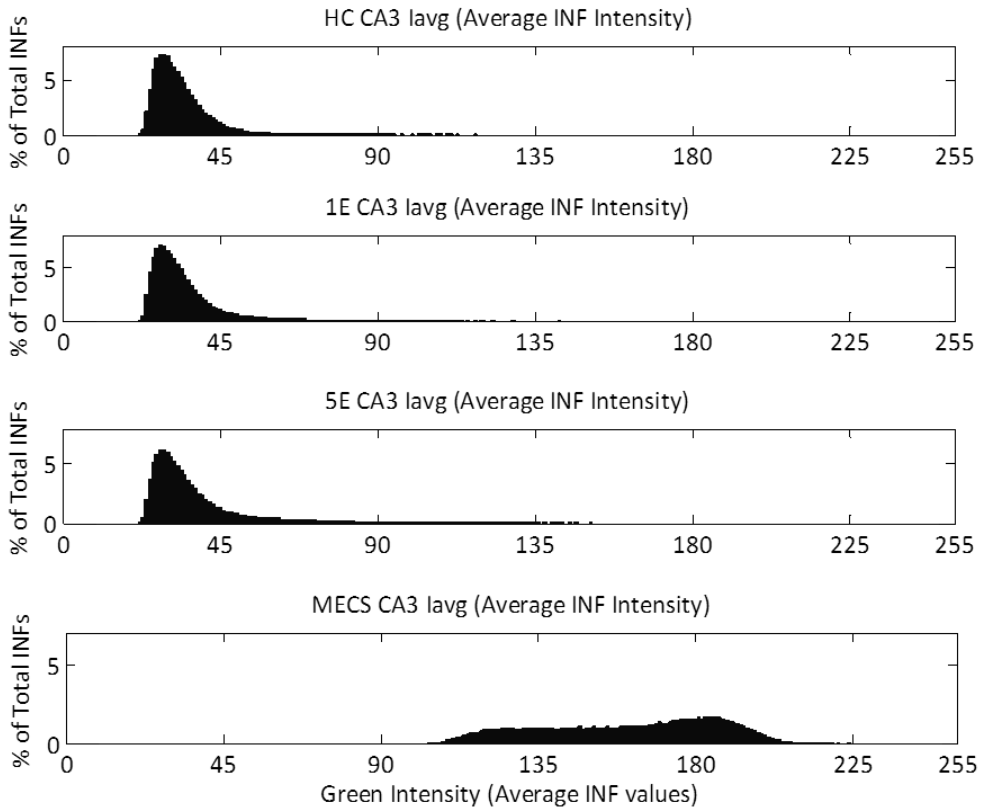

Figure 10. Percentage distributions of all INFs according to average INF-pixel intensity in CA3.

d) Dentate gyrus Average INF Intensity

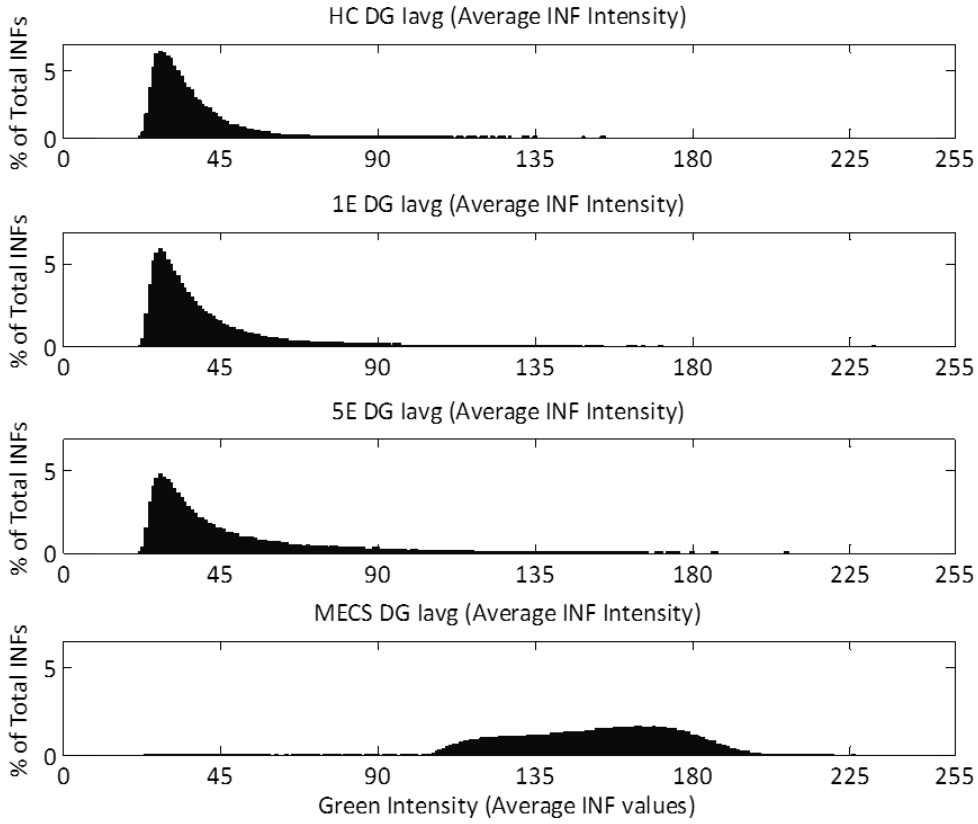

Figure 11. Percentage distributions of all INFs according to average INF-pixel intensity in dentate gyrus.

2. Savg (INF Area in pixels)

a) Dorsal subiculum INF Sizes

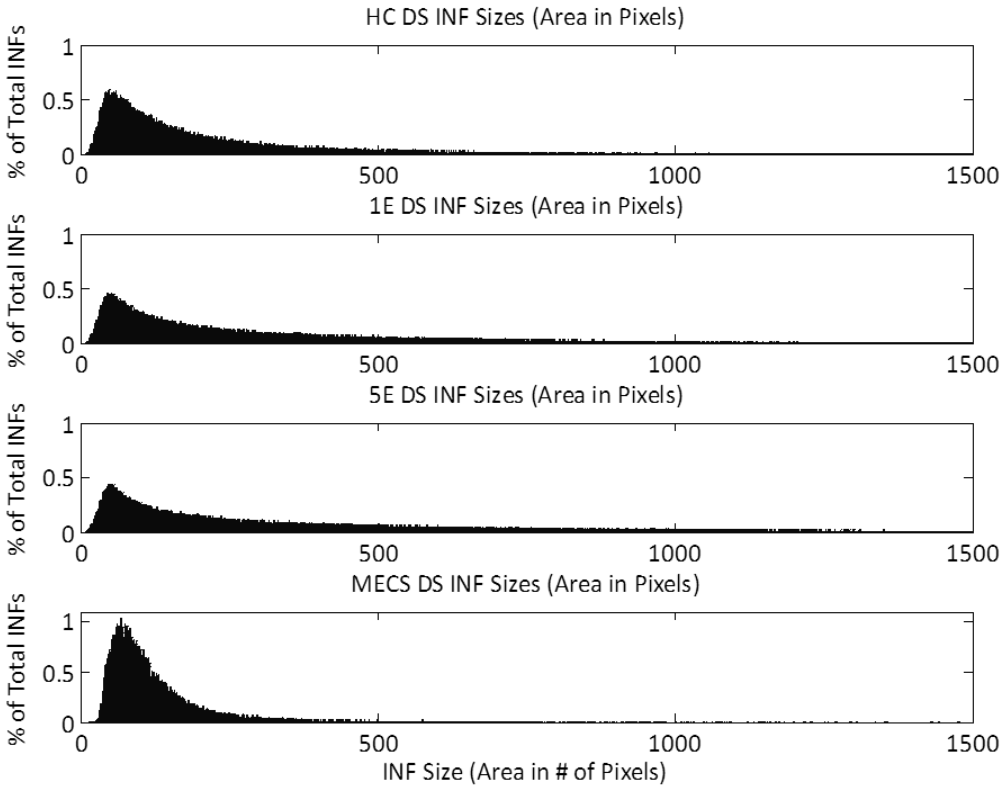

Figure 12. Percentage distributions of all INFs according to size (area in pixels) in dorsal subiculum.

b) CA1 INF Sizes

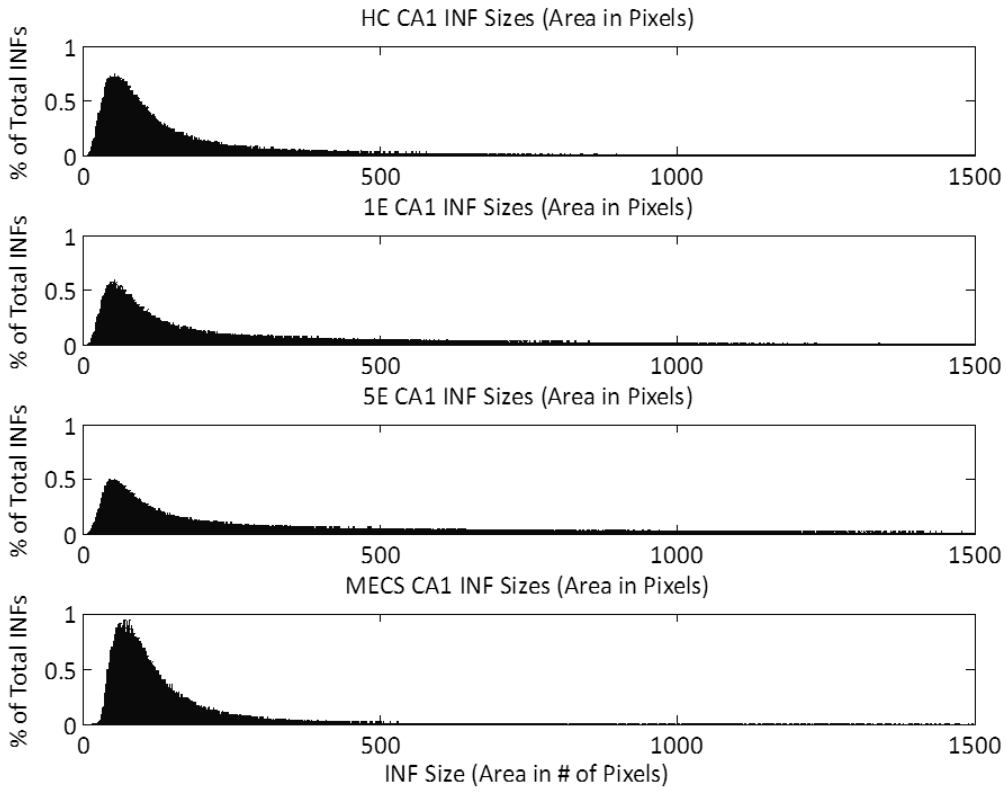

Figure 13. Percentage distributions of all INFs according to size (area in pixels) in CA1.

c) CA3 INF Sizes

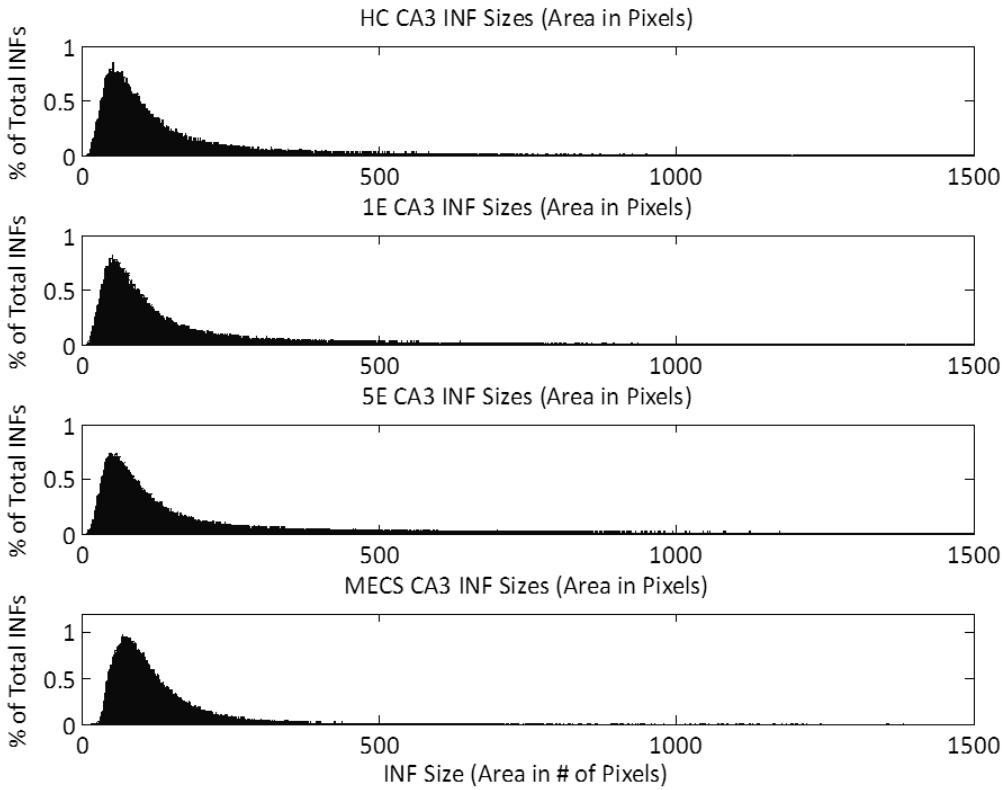

Figure 14. Percentage distributions of all INFs according to size (area in pixels) in CA3.

d) Dentate gyrus INF Sizes

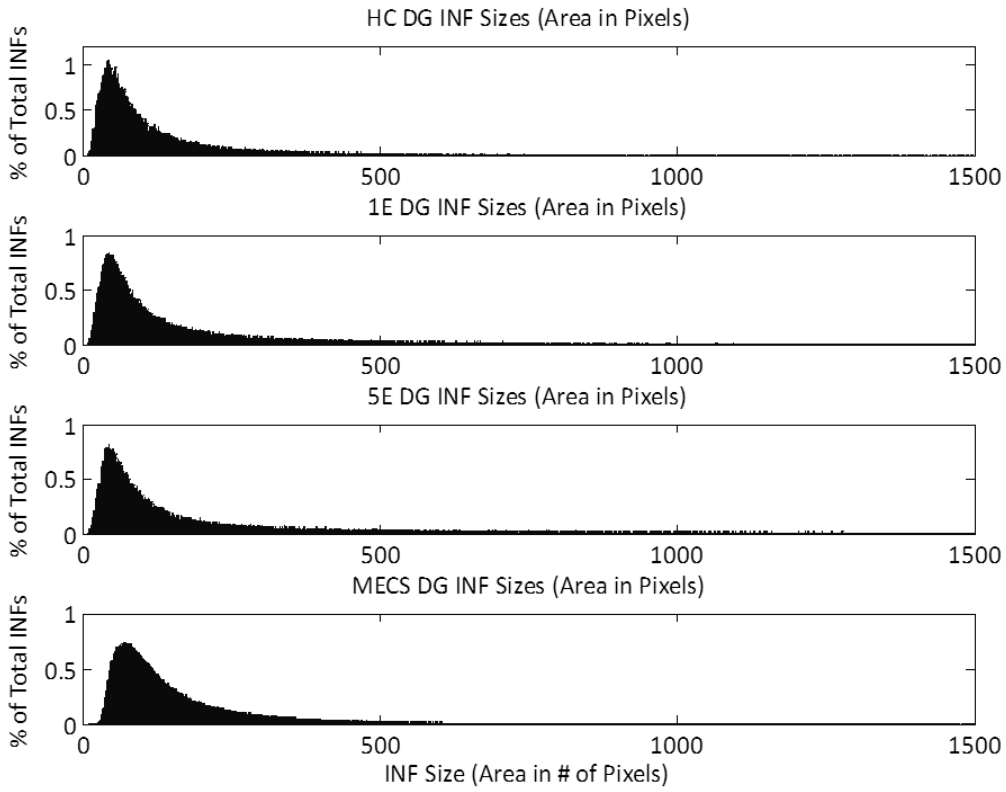

Figure 15. Percentage distributions of all INFs according to size (area in pixels) in DG.

Activation proportions across sub-regions according to condition

Based on expression proportions (single INF counts/total neurons), the dorsal subiculum showed high INF expression across all conditions and in both CR and CD cohorts (Figure 16). Dorsal subiculum expression levels were significantly higher than DG in HC[16], 1E[17], and 5E[18] conditions. The lowest expression levels were observed in the dentate gyrus. MECS animals showed the greatest expression level of all conditions.

[16] ($t(9)=6.75$, $p<0.001$)

The INF expression ratios in all regions from HC to 1E to 5E conditions demonstrated a flat gradient; i.e. there were no significant increases in recruitment of active cells with increased environmental exposure. Even from HC to 5E, only DS[19] showed significant recruitment, but not CA1[20], CA3[21], or DG[22]. When both cohorts were pooled, and normalized by MECS values, activation proportions decreased from DS > CA1 > CA3 >DG (Figure 17).

In CA1, there was a significant effect of condition on expression ratios[23] and paired-sample t-tests confirmed higher values in MECS than 5E[24], than 1E[25]; and higher than HC[26]. There were no significant differences between values from HC to 1E[27], from HC to 5E[28]; and also from 1E to 5E[29].

In CA3, home-cage INF expression was almost equal[30] to 1E, and also with 5E[31]. There was no difference between 1E and 5E values[32]. Paired-sample t-tests confirmed significantly higher values in MECS than 5E[33]; than 1E[34]; and higher than HC[35].

---

[17] (t(9)=6.75, p<0.001)
[18] (t(12)=9.05, p<0.001)
[19] DS: HC to 5E showed significant increase in expression[F(22)=4.91, p=0.04]
[20] CA1: HC to 5E did not show significant increase in expression [F(22)=1.78, p=0.20]
[21] CA3: HC to 5E did not show significant increase in expression [F(22)=0.07, p=0.80]
[22] DG: HC to 5E did not show significant increase in expression [F(22)=2.8, p=0.11]
[23] [F(3,22)=18.77, p<0.0001]
[24] (t(7)=9.10, p<0.0001)
[25] (t(7)=-8.07, p<0.0001)
[26] (t(7)=-7.43, p=0.0001)
[27] (t(7)=-0.759, p=0.473)
[28] (t(7)=-1.485, p=0.181)
[29] (t(7)=-0.92, p=0.389)
[30] (t(7)=0.054, p=0.96)
[31] (t(7)=-0.66, p=0.53)
[32] (t(7)=-0.788, p=0.46)
[33] (t(7)=6.55, p=0.0003)
[34] (t(7)=-5.50, p=0.001)
[35] (t(7)=-10.62, p<0.0001)

In summary, activation proportions (proportions of INFs in each sub-regional population) did not differ significantly between HC, 1E, or 5E conditions, in any of DS, CA1, CA3, or DG regions. HC proportions were generally equal to or slightly less than 1E and 5E conditions. MECS activation proportions were highest across all sub-regions.

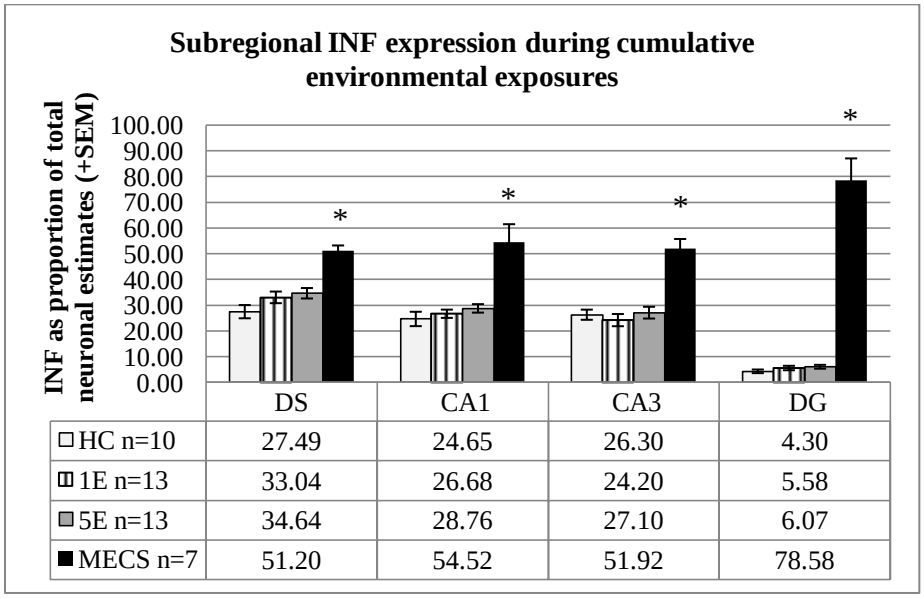

	DS	CA1	CA3	DG
HC n=10	27.49	24.65	26.30	4.30
1E n=13	33.04	26.68	24.20	5.58
5E n=13	34.64	28.76	27.10	6.07
MECS n=7	51.20	54.52	51.92	78.58

Figure 16. Total INFs expressed as a proportion of estimated total neuronal nuclei across sub-regions, according to test condition. Subjects were pooled from both cohorts since no effect of cued-transport was observed. Dorsal subiculum showed overall highest expression ratios. DG showed lowest IEG expression. No significant differences observed between HC and 1E, or between 1E and 5E conditions in either CR or CD cohort.

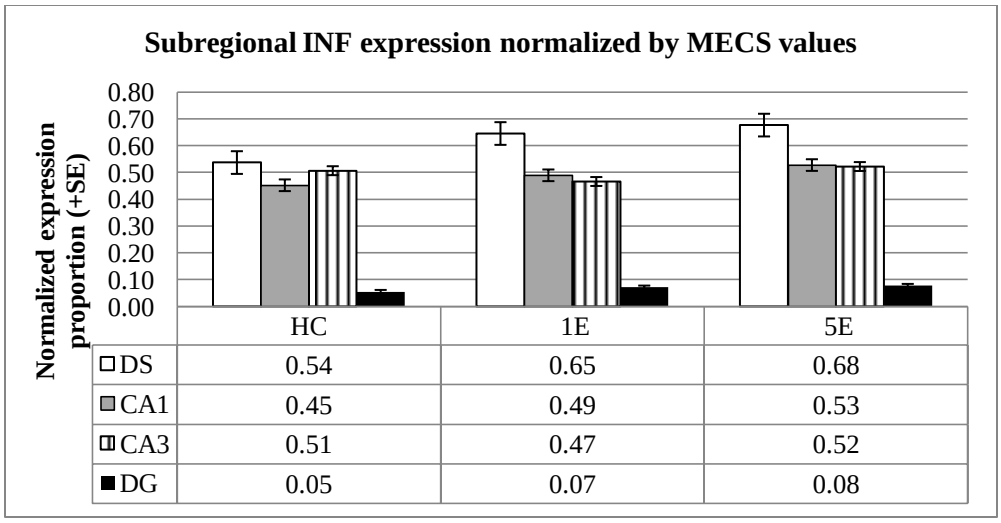

	HC	1E	5E
DS	0.54	0.65	0.68
CA1	0.45	0.49	0.53
CA3	0.51	0.47	0.52
DG	0.05	0.07	0.08

Figure 17. Normalized sub-regional expression levels. Expression averages across conditions divided by region-specific MECS values. Dorsal subiculum (DS) activation proportions were higher than CA1, CA3, and DG.

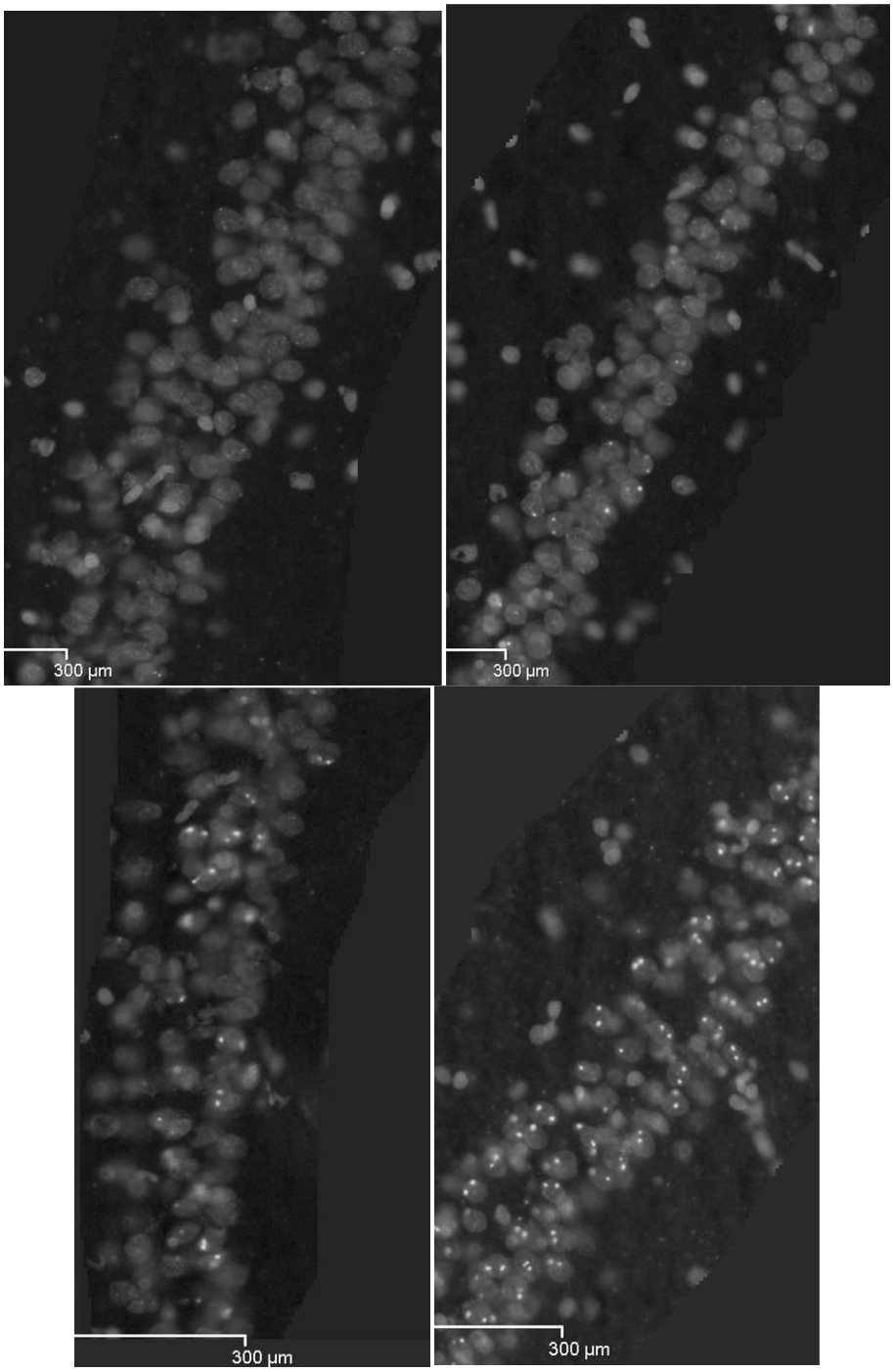

Figure 18. Sample fluorescent images of CA1 (FITC-labeled for *Homer1a* intranuclear foci, counterstained with DAPI); from conditions HC, 1E, 5E, and MECS (left to right), shown at 20X magnification.

DISCUSSION

General Conclusions

Rats were introduced to either one or five different environments and automated INF characterization was used to quantify transcription foci characteristics of *Homer1a* expressed in four hippocampal subfields: dentate gyrus (DG), CA3, CA1, and dorsal subiculum (DS). Systematic intranuclear transcription foci characterization revealed non-Boolean functions of size (area) and intensity, and both parameters increased monotonically as environmental exposures (and, presumably, total neural activity) also increased. Electroconvulsive shock treatments resulted in the most intense and largest foci out of all conditions.

Magnitudes of firing rates may be conveyed in incremental INF intensity and size

It was previously assumed that the signal amplification steps during *in situ* hybridization tissue processing obliterated information regarding neuronal activation magnitudes. The most intense INFs were observed when neural activity was induced by electroconvulsive shock (seizure activation). The results here suggest that cumulative environmental exposure leads to increased neuronal activation and subsequently increases visible parameters (i.e., intensity and size of transcriptional foci). These data also suggest that the complex biochemical cascades occurring during electro-transcriptional coupling (Link et al., 1995; Atar et al., 1995; Flavell & Greenberg, 2008; Fields et al., 1997) may manifest as visible and quantifiable variations in INF characteristics. The connection between electrical activation and transcriptional activity in neurons is tightly coupled, and most likely employs a reciprocal feedback mechanism

such that one can influence or modify the other process, leading to long-term changes in neuronal networks (Kubik, Miyashita, & Guzowski, 2007; Guzowski et al., 2006; Tully, 1997). As a result of electrical stimulation (i.e. generation of an action potential), signaling and transcription factors are phosphorylated or otherwise activated to initiate downstream molecular processes. It is probable that the onset of electrical activation generating an action potential induces Ca^{2+} ion influx, leading to downstream cascades to initiate transcription factor binding to promoter sequences of specific IEGs may dictate the number of factors binding to promoters, thus increasing transcription cycles within transcription factories (Lanahan & Worley, 1998). Although the exact stoichiometry between action potentials and transcriptional cycles remains unclear, there is strong biochemical evidence that firing rates are directly proportional to cycles of transcription (Atar et al., 1995; Fields et al., 1997). The variable intensity and size of transcriptional foci shown here most likely indicate varying volumes of IEG transcripts generated within localized transcription factories (Jackson et al., 1993).

These results are significant findings for the field of IEG imaging for a number of reasons. First, it is evident that previous Boolean approaches are overly simplistic and may eliminate important neural coding information relating to network firing properties. The broad assumption that gene transcription and neuronal activation are finite and homogeneous events in all active principal neurons is obviously flawed. The current data suggest that firing rates vary depending on the behavioural task and also activation intensity. Second, the current findings indicate the need for a more conscientious approach in the application of IEG imaging techniques as timing, behavioural intensity, and prior experience are influential factors on IEG transcription dynamics. The

characterization of small and faint but numerous foci in home-cage controls necessitates the consideration of arbitrary thresholds in imaging parameters. These thresholds are usually set such that the home-cage activation shows the lowest expression (Chawla et al., 2005; Burke et al., 2005; Guzowski et al., 1999) but the current data show that it may be inaccurate to assume low or zero activation in the home-cage subjects. In addition, the observation that IEGs are continually expressed at a baseline level in resting or home-cage animals indicate that a fraction of previously reported behaviourally-activated IEG expression probably relates to home-cage activity prior to the test or experience. That is, IEG expression levels may not correspond entirely to the limited time window of the arbitrary ~5 minutes of behavioural manipulation; there could be portions of home-cage noise or baseline transcription not directly triggered by the chosen behavioural event. Finally, the finding of non-Boolean INF properties is important for IEG studies because it essentially reveals a new dimension of IEG imaging. Traditionally, IEG images offer 'cell-counts' or 'activated neuronal proportions' to show increased network engagement in a certain task or epoch. While activation proportions are still available, the current findings could provide more intricate and precise parameters (e.g. firing rates, firing intensity, and activation duration) in decoding neuronal circuitry. The potential applications are too numerous to list exhaustively here. However, one particular example of application could be to reproduce the findings reported by Marrone et al. (2008) which described high degree of reactivation in the rest period following a novel environmental experience. The activity profile at rest seemed to represent a subset of the activated population during the wakeful experience immediately prior to the rest period. Applying non-Boolean INF quantification to this behavioural paradigm could potentially verify

whether this reported replay in rest faithfully replicates firing rates during the active experience, or whether spike rates are scaled down during replay.

Comparing current methods with previous approaches in IEG imaging

The non-Boolean nature of INF intensity described here coincides with previous reports of variable INF parameters although there are numerous methodological differences between the current study and previous experiments.

First, Miyashita et al. (2009) and Penner et al., (2011) both observed incremental variations in *Arc*-INF intensity that matched the observations we describe here. However, both of these studies acquired fluorescent images with multi-layer confocal scanning whereas we used a digital Nanozoomer (Olympus) scanner to acquire single-layer images. Regardless, it appears that both image acquisition methods reliably detect non-Boolean variations in INF characteristics. In addition, behavioural manipulations in both previous studies (overtraining of track-running; Miyashita et al., 2009, or, spatial exploration in aged rats; Penner et al., 2011) differed from the current environmental paradigm but we were still able to replicate similar results.

We also employed a different type of automated quantification of INF parameters, GreenDot.exe, instead of MetaMorph (Universal Imaging), which was used by Penner et al., (2011) or a manual blind counter (Miyashita et al., 2009). There were also slight variations in the FISH process (use of FITC instead of DIG for fluorescent probe detection, etc.) but these deviations were inconsequential in procuring results that align with previous reports.

Non-Boolean variations are robust and consistent across behaviours and imaging methods

Robust and incremental variations between INF intensity and size were observed between behavioural conditions such that both parameters increased as a result of cumulative environmental exposure. Although the current data were analyzed with a novel imaging protocol on a digital Nanozoomer, these results replicated a similar effect that was observed with confocal imaging (Miyashita et al., 2009; Penner et al., 2011). Wherein we permitted random foraging of open environments, Miyashita et al. (2009) confined behavioural epochs to lap-running, but both types of tasks resulted in non-Boolean INFs, suggesting a robust effect across variable tasks.

In addition, since samples of all conditions (HC, 1E, 5E, MECS) were counterbalanced within each FISH batch, it is highly unlikely the results arose from coincidental variations in tissue processing. Subjects were also oversampled, compared to previous sample sizes of 3-4 sections per animal (Miyashita et al., 2009), so the non-Boolean effects are most likely not a chance observation from an undersampling error. As well, since the experiment was essentially conducted twice, and the effect was observed in both cohorts (cue-deprived versus cue-available transport), we demonstrated that non-Boolean variations are reproducible and robust. Finally, the monotonic increases in INF intensity are most likely a result of differential fluorescein uptake (green fluorescence) instead of coincidental increases in DAPI concentration across conditions contributing to the intensifying signal. That is, since statistical tests did not show significant changes in blue channel intensity in INF pixels across test conditions (Appendix II), the increased intensity is not due to cumulative bleedthrough in the

blue/DAPI channel since the DAPI and fluorescein emission spectra overlap. Furthermore, all sub-images were pre-processed to minimize blue-green channel bleedthrough noise prior to automated INF detection, to preemptively eliminate artifacts from this spectral overlap.

Development and refinement of automated IEG quantification methods

These findings may have revealed the capability of quantifying neuronal activity in a fluorescent image for direct quantification of firing rates to complement electrophysiological techniques. The use of automated intranuclear foci quantification was introduced to increase data throughput and permit future adaptations for serial reconstruction. It is also possible that a steadily low level of baseline transcription occurs in home-cage controls as a process of continual updating of recent and past experiences (Marrone et al., 2008). Previous studies may have eliminated these faint and dim foci because of high confocal intensity thresholds and subjective human counting, both variables that may be eliminated with automated quantification.

It is the hope that automated characterization and quantification of INF will become a reliable and consistent method to increase data throughput and decrease human hours in IEG image analysis. However, further interpretation of the current data reveals technical and methodological aspects that require improvement. The current data shows some areas of discrepancies that will require further verification. For one, relatively large variations were reported in INF sizes in MECS images across all sub-regions. These large differences in variations could be the result of saturation levels in MECS images, leading to faulty INF-border detection; or false-positive INFs due to the noisy nature of 2D MECS images (as signal can penetrate from z-layers above and below the plane of

focus). Secondly, it will be important for the automated analysis program to reliably process confocal images of the same brain sections for volumetric information in 3D, as well as multi-layer scans from both confocal and Nanozoomer images. Lastly, while large samples of the current data were rigourously confirmed with manual verification of 2D data using freeware (ImageJ, NIH), the sampling is limited due to time and labour constraints. It will be indispensable for future software versions to permit convenient methods for manual verification in 3D (data from multiple focal planes or layers).

Anomalous INF expression levels in CA1/CA3 suggest aberrant activation proportions

Activation proportions were estimated in the current study by quantifying detected INFs as proportions of total neurons. This yielded expression levels that should have been directly proportional to percentages of activated neurons. However, it is important to reiterate that expression levels reported in the Results section reflect total INF counts, but should not be interpreted as direct cell counts since each neuron would express two INFs if 3D analyses were applied. Regardless, the current activation values do not increase substantially from HC to 1E to 5E in any hippocampal subfield, a trend that does not match previously documented activation proportions (Vazdarjanova & Guzowski, 2004; Chawla et al., 2005). These discrepancies are especially evident in CA1 and CA3. Vazdarjanova and Guzowski (2004) reported about 30-35% neuronal activation in CA1 after exposures to environments of comparable size to the apparatus used in the 1E test, and CA3 showed about 18-20% activation. In the present study, expression levels in CA3 were close to and even exceeded averages in CA1. In addition, it is still unclear whether DS activity is less sparse or equal to activation probabilities in CA1 (Barnes,

McNaughton, Mizumori, & Leonard, 1990) as the values of activation were fairly similar across test conditions in DS and CA1.

The anomalous results in HC, 1E, and 5E INF counts across sub-regions could possibly be attributed to erroneous inclusion of background or non-INF noise by the automated software system. That is, it is likely that INF counts were highly inflated, even bypassing detection by manual verification (which was routinely performed). By lowering the intensity thresholds past the usual minimum used in confocal studies, the current analyses were able to detect dim and small HC INFs but may have included a high degree of background artifacts. In addition, it is also possible that the method employed in the current analysis does not accurately estimate neuron totals. In effect, counting total blue pixels within a specified intensity range to estimate total nuclei counts is likely an overly gross measure of total cell counts. It is probable that applying higher intensity and size thresholds would eliminate the bulk of the "noise" included in the INF counts which resulted in the anomalous HC, 1E, and 5E activation proportions. Therefore, it will be necessary to employ more accurate methods of nuclei segmentation and quantification in future verifications of these neuronal activation proportions.

In addition, the flat gradient of activation in 5E/1E conditions, especially in CA1 and CA3, could be explained by failure of the current methods to induce global remapping (orthogonalization of place cell activity) (Leutgeb et al., 2005). Instead, it is possible that rate remapping (redistribution of place cell firing rates) was observed as a result of the passive transport of rats from one room to another. Rate remapping would explain the lack of increase in the number of active place cells in 1E and 5E conditions and also why we observed increasing intensity and size in the same population of

neurons. Further systematic investigations will be necessary to substantiate these predictions but it is possible that the same population of place cells was continuously re-activated in the 5E locations, leading to prolonged activation, and subsequently prolonged *Homer1a* transcription.

Future directions

The idea that static IEG images could be used to detect both the identity of activated neurons and magnitudes of neuronal activation (i.e. firing rates) has significant implications for the field of brain imaging. For example, is one action potential responsible for triggering a set number of transcription cycles (*t*), such that traversal of the same place field *n* times in a behavioural epoch, results in a number of IEG transcripts that coincides with *n* X *t*? This remains to be investigated systematically, for example, through the use of direct quantification of synthesized RNA during controlled place field firing similar to the PCR quantification performed by Miyashita et al. (2009) and Penner et al. (2011). However, Miyashita et al., (2009) did not detect significant increases in mRNA as a result of overtraining in CA3 and CA1; but Penner et al. (2011) reported decreases in mRNA in aged animals in DG. Both of these experiments studied varying aspects of behaviour (overtraining versus aging), although both reported significant changes in *Arc*-INF intensity across test groups. Therefore, the imminent goal is to integrate data from these studies with the current non-Boolean INF data in order to compile a coherent and holistic story linking behavioural activation, mRNA transcription levels, and resulting INF characteristics. In addition, biomolecular techniques (e.g.

Northern blot quantification of transcription factors) could further characterize differential upregulation during electro-transcriptional coupling. Ideally, this quantification would occur in tissue preserved immediately following electrophysiological recordings to confirm the direct coupling between electrical activity and the onset of genetic transcription.

Another avenue of confirmation lies in the recently refined single-molecule FISH procedures which provide accurate integer counts of mRNA copy numbers in individual activated neurons (Raj et al., 2008). The continuous variation in intensity and size of transcriptional foci most likely indicates variable volumes of IEG transcripts generated from repeated cycles of parallel RNA-polymerase activity targeted at the IEG loci.

In the present tests, animals were allowed to freely navigate novel or familiar environments of relatively uniform size, but their trajectories were not systematically controlled. Therefore, the exact neural firing patterns in hippocampal populations can only be roughly correlated with the observed increases in intensity and size of induced INFs. Although there appears to be a consistent increase in both INF intensity and size parameters correlated with increased navigational area (cumulative area from subsequent environmental exposures), the present paradigm cannot relay an exact neuronal activation link with the results. That is, firing rates of pyramidal cells across hippocampal sub-regions cannot be derived from these inexact testing procedures. In a follow-up experiment, animals will be trained to run circular laps on a small, round track. Subjects will be assigned to traverse the track in a single direction for food once, five, ten, or twenty times and *Homer1a* INF intensity and size will be systematically analyzed. The robust re-activation of a consistent subset of place cell activity tagged to the circular track

on each repeated traversal has been previously reported (Wilson & McNaughton, 1993; Leutgeb et al., 2004; O'Keefe & Conway, 1978). Previous studies have also linked the co-activation of pyramidal place cell activity coupled to IEG transcription (Guzowski et al., 2001; Vazdarjanova et al., 2002) so it can be inferred with confidence that one traversal of a distinct place field should activate a set quantity of IEG transcription cycles. Hopefully, this follow-up study will exploit the systematic control of repeated place cell firing to provide a stronger, definitive link between repeated neuronal activity and increasing INF intensity and size.

In re-examining the behavioural time course used in the present studies, there was a substantial timing difference between 5E and 1E subjects. The 5E animals were actually sacrificed later than 1E relative to both groups' first environmental exposures since it took two minutes to explore each of the five different rooms, whereas the 1E subject was given five minutes for a single environment. This discrepancy convolutes the direct connection between firing rates and transcription time since it is likely that subjects in 5E were sacrificed about 35-40 minutes from its first environment. Nonetheless, this inequality still supports the hypothesis that increased transcription duration leads to increased INF intensity and size since 5E INFs were larger and more intense, indicating persistent or cumulative neuronal firing during the additional time. Another future manipulation in the study would include the equalization of timing in the rest period between 1E and 5E to eliminate the increased time as a factor of transcription rate. In addition, it would be beneficial to quantify systematic changes in INF intensity and size at progressive time-points post-activation. For example, rats could receive a single

MECS-treatment and sacrificed at 2-minute intervals from 0 to 60 minutes post-treatment to plot the exact time-course of INF accumulation and dissipation.

Additionally, in the current study, only single-layer z-stack analyses were performed, which would have led to a consistent degree of measurement error since the data only illustrates changes in 2D. In effect, the inclusion of partial INFs would underestimate certain data points, or the inclusion of out-of-focus INFs from below or above the focal layer would have inflated actual size values. Follow-up studies will require verification of the current Nanozoomer data with standard confocal imaging procedures, combined with 3D volumetric measurements. Thus, these data will require replication using laser scanning confocal quantification, as previously used in other IEG analysis studies (Guzowski et al., 2002; Chawla et al., 2005; Miyashita et al., 2009). This step is important for confirming that confocal imaging does not obliterate the varying degrees of intensity or size beyond detection due to the intrinsic deconvolving properties of the laser technology. In order to accommodate all four sub-regions, posterior HPC sections were analyzed here. Future studies should incorporate sections from anterior HPC and also other cortical or subcortical regions to verify similar trends throughout the brain.

Non-Boolean INF characteristics permit broadening of IEG imaging applications

The observation that INF intensity and size (area) may represent non-Boolean values could indicate that FISH IEG images may contain more electro-transcriptional coupling information than previously accepted. Despite several methodological approaches which require further enhancement, the current data suggest that potentially,

magnitude of neuronal activity (i.e. firing) may be quantified directly from a static fluorescent image.

Traditional Boolean quantification approaches may be overly reductionist and neglect information relating to a distinct neural coding window. It is likely that the proportional relationship between neuronal activation rates and transcription levels can be quantified from static fluorescent images, offering an essential parameter in characterizing whole-brain neuronal circuits. While IEG imaging has previously served as a powerful tool for mapping functional circuits engaged in specific cognitive processes, the reported data strongly suggest that IEG analyses may also permit real-time measurements of variable neural activation in discrete populations. The current data permit greater ranges of the application of IEG imaging and it is evident that IEG imaging will continue to gain popularity as a relevant method for functional and anatomical studies as these and other technical improvements are reported (Chawla et al., 2004; Pevzner et al., 2010). IEG imaging techniques, in complementation with techniques such as electrophysiological recordings, etc., will continue to answer important theoretical questions relating to neuronal circuit dynamics and population activity patterns within the field of learning and memory, cognitive processing, and an expanding list of other neuroscientific domains.

REFERENCES

Atar, D., Backx, P.H., Appel, M.H., Gao, W.D., & Marban, E. (1995). Excitation-transcription coupling mediated by zinc influx through voltage-dependent calcium channels. *The Journal of Biological Chemistry*, *270*(6), 2473-2477.

Barnes, C.A., Jung, M.W., McNaughton, B.L., Korol, D.L., Andreasson, K., & Worley, P.F. (1994). LTP saturation and spatial learning disruption: effects of task variables and saturation levels. *Journal of Neuroscience*, *14*, 5793-5806.

Barnes, C.A., McNaughton, B.L. Mizumori, S.J.Y., Leonard, B.W., & Lin, L.-H. (1990). Comparison of spatial and temporal characteristics of neuronal activity in sequential stages of hippocampal processing. *Progress in Brain Research, 83,* 287-300.

Bliss, T.V., & Collingridge, G.L. (1993). A synaptic model of memory: long-term potentiation in the hippocampus. *Nature*, *361*, 31-39.

Bottai, D., Guzowski, J.F., Schwarz, M.K., Kang, S.H., Xiao, B., Lanahan, A., Worley, P., & Seeburg, P.H. (2002). Synaptic activity-induced conversion of intronic to exonic sequence in *Homer1* immediate early gene expression. *The Journal of Neuroscience*, *22*, 167-175.

Brakeman, P.R., Lanahan, A.A., O'Brien, R., Roche, K., Barnes, C.A., Huganir, R.L., & Worley, P.F. (1997). Homer: a protein that selectively binds metabotropic glutamate receptors. *Nature*, *386*, 284-288.

Burke, S.N., Chawla, M.K., Penner, M.R., Barnes, C.A., & McNaughton, B.L. (2005). Differential encoding of behavior and spatial context in deep and superficial layers of neocortex. *Neuron, 45*, 667-674.

Chawla, M.K., Lin, G., Olson, K., Vazdarjanova, A., Burke, S.N., McNaughton, B.L., Worley, P.F., Guzowski, J.F., Roysam, B., & Barnes, C.A. (2004). 3D-CatFISH: a system for automated quantitative three-dimensional compartmental analysis of temporal gene transcription activity imaged by fluorescence in situ hybridization. *Journal of Neuroscience Methods*, *139*, 13-24.

Chawla, M.K., Guzowski, J.F., Ramirez-Amaya, V., Lipa, P., Koffman, K.L., Marriott, L.K.,… Barnes, C.A. (2005). Sparse, environmentally-selective expression of Arc RNA in the upper blade of rodent fascia dentata by brief spatial experience. *Hippocampus, 15*, 579-586.

Cole, A.J., Saffen, D.W., Baraban, J.M., & Worley, P.F. (1989). Rapid increase of an immediate-early gene messenger RNA in hippocampal neurons by synaptic NMDA receptor activation. *Nature, 340*, 474-476.

Cole, A.J., Abu-Shakra, S., Saffen, D.W., Baraban, J.M., & Worley, P.F. (1990). Rapid rise in transcription factor mRNAs in rat brain after electroshock-induced seizures. *Journal of Neurochemistry*, *55*(6), 1920-1927.

Femino, A.M., Fay, F.S., Fogarty, K., & Singer, R.H. (1998). Visualization of single RNA transcripts in situ. *Science*, *280*, 585- 590.

Fields, R.D., Eshete, F., Stevens, B., & Itoh, K. (1997). Action potential-dependent regulation of gene expression: temporal specificity in Ca^{2+}, cAMP-responsive element binding proteins, and mitogen-activated protein kinase signaling. *Journal of Neuroscience*, *17*, 7252-7266.

Flavell, S.W., & Greenberg, M.E. (2008). Signaling mechanisms linking neuronal activity to gene expression and plasticity of the nervous system. *Annual Review of Neuroscience, 31*, 563-90.

Grande, M.A., van der Kraan, I., de Jong, L., & van Driel, R. (1997). Nuclear distribution of transcription factors in relation to sites of transcription and RNA polymerase II. *Journal of Cell Science*, 110, 1781-1791.

Greenberg, M.E., Thompson, M.A., & Sheng, M. (1992). Calcium regulation of immediate early gene transcription. *Journal of Physiology*, 86, 99-108.

Guzowski, J.F., Knierim, J.J., & Moser, E.I. (2004). Ensemble dynamics of hippocampal regions CA3 and CA1. *Neuron, 44*, 581-584.

Guzowski, J.F., Lyford, G.L., Stevenson, G.D. Houston, F.P. McGaugh, J.L., Worley, P.F., & Barnes, C.A. (2000). Inhibition of activity-dependent arc protein expression in the rat hippocampus impairs the maintenance of long-term potentiation and the consolidation of long-term memory. *Journal of Neuroscience, 20*, 3993-4001.

Guzowski, J., McNaughton, B.L., Barnes, C.A., & Worley, P.F. (1999). Environment-specific expression of the immediate-early gene *Arc* in hippocampal neuronal ensembles. *Nature*, *2*(12), 1120-1124.

Guzowski, J.F., McNaughton, B.L., Barnes, C.A., & Worley, P.F. (2001). Imaging neural activity and temporal and cellular resolution using FISH. *Current Opinion in Neurobiology, 11*, 579-84.

Guzowski, J.F., Miyashita, T., Chawla, M.K., Sanderson, J., Maes, L.I., Houston, F.P.,… Barnes, C.A. (2006). Recent behavioural history modifies coupling between cell activity and *Arc* gene transcription in hippocampal CA1 neurons. *Proceedings of National Academy of Sciences*, *103*, 1077-1082.

Guzowski, J.F., Setlow, B., Wagner, E.K., & McGaugh, J.L. (2001). Experience-dependent gene expression in the rat hippocampus after spatial learning: a comparison of the immediate-early genes Arc, c-fos, and zif268. *Journal of Neuroscience, 21*(14), 5089-5098.

Guzowski, J.F., Timlin, J.A., Roysam, B., McNaughton, B.L., Worley, P.F., & Barnes, C.A. (2005). Mapping behaviourally relevant neural circuits with immediate-early gene expression. *Current Opinion in Neurobiology*, *15*, 599-606.

Hardingham, G.E., Chawla, S., Johnson, C.M., & Bading, H. (1997). Distinct functions of nuclear and cytoplasmic calcium in the control of gene expression. *Nature, 385*, 260- 265.

Iborra, F.J., Pombo, A., Jackson, D.A., & Cook, P.R. (1996). Active RNA polymerases are localized within discrete transcription ‘factories’ in human nuclei. *Journal of Cell Science, 109*, 1427-1436.

Imamura, N., Nonaka, A., Yamamoto, H., Matsuki, N., & Nomura, H. (2011). Experience-dependent Homer1a expression in excitatory and inhibitory neurons. *NeuroReport*, *22*, 353- 357.

Inoue, N., Nakao, H., Migishima, R., Hino, T., Matsui, M., Hayashi, F.,… Inokuchi, K. (2009). Requirement of the immediate early gene vesl-1S/homer-1a for fear memory formation. *Molecular Brain*, *2*, 7-12. Retrieved September 23, 2011 from www.molecularbrain.com/content/2/1/7.

Jackson, D.A., Hassan, A.B., Errington, R.J., & Cook, P. R. (1993). Visualization of focal sites of transcription within human nuclei. *European Molecular Biology Organization Journal*, *12*, 1059-1065.

Kandel, E.R. (2001). The molecular biology of memory storage: a dialogue between genes and synapses. *Science*, *294*, 1030-1038.

Kato, A., Ozawa, F., Saitoh, Y., Fukazawa, Y., Sugiyama, H., & Inokuchi, K. (1998). Novel members of the Vesl/Homer family of PDZ proteins that bind metabotropic glutamate receptors. *Journal of Biological Chemistry*, *273*, 23969-23975.

Kelly, M.P., & Deadwyler, S.A. (2003). Experience-dependent regulation of the immediate-early gene arc differs across brain regions. *Journal of Neuroscience*, *23*, 6443-6451.

Kubik, S., Miyashita, T., & Guzowski, J.F. (2007). Using immediate-early genes to map hippocampal sub-regional functions. *Learning and Memory*, *14*, 758-770.

Lanahan, A., & Worley, P.F. (1998). Immediate-early genes and synaptic function. *Neurobiology of Learning and Memory*, *70*, 37-43.

Leutgeb, S., Leutgeb, J.K., Barnes, C.A., Moser, E.I., McNaughton, B.L., & Moser, M.-B. (2005). Independent codes for spatial and episodic memory in the hippocampus. *Science*, *309*, 619-623.

Link, W., Konietzko, U., Kauselmann, G., Krug, M., Schwanke, B., Frey U., & Kuhl, D. (1995). Somatodendritic expression of an immediate early gene is regulated by synaptic activity. *Proceedings of the National Academy of Sciences*, *92*, 5734-5738.

Lyford, G.L., Yamagata, K., Kaufmann, W.E., Barnes, C.A., Sanders, L.K., Copeland, N.G., Gilbert, D.J., Jenkins, N.A., Lanahan, A.A., & Worley, P.F. (1995). Arc, a growth factor and activity-regulated gene, encodes a novel cytoskeleton-associated protein that is enriched in neuronal dendrites. *Neuron*, *14*, 433-445.

Marrone, D.F., Schaner, M.J., McNaughton, B.L., Worley, P.F., & Barnes, C.A. (2008). Immediate-early gene expression at rest recapitulates recent experience. *Journal of Neuroscience*, *28*(5), 1030-1033.

Martin, S., & Pombo, A. (2003). Transcription factories: quantitative studies of nanostructures in the mammalian nucleus. *Chromosome Research*, *11*, 461-470.

McNaughton, B.L. (1982). Long-term synaptic enhancement and short-term potentiation in rat fascia dentate act through different mechanisms. *Journal of Physiology*, *324*, 249-262.

Mitchell, J.A., & Fraser, P. (2008). Transcription factories are nuclear subcompartments that remain in the absence of transcription. *Genes & Development*, *22*, 20-25.

Miyashita, T., Kubik, S., Haghighi, N., Steward, O., & Guzowski, J.F. (2009). Rapid activation of plasticity-associated gene transcription in hippocampal neurons provides a mechanism for encoding of one-trial experience. *The Journal of Neuroscience*, *29*(4), 898-906.

Morgan, J.I., Cohen, D.R., Hempstead, J.L., & Curran, T. (1987). Mapping patterns of c-fos expression in the central nervous system after seizure. *Science*, *237*, 192-7.

Naisbitt, S., Kim, E., Tu, J., Xiao, B, Sala, C., Valtschanoff, J., Weinberg, R., Worley, P., & Sheng, M. (1999). Shank, a novel family of postsynaptic density proteins that binds to the NMDA receptor/PSD-95/ GKAP complex and cortactin. *Neuron*, *23*, 569-582.

Nyguyen, T.V., Kobierski, L., Comb, M, & Hyman, S.E. (1990). The effect of depolarization on expression of the human proenkephalin gene is synergistic with cAMP and dependent upon a cAMP-inducible enhancer. *Journal of Neuroscience*, *10*, 2825- 2833.

Osborne, C.S., Chakalova, L., Brown, K.E., Carter, D., Horton, A., Debrand, E.,… Fraser, P. (2004). Active genes dynamically colocalize to shared sites of ongoing transcription. *Nature Genetics*, 36, 1065-1071.

Osborne, C.S., Chakalova, L., Mitchell, J.A., Horton, A., Wood, A.L., Bolland, D.J.,… Fraser, P. (2007). Myc dynamically and preferentially relocates to a transcription factory occupied by Igh. *Plos Biology*, 5, 1763-1772.

Paxinos, G., & Watson, C. (2007). *The Rat Brain in Stereotaxic Coordinates* (6th ed.). Sydney, Australia: Academic Press.

Penner, M.R., Roth, T.L., Chawla, M.K., Hoang, L.T., Roth, E.D., Lubin, F.D.,… Barnes, C.A. (2011). Age-related changes in Arc transcription and DNA methylation within the hippocampus. *Neurobiology of Aging*, *32*, 2198-2210.

Raj, A., van den Bogaard, P., Rifkin, S.A., van Oudenaarden, A., & Tyagi, S. (2008). Imaging individual RNA molecules using multiple singly labeled probes. *Nature Methods*, *5*, 877- 879.

Sato, M., Suzuki, K., & Nakanishi, S. (2001). NMDA receptor stimulation and brain-derived neurotrophic factor upregulate Homer 1a mRNA via the mitogen-activated protein kinase cascade in cultured cerebellar granule cells. *Journal of Neuroscience*, *21*, 3797-3805.

Sheng, M., & Greenberg, M.E. (1990). The regulation and function of c-fos and other immediate-early genes in the nervous system. *Neuron*, 4, 447-485.

Sheng, M. & Kim, E. (2000). The Shank family of scaffold proteins. *Journal of Cell Science*, 113, 1851-1856.

Tu, J.C., Xiao,B., Yuan, J., Lanahan, A., Leoffert, K., Li, M.,… Worley, P.F. (1998). Homer binds a novel proline rich motif and links group 1 metabotropic receptors with IP3 receptors. *Neuron, 21*, 717-726.

Tully, T. (1997). Regulation of gene expression and its role in long-term memory and synaptic plasticity. *Proceedings of the National Academy of Sciences*, *94*, 4239-4241.

Ugo Basile. (2009, March). Manufacturer's Instruction Manual for ECT Unit Model 57800. Revision 1. [Instruction Manual]. Varese, Italy.

Vazdarjanova, A., & Guzowski, J.F. (2004). Differences in hippocampal neuronal population responses to modifications of an environmental context: Evidence for distinct, yet complementary, functions of CA3 and CA1 ensembles. *Journal of Neuroscience*, *24*, 6489-6496.

Vazdarjanova, A., McNaughton, B.L., Barnes, C.A., Worley, P.F., & Guzowski, J. (2002). Experience-dependent coincident expression of the effector immediate-early genes *Arc* and *Homer1a* in hippocampal and neocortical neuronal networks. *Journal of Neuroscience*, 22, 10067-10071.

Vazdarjanova, A., Ramirez-Amaya, V., Insel, N., Plummer, T.K., Rosi, S., Chowdhury,... Barnes, C.A. (2006). Spatial exploration induces Arc, a plasticity-related immediate-early gene, only in calcium/calmodulin-dependent protein kinase II-positive principal excitatory and inhibitory neurons of the rat forebrain. *Journal of Comparative Neurology*, *498*(3), 317-29.

Wansink, D.G., Schul, W., van der Kraan, I., van Steensel, B., van Driel, R., & de Jong, L. (1993). Fluorescent labeling of nascent RNA reveals transcription by RNA polymerase II in domans scattered through the nucleus. *Journal of Cell Biology*, 122, 283-293.

Xia, Z., Dudek, H., Miranti, C.K., & Greenberg, M.E. (1996). Calcium influx via the NMDA receptor induces immediate early gene transcription by a MAP kinase/ERK-dependent mechanism. *Journal of Neuroscience*, *16*, 5425-5436.

Xiao, B., Tu, J.C., & Worley, P.F. (2000). Homer: a link between neural activity and glutamate receptor function. *Current Opinion in Neurobiology*, *10*, 370-374.

Xiao, B., Jian, C.T., Petralia, R.S., Yuan, J.P., Doan, A., Breder, C.D., Ruggiero, A., Lanahan, A., Wenthold, R.J., & Worley, P.F. (1998). Homer regulates the association of group 1 metabotropic glutamate receptors with multivalent complexes of homer-related, synaptic proteins. *Neuron, 21*, 707-716.

Yamamoto, K., Sakagami, Y., Sugiura, S., Inokuchi, K., Shimohama, S., & Kato, N. (2005). Homer1a enhances spike-induced calcium influx via L-type calcium channels in neocortex pyramidal cells. *European Journal of Neuroscience*, *22*, 1338 – 1348.

APPENDIX I
SUPPLEMENTARY MATERIAL: METHODS AND PROCEDURES

Behaviour

Initially, the complete data set was comprised of two separate cohorts. Both cohorts received identical treatment except that one cohort (cue-deprived transport) was moved between locations in a covered transport cage. Meanwhile, the other cohort (cue-available transport, or cue-rich transport) was moved in a transparent cage and also received 3 days of transport habituation. However, results showed no difference between the two cohorts and so both groups of data were combined in the official Results. In the cue-deprived (CD) transport, 21 naïve Long-Evans rats were separated into home-cage, 1-environment (1E), 5-environment (5E) or maximal electroconvulsive shock (MECS) groups. In the cue-available transport cohort (CA), 28 naïve rats (22 Long-Evans, 6 Brown-Norways) were also assigned to home-cage, 1-environment (1E), 5-environment (5E) or maximal electroconvulsive shock (MECS) groups. The only difference between the two cohorts was that the cue-available cohort were transported in uncovered carrying-cages for 5 transport- training days, exposed to a darkened antechamber for a minimum of 3 hours per day, and then transported in uncovered carrying-cages to the five environmental testing room in the same order as the CD cohort as test day. All subjects were housed in pairs in a 12-hour dark/light cycle colony room on an *ad libitum* feeding schedule. Home-cages were clear plastic shoe-boxes with bases that measured 24cm X

45.5cm, and 21cm in height. All subjects were handled daily for 10 minutes for two full weeks prior to their designated test day animals. On test day, all subjects were transported with their home-cages covered with a dark blanket (CD group) or with a transparent cage (CA group), and rested for at least one hour in a darkened antechamber to lower global activity and control for extraneous disruptions. In the home-cage control group (n=10; ages P107, P218, P108, P168, P219, P155, P155, P180, P136, P141), all subjects were removed directly from the darkened antechamber in their cage for immediate sacrifice in the surgical suite. For the 1E group (n=14, ages P107, P218, P224, P108, P168, P168, P219BN, P219BN, P155,P155, P180, P136, P136, P141), animals were transported in a transport cage identical to the home-cage, to a testing room and animals were placed by the experimenter in a new environment in the form of a triangular enclosure that measured 84cm X 81cm with walls 50cm in height. Walls were covered with vertical black stripes while the flooring was covered with gritty sandpaper. 1E rats traversed this environment freely with the experimenter nudging the rat gently to ensure full coverage of the space. After a 5-minute exploration period, rats were transported in its covered carrying-cage to the darkened antechamber and rested in its home-cage for 25 minutes prior to sacrifice. In the 5E group (n=15, ages P107, P218, P224, P224, P108, P168, P168, P219BN, P219BN, P155, P155, P180, P136, P136, P141), subjects were transported in a covered carrying-cage, and transported to five different testing rooms for 2 minutes per trial. The order of environments exposed were a triangular enclosure (same as those navigated by 1E rats), a square enclosure on a wooden desk (71cm X 71cm X 10cm), a trapezoid metal tank (area=6480cm^2), a circular track elevated by 19cm (area=4449cm^2), and another square enclosure with 3 pillars scattered (71cm X 71cm X

10cm walls). Following the five environmental exposures of 2-minutes each, 5E animals were returned to the darkened antechamber, rested for 25 minutes, and then rushed to the surgical suite for immediate sacrifice. Finally, in the MECS positive control group (n=10, ages P23, P67, P2, and P168, P219BN, P155, P155, P180, P136, P141), animals were removed from the dark antechamber, administered a single MECS event, and then returned to the antechamber to rest for 28 minutes and then sacrificed. Earclips connected to a research-grade ECT (electroconvulsive therapy) unit (Ugo Basile 57800) were used to deliver pulses of electrical current to electrically drive all IEG-expressing cells produce RNA transcripts (Cole, Abu-Shakra, Saffen, Baraban, & Worley, 1990). Subjects receiving MECS treatment served as the maximal level positive control. The parameters for all MECS administrations were as follows: frequency of 100pulses/second; pulse width of 0.5ms, shock duration of 1.1s and 85mA of current. These parameters were calculated from the manufacturer's guide (Ugo Basile, 2009).

Fluorescent *in situ* hybridization

Coronal sections containing the region of interest (start of dorsal subiculum in anterior-posterior axis until its fusion with ventral subiculum) were selected for *H1a*-single label FISH processing. Slides represented 20μm serial sections from -4.92mm until -6.96mm from bregma. *Homer1a* DNA templates were generated from the restriction digestion of plasmids provided in house via a previously described process (reference) and oligonucleotide riboprobes were then synthesized with from this digested template. All solutions and washes were carried out with water processed with a Barnstead Nanopure system filtering at 18.2mOhms to ensure the removal of DNAses and RNAses. Slides were removed from -80^{o}C storage, thawed for 20-40 minutes at room temperature

(~21^{o}C), and then fixed in 4% paraformaldehyde for 7 minutes at 4^{o}C. Following a 2XSSC wash, slides were then treated with acetic anhydride in triethanolamine buffer for 10 minutes to lower background signal by binding to polar groups that bind to the probe, followed by a 5 minute 1:1 acetone-methanol treatment (perforate nuclear envelope to enable probe penetration). Sections were then pre-hybridized with hybridization buffer for a minimum of 1 hour to prevent background staining, and then incubated overnight (16 hours) in the hybridization oven with H1a-conjugated fluoroprobes. Then, slides were cooled for 15 minutes, incubated with RNAse A for 30 minutes to digest single-stranded RNA that has not bound to the probe and then washed in a succession of buffers in increasing stringency. To quench the endogenous peroxidases that would bind to the antibody, slides were washed in 2% hydrogen peroxide for 15 minutes, and washed in buffered solution. TSA blocking buffer with 5% normal sheep serum was pipetted onto each slide to block all non-specific binding sites for anti-FITC to reduce the background and incubated for 40 minutes at room temperature. Anti-fluorescein was added to the slides and incubated in the fridge at 4^{o}C for 18 hours. Following three more washes in buffered solution, slides were then incubated with 1:100 fluorescein-tyramide for 30 minutes, washed, and counter-stained with DAPI (Sigma), and coverslipped with VectaShield Mounting Media for Fluorescence (Vector Labs).

Automated IEG foci quantification

In-house software programmed in Visual Basic C++ (GreenDot.exe) was used for automated characterization of green *Homer1a* intranuclear foci (INF). Each sub-image that contained segments of the ROIs were fed through the algorithm such that putative

INFs were detected by a horizontal line probe scan which searched for green channel intensity increases in a step-wise function followed by a rotational confirmational scan to ensure circular Gaussian spread using a Markhov chain parameter as the guiding principle. Detection criteria required that each putative green pixel counted in an INF must have contained minimum blue pixel content (from DAPI counterstain to ensure its inclusion within a neuronal nucleus). The neighbouring green pixels were required to meet the Gaussian increase pattern to distinguish from diffuse background noise acquired during the FISH process. Total INF counts per image were outputted along with the total blue pixel count quantifying the amount of blue pixels that fell within nuclear intensity range in a rough attempt to eliminate small glial nuclei (which appear as intensely bright and uniformly stained nuclei, ~5μm in diameter). This total blue pixel count (in theory, the total neuronal nuclei pixel count) was then divided by a predetermined average area of hippocampal neuronal nuclei size (previous systematic sampling from randomized hippocampal DAPI images). For each ROI, four parameters were calculated in addition to the total estimate of individual foci detected: a) total peak foci intensity of all foci; b) total average intensity values; c) total pixels included in all foci; d) total blue intensity values within identified foci. Manual counting was used as a verification of software detection accuracy for randomly-selected images. All signal statistics were collated into a comma-separated values file (.CSV), then exported into a Microsoft Excel file.

APPENDIX II
SUPPLEMENTARY MATERIAL: NON-BOOLEAN VARIATION IN FOCI INTENSITY AND SIZE

Results

Subjects were actually divided in two cohorts: cue-deprived transport (CD) and cue-available transport (CR). The only two differences between the two cohorts was that 1) CD rats were transported between dark room and test environments in a lab-coat covered transport cage, while CR animals were moved from place to place in a clear, transparent cage; and 2) CR animals received a brief period of transport-habituation to all environments prior to test day but never experienced the actual apparatuses. However, the following analyses showed no statistically significant differences in any parameter between the two cohorts, and as such are treated as a single test group in the official Results.

1. Mean maximum INF intensity (I_{max})

To tabulate data regarding mean peak INF intensity (I_{max}), the sum of all INF "origin" or maximum intensity values was divided by the total number of INFs per sub-image, and tabulated across sub-regions, and also across test conditions.

1a. Cue-Deprived (CD) Transport Cohort

Refer to Table II.1 for statistical data. The effect of condition on I_{max} in dorsal subiculum was significant by a one-way ANOVA[1]. In DS, HC I_{max} was lower than 1E[2]; 5E was higher than 1E[3]; 5E was higher than HC[4]. MECS I_{max} was significantly higher than 5E[5]; than 1E[6] and higher than HC[7].

In CA1, there was a significant effect of condition on I_{max}[8] while paired-sample T-tests confirmed that 1E I_{max} was higher than HC I_{max}[9], 5E was higher than 1E[10], and 5E was also higher than HC[11]. MECS I_{max} was significantly higher than 5E[12], higher than 1E[13]; and higher than HC[14].

In CA3, there was a significant effect of condition on I_{max}[15] while paired-sample T-tests confirmed that 5E was higher than 1E[16]; and 5E was higher than HC[17]. There was no significant difference between HC and 1E I_{max} values[18]. MECS I_{max} was significantly higher than 5E[19]; higher than 1E[20]; and higher than HC[21].

In DG, there was a significant effect of condition on I_{max}[22], and paired-sample T-tests confirmed that 1E I_{max} was higher than HC[23], and 5E was higher than HC[24]. There was no significant difference between 1E and 5E I_{max} values[25]. MECS was higher than 5E[26]; higher than 1E[27]; and higher than HC[28].

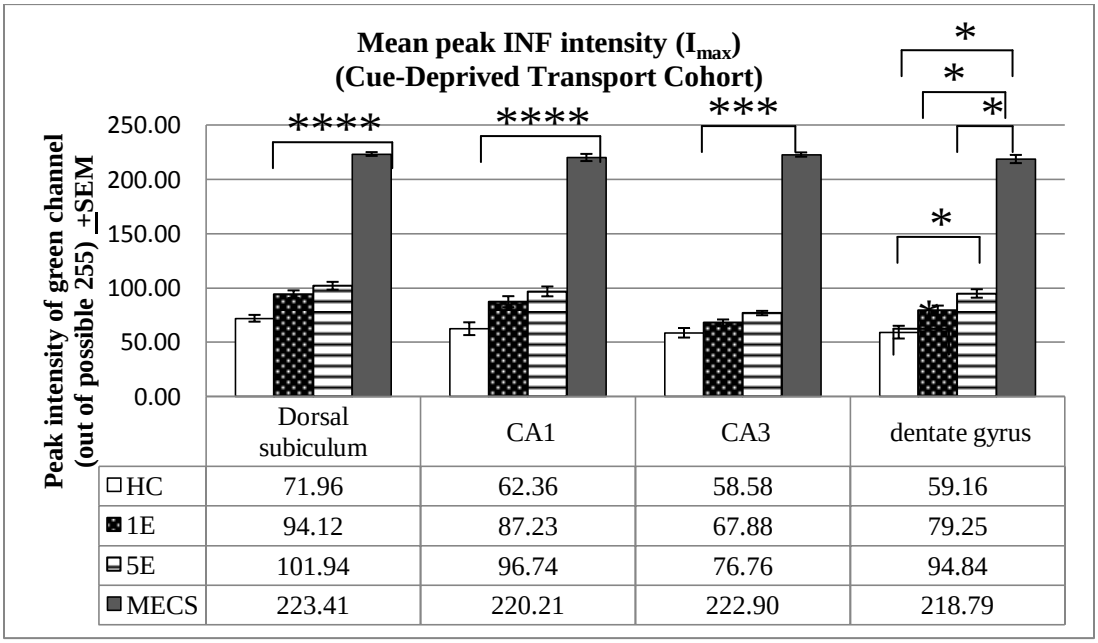

Figure II.1 Mean peak green intensity (I_{max}) of INFs showed monotonic increase with cumulative environmental exposure in cue-deprived transport cohort. Significant increase observed in all sub-regions.

Table II.1 Statistical data reporting overall significant effect of cumulative environment on I_{max} in CD cohort.

[1] [F(3,13)=304.85, p<0.001]	[2] (t(4)=-5.302, p=0.006)	[3] (t(4)=-3.764, p=0.02)
[4](t(4)=-6.429, p=0.003)	[5] (t(4)=-29.83, p<0.001)	[6] (t(4)=34.9, p<0.001)
[7] (t(4)=96.44, p<0.001)	[8][F(3,13)=149.94, p<0.001]	[9](t(4)=-6.824, p=0.002)
[10] (t(4)=-3.05, p=0.038)	[11] (t(4)=-7.92, p=0.001)	[12] (t(4)=-35.45, p<0.001))
[13] (t(4)=35.75, p<0.001)	[14] (t(4)=53.99, p<0.001)	[15] [F(3,13)=502.17; p<0.0001]
[16] (t(4)=-4.186, p=0.013)	[17] (t(4)=-3.96, p=0.017)	[18] (t(4)=-5.54, p=0.064)
[19] (t(4)=-60.59, p<0.0001)	[20] (t(4)=44.60, p<0.0001)	[21] (t(4)=53.75, p<0.0001)
[22][(F(3,13)=185.48, p<0.0001]	[23] (t(4)=-4.216, p=0.01)	[24] (t(4)=-5.01, p=0.007)
[25] (t(4)=-2.73, p=0.05)	[26] (t(4)=-24.02, p<0.0001)	[27] (t(4)=31.52, p<0.0001)
[28] (t(4)=61.79, p<0.0001)		

1b. Cue-available Transport (CR) Cohort

See Figure II.2 and refer to Table II.2 for statistical data. The effect of condition on I_{max} in dorsal subiculum (DS) was reported to be significant by one-way ANOVA[29], and paired-sample T-tests confirmed that 5E I_{max} was higher than 1E[30], and 5E was higher than HC[31]. The difference between 1E and HC was not significant[32]. MECS values were higher than 5E[33]; higher than 1E[34]; and higher than HC[35].

In CA1, there was a significant effect of condition on I_{max}[36] and paired-sample T-tests confirmed that 1E I_{max} values were higher than HC[37], 5E higher than HC[38], and 5E was higher than 1E[39]. MECS values were higher than 5E[40]; 1E[41]; and HC[42].

In CA3, there was an effect of condition on I_{max}[43], and paired-sample T-tests reported significantly higher I_{max} in 5E versus 1E[44]; and 5E versus HC[45]. There was no significant difference between HC and 1E 1_{max}[46]. MECS was higher than 5E[47]; higher than 1E[48]; and higher than HC[49].

In DG, there was a significant effect of condition on I_{max}[50] and paired-sample T-tests confirmed significantly higher I_{max} values in 1E versus HC[51], 5E versus HC[52]. There was no significant difference between 1E and 5E[53]. MECS was higher than 5E[54]; higher than 1E[55]; and higher than HC[56].

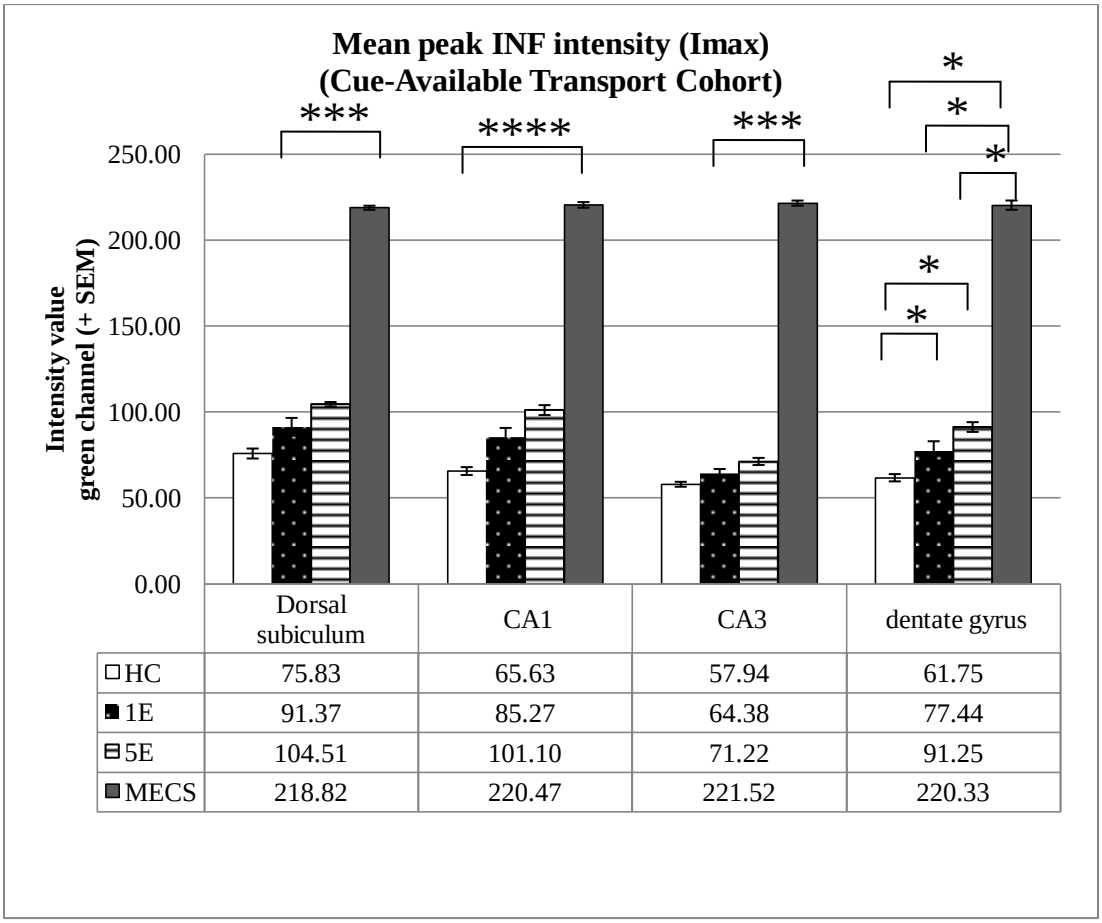

	Dorsal subiculum	CA1	CA3	dentate gyrus
HC	75.83	65.63	57.94	61.75
1E	91.37	85.27	64.38	77.44
5E	104.51	101.10	71.22	91.25
MECS	218.82	220.47	221.52	220.33

Figure II.2 Mean maximum green intensity (I_{max}) of INFs showed monotonic increase with cumulative environmental exposure in CA transport cohort. Significant increase observed in all sub-regions.

Table II.2 Statistical data showing overall significant effect of cumulative environmental exposure on I_{max} in CA cohort.

[29] [F(3,22)=225.73, p<0.001]	[30] (t(7)=-2.43, p=0.045)	[31] (t(7)=-11.21, p< 0.0001)
[32] (t(7)=-2.34, p=0.05)	[33] (t(7)=-98.53, p<0.0001)	[34] (t(7)=25.02, p<0.0001)
[35] (t(7)=55.87, p<0.0001)	[36][F(3,22)=208.27, p<0.0001]	[37] (t(7)=-3.02, p=0.02)
[38] (t(7)=-12.05, p<0.0001)	[39] (t(7)=-2.603, p=0.04)	[40] (t(7)=-52.42, p<0.0001)
[41] (t(7)=24.13, p<0.0001)	[42] (t(7)=107.02, p<0.0001)	[43][F(3,22)=914.27, p<0.0001]
[44] (t(7)=-2.83, p=0.03)	[45] (t(7)=-6.177, p<0.01)	[46](t(7)=-2.27, p=0.06)
[47] (t(7)=-88.21, p<0.0001)	[48] (t(7)=64.68, p<0.0001)	[49] (t(7)=156.54, p<0.0001)
[50][F(3,22)=218.96, p<0.0001]	[51] (t(7)=-2.81, p=0.03)	[52] (t(7)=-11.29, p<0.0001)
[53] (t(7)=-2.304, p=0.05)	[54] (t(7)=-64.05, p<0.0001)	[55] (t(7)=27.28, p<0.0001)
[56] (t(7)=85.73, p<0.0001)		

1c. Raw differences in maximum intensity values between CA and CD counterparts

The increases in I_{max} between all conditions were compared (1E to HC; 5E to 1E; and 5E to HC) to measure a) whether there were robust increase patterns as a result of increased behavioural exposure (Table II.3) and b) whether cue-deprived or cue-available transportation affected maximum intensity (Table II.4).

Table II.3 Comparison of absolute increase in average maximum intensity (green intensity value of 'origin' of all INFs (I_{max}). Significant increase in I_{max} across all sub-regions between HC to 1E, 1E to 5E, and HC to 5E. Lowest absolute increases were observed in CA3 between HC and 1E averages, and highest increases observed in regions DG and CA1 between 5E and HC.

Difference in I_{max}	**Dorsal subiculum**		**CA1**		**CA3**		**Dentate gyrus**	
	CD	CA	CD	CA	CD	CA	CD	CA
$1E_{imax}$-HC_{imax}	22.17	14.81	24.88	19.65	9.30	6.44	20.09	15.70
$5E_{imax}$-$1E_{imax}$	7.82	13.87	9.50	15.83	8.88	6.85	15.59	13.80
$5E_{imax}$-HC_{imax}	29.98	28.67	34.38	35.48	18.18	13.29	35.68	29.50
$MECS_{imax}$– $5E_{imax}$	121.47	114.31	123.47	119.37	146.14	150.3	123.95	129.08
$MECS_{imax}$ – $1E_{imax}$	129.29	127.45	132.98	135.20	155.02	157.14	139.54	142.89
$MECS_{imax}$ - HC_{imax}	151.45	142.99	157.85	154.84	164.32	163.58	159.63	158.58

There was no statistically significant effect of cued-transport on I_{max} in any region or condition except for between MECS values in DS-CD versus DS-CA[57]. In HC condition, there were no differences between DS-CD and DS-CA I_{max}[58], CA1-CD and CA1-CA[59], CA3-CD and CA3-CA[60], nor between DG-CD and DG-CA[61]. In 1E condition, there were no differences between CD and CA cohorts in DS[62], CA1[63], CA3[64], nor in DG[65]. In 5E condition, no regions showed significant differences between CD and CA cohorts; DS[66], CA1[67], CA3[68]; DG[69]. For MECS, no other sub-region showed significant difference in I_{max} between CD and CA cohorts: CA1[70], CA3[71] and DG[72].

Table II.4 Statistical data showing no significant effect of transport method on I_{max} between CD and CA cohorts.

[57] (t(3)=3.37, p=0.04)	[58](t(5)=-1.27, p=0.258)	[59] (t(5)=-0.834, p=0.442)
[60] (t(5)=0.229, p=0.828)	[61] (t(5)=-0.667, p=0.535)	[62] (t(7)=0.513, p=0.624)
[63] (t(7)=0.282, p=0.786)	[64] (t(7)=1.205, p=0.267)	[65] (t(7)=0.314, p=0.763)
[66] (t(7)=-0.904, p=0.396)	[67] (t(7)=-1.467, p=0.186)	[68] (t(7)=2.362, p=0.05)
[69] (t(7)=0.935, p=0.381)	[70] (t(3)=-0.097, p=0.929)	[71] (t(3)=0.483, p=0.662)
[72] (t(3)=-0.343, p=0.754)		

1d. Differences across sub-regions in maximal INF intensity (I_{max})

Through one-way ANOVA and paired-sample t-tests, the effect of sub-region on I_{max} was analyzed. This measured whether INFs expressed in cells of different regions varied significantly in I_{max}. All statistical tests employed an alpha level of 0.05 where appropriate. Refer to Table II.5 for statistical data relating to the effect of sub-region on I_{max} values.

Refer to Figure II.3. Within the cue-deprived transport cohort, there were several significant differences between regions in I_{max} values within specific behavioural conditions. In the CD-HC condition, one-way ANOVA reported no significant differences between I_{max} between regions[73] but paired-sample t-tests confirmed higher I_{max} in DS versus CA3[74]; DS higher than DG[75] and CA1 was higher than DG[76].

In the CD-1E condition, there was a significant difference between regions in I_{max}[77] and paired-sample t-tests confirmed higher DS I_{max} than CA3[78]; DS was higher than DG[79]; CA1 was higher than CA3[80]; and DG was higher than CA3[81]. CA3 contained the lowest I_{max} values amongst all regions.

In CD-5E condition, there was a significant regional effect on I_{max}[82] and paired-sample t-tests confirmed higher intensities in DS than CA3[83], higher DS than DG intensities[84], higher DG than CA3[85], and CA1 higher than CA3[86]. Thus in CD-5E, CA3 contained the lowest I_{max}. In CD-MECS condition, one-way ANOVA reported no difference among regions[87].

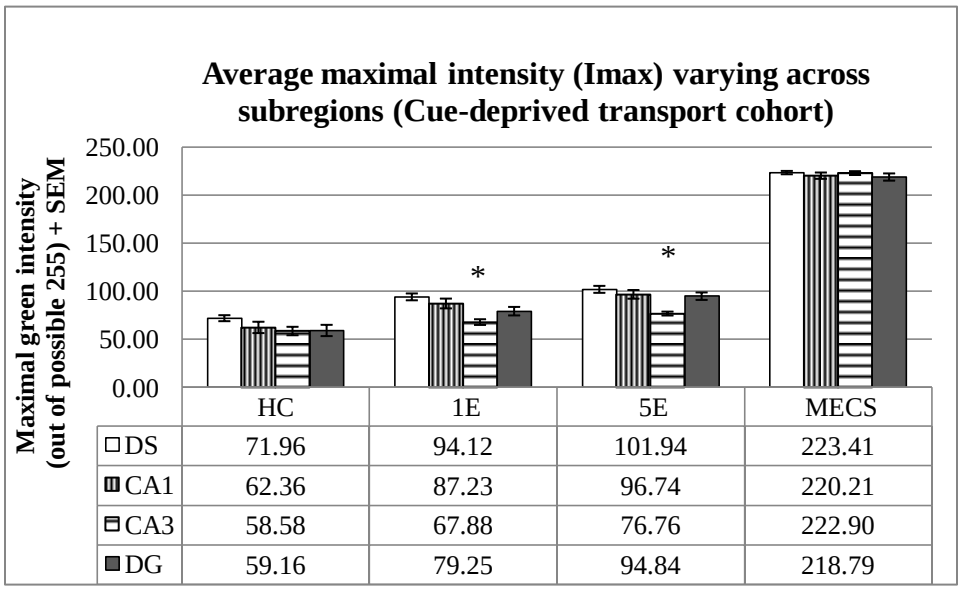

	HC	1E	5E	MECS
DS	71.96	94.12	101.94	223.41
CA1	62.36	87.23	96.74	220.21
CA3	58.58	67.88	76.76	222.90
DG	59.16	79.25	94.84	218.79

Figure II.3 Peak INF intensity (I_{max}) compared for cross-regional differences, separated by condition in CD transport group. Lowest values observed in CA3.

Table II.5 Statistical data showing mild effect of sub-region on I_{max} in CD cohort. Lowest values observed in CA3.

[73] [F(3, 12)=1.56, p=0.25]	[74] (t(3)=5.607, p=0.01)	[75] (t(3)=3.607, p=0.037)
[76] (t(3)=-8.674, p=0.003)	[77] [F(3,16)=7.576, p=0.002]	[78] (t(4)=4.93, p=0.008)
[79] (t(4)=2.96, p=0.04)	[80] (t(4)=3.946, p=0.017)	[81] (t(4)=-4.3, p=0.012)
[82][F(3,16)=9.069, p=0.001]	[83] (t(4)=5.893, p=0.004)	[84] (t(4)=7.437, p=0.002)
[85] (t(4)=-4.034, p=0.016)	[86] (t(4) =4.336, p=0.012)	[87] [F(3,8)=0.604, p=0.631]

Refer to Figure II.4 and Table II.6 (statistical data). Within the cue-available (CA) transport cohort, there were several significant differences between regions in regards to I_{max} values within specific behavioural conditions. In CD-HC condition, one-way ANOVA reported significant effect of region on I_{max} values[88], while paired-sample t-tests

confirmed higher I_{max} in DS than CA1[89]; higher in CA1 than CA3[90]; higher DS than DG[91]; and higher DS than CA3[92].

In CD-1E condition, there was a significant effect of region on I_{max} values[93] and t-tests confirmed higher values in DS versus CA1[94]; higher I_{max} in DS than CA3[95]; higher CA1 than CA3[96]; and higher DG than CA3[97]. Thus, in CD-1E, I_{max} were lowest in CA3.

In CD-5E condition, there was a significant effect of region on I_{max} values[98]; while paired-sample t-tests confirmed higher values in CA1 versus CA3[99]; higher DS than CA3[100]; higher DS versus DG[101]; higher DG than CA3[102]; and higher CA1 than DG[103]. Thus, in CD-5E, I_{max} were lowest in CA3.

In CD-MECS, there was no significant effect of region on I_{max} [104] while paired-sample t-tests confirmed only significance between CA3 and DS[105].

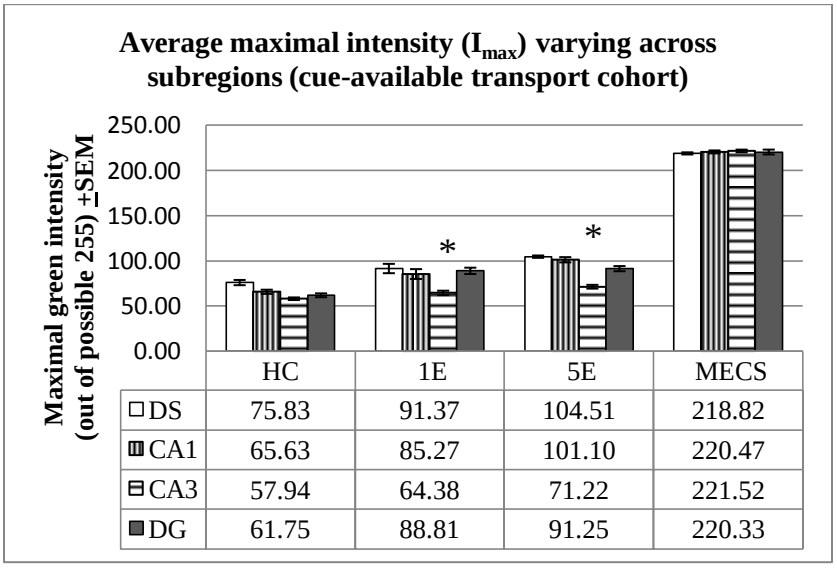

	HC	1E	5E	MECS
DS	75.83	91.37	104.51	218.82
CA1	65.63	85.27	101.10	220.47
CA3	57.94	64.38	71.22	221.52
DG	61.75	88.81	91.25	220.33

Figure II.4 Peak INF intensity (I_{max}) compared for cross-regional differences, separated by condition in CA transport cohort. Lowest values observed in CA3.

Table II.6 Statistical data showing mild effect of region on CA cohort. Lowest values observed in CA3.

[88] [F (3,20)=11.738, p=0.0001]	[89] (t(5)=3.89, p=0.012)	[90] (t(5)=5.82, p=0.002)
[91] (t(5)=3.027, p=0.029)	[92] (t(5)=7.48, p=0.0007)	[93] [F(3,28)=8.11, p=0.0005]
[94] (t(7)=2.544, p=0.038)	[95] (t(7)=7.807, p=0.0001)	[96] (t(7)=5.77, p=0.0007)
[97] (t(7)=-6.182, p=0.0005)	[98] [F(3,28)=39.95, p<0.0001]	[99] (t(7)=12.259, p<0.0001)
[100] (t(7)=20.571, p<0.0001)	[101] (t(7)=6.848, p=0.0002)	[102] (t(7)=-9.07, p<0.0001)
[103] (t(7)=4.511, p=0.003)	[104] [F(3,12)=0.366, p=0.779]	[105] (t(3) =-4.034, p=0.027)

1e. Post-hoc test results of collapsed data (I_{max})

Table II.7 Bonferroni post-hoc tests to determine which conditions differed in I_{max} values when both cohorts were combined and grouped according to HC, 1E, 5E, or MECS.

Region	Condition	Condition	Critical Value	Bonferroni p=value	Significant?
DS	5E n=13	MECS n=7	0.008333	8.46E-21	**Yes**
DS	HC n=10	MECS n=7	0.01	1.91E-18	**Yes**
DS	1E n=13	MECS n=7	0.0125	5.04E-16	**Yes**
DS	HC n=10	5E n=13	0.016667	1.87E-10	**Yes**
DS	HC n=10	1E n=13	0.025	0.000372	**Yes**
DS	1E n=13	5E n=13	0.05	0.006404	**Yes**
CA1	5E n=13	MECS n=7	0.008333	8.62E-18	**Yes**
CA1	HC n=10	MECS n=7	0.01	1.27E-17	**Yes**
CA1	1E n=13	MECS n=7	0.0125	1.49E-15	**Yes**
CA1	HC n=10	5E n=13	0.016667	3E-09	**Yes**
CA1	HC n=10	1E n=13	0.025	0.000208	**Yes**
CA1	1E n=13	5E n=13	0.05	0.006344	**Yes**
CA3	5E n=13	MECS n=7	0.008333	1.9E-22	**Yes**
CA3	1E n=13	MECS n=7	0.01	7.74E-22	**Yes**
CA3	HC n=10	MECS n=7	0.0125	3.39E-20	**Yes**
CA3	HC n=10	5E n=13	0.016667	3.87E-06	**Yes**
CA3	1E n=13	5E n=13	0.025	0.005437	**Yes**
CA3	HC n=10	1E n=13	0.05	0.010421	**Yes**
DG	5E n=13	MECS n=7	0.008333	2.1E-18	**Yes**
DG	HC n=10	MECS n=7	0.01	1.48E-17	**Yes**
DG	1E n=13	MECS n=7	0.0125	6.09E-16	**Yes**
DG	HC n=10	5E n=13	0.016667	5.33E-09	**Yes**
DG	HC n=10	1E n=13	0.025	0.001435	**Yes**
DG	1E n=13	5E n=13	0.05	0.002649	**Yes**

2. Average INF size (area measured in pixels, S_{avg})

The total number of pixels which constituted all detected INFs was summed and averaged across regions and test conditions. Size (S_{avg}) was defined as the total 2D area (measured in pixels) of INFs detected in a single z-plane. There was a general trend of increase in INF size as behavioural exposure also increased in both CD and CA transportation cohorts. At the time this thesis was written, the software program identified INFs in MECS condition in dentate gyrus with faulty border detection and thus the INF sizes were most likely inflated but there was a general trend of increase both by including and excluding the MECS values in statistical analyses. All statistical tests employed alpha level of 0.05 where appropriate.

2a. Cue-Deprived (CD) transport cohort

Refer to Figure II.5. INF size (S_{avg}) detection for MECS groups appeared to return faulty values as the thresholds for INF borders were did not match manual verification. This was potentially a result of image saturation or close proximity of INFs in MECS images. Thus, statistical test values both including and excluding MECS condition INF sizes are reported in order to investigate the significance of size increases between HC, 1E, and 5E in an unbiased manner. Refer to Table II.8 for all statistical data relating to effect of condition on average INF size in CD cohort.

In dorsal subiculum (DS), one-way ANOVA including MECS S_{avg} reported non-significant differences between conditions[106] but paired-sample T-tests showed significant differences in S_{avg} between 1E and 5E[107] and between HC and 5E[108], while the

S_{avg} between HC and 1E was not significantly different[109]. In DS, there was a significant effect of condition on S_{avg} when MECS values were excluded[110].

In CA1, the inclusion of MECS in the one-way ANOVA test did not yield a significant difference in S_{avg}[111] but paired-sample T-tests showed a significant difference between HC and 5E[112]. There were no significant differences between HC and 1E INF S_{avg}[113], or between 1E and 5E[114]. The one-way ANOVA excluding MECS yielded significant effect of condition on size[115].

S_{avg} in CA3 did not change significantly between conditions, except from HC to 5E[116]. One-way ANOVA including MECS values[117] and excluding MECS values[118] both reported no difference between conditions in CA3, and paired-sample T-tests confirmed non-difference between 1E and HC[119] and between 1E and 5E[120].

In DG, both one-way ANOVA tests including MECS[121] and excluding MECS INF sizes[122] showed significant differences in S_{avg} between conditions. Paired-sample t-tests in DG confirmed no differences between 1E and HC[123] nor between 1E and 5E[124]. The only significant difference in S_{avg} occurred between HC and 5E[125].

Across regions in the CD transport cohort, MECS values were not included in paired-sample t-tests between individual regions as these values await intensive manual verification as the software outputted values lower than expected in DS, CA1, and CA3 but overly inflated values in DG.

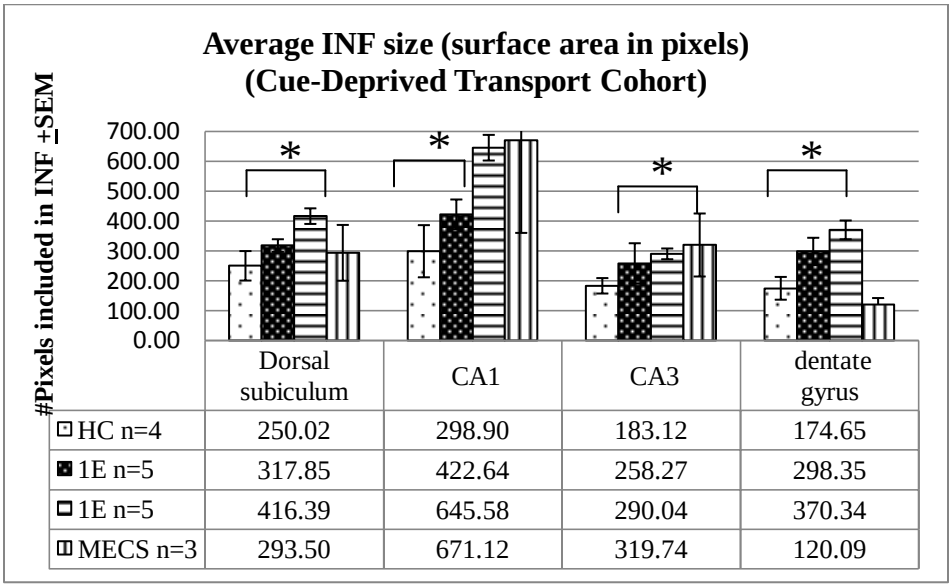

	Dorsal subiculum	CA1	CA3	dentate gyrus
HC n=4	250.02	298.90	183.12	174.65
1E n=5	317.85	422.64	258.27	298.35
1E n=5	416.39	645.58	290.04	370.34
MECS n=3	293.50	671.12	319.74	120.09

Figure II.5 Average size of INFs (S_{avg}) expressed as areas in pixels across behavioural conditions, within sub-regions, in cue-deprived (CD) transport cohort. Overall significant effect of cumulative environmental exposure on S_{avg} across all regions.

Table II.8. Statistical data showing significant effect of cumulative environmental exposure on S_{avg} (average INF size) in CD cohort.

[106] [F(3,13)=2.80, p=0.081]	[107] (t(4)=-4.333, p=0.012)	[108] (t(4)=-6.117, p=0.004)
[109] (t(4)=-2, p=0.116)	[110] [F(2,12)=8.1, p=0.006]	[111][F(3,13)=2.21, p=0.136]
[112] (t(4)=-5.166, p=0.006)	[113](t(4)=-1.497, p=0.209)	[114] (t(4)=-2.5, p=0.067)
[115] [F(2,12)=10.43, p=0.002]	[116] (t(4)=-3.58, p=0.02)	[117] [F(3,13)=0.979, p=0.433]
[118] [F(2,11)=1.37, p=0.294]	[119] (t(4)=-0.899, p=0.419)	[120] (t(4)=-0.556, p=0.608)
[121] [F(3,13)=6.55, p=0.006]	[122] [F(2,11)=5.988, p=0.017]	[123] (t(4)=-1.882, p=0.133)
[124] (t(4)=-1.25, p=0.279)	[125] (t(4)=-7.493, p=0.002)	

2b. Cue-available (CA) Transport Group

Refer to Figure II.6. INF size (S_{avg}) for MECS conditions in CA transport group appeared to return faulty values as the thresholds for INF borders were not accurate potentially due to image saturation or close proximity of INFs in MECS images. Thus, statistical test values both including and excluding MECS condition INF sizes were included in order to investigate the significance of size increases between HC, 1E, and 5E in an unbiased manner. Refer to Table II.9 for statistical data referenced.

In DS, one-way ANOVA testing reported significant differences between conditions including MECS S_{avg}[126] and also excluding MECS S_{avg}[127] while paired-sample T-tests confirmed S_{avg} differed significantly between 1E and HC[128]; 5E and HC[129]; and between 1E and 5E[130]. MECS S_{avg} was higher than 5E[131]; than 1E[132]; and higher than HC[133].

In CA1, there was a significant effect of condition on S_{avg} including MECS values[134] while paired-sample T-tests confirmed significantly higher S_{avg} in 1E versus HC[135]; higher S_{avg} in 5E versus 1E[136]; and higher S_{avg} in 5E versus HC[137]. When MECS values were excluded, one-way ANOVA testing still confirmed the effect of behavioural condition on S_{avg} in CA1[138]. MECS S_{avg} was higher than 5E[139]; than 1E[140]; and higher than HC[141].

In CA3, one-way ANOVA reported significant effect of condition on S_{avg} when MECS sizes were included[142] but t-tests only confirmed significantly higher 5E S_{avg} versus HC[143]. There were no differences in S_{avg} between HC and 1E[144] or between 1E and 5E[145]. With the exclusion of MECS INF sizes, one-way ANOVA also confirmed

significantly different S_{avg} across conditions[146]. MECS S_{avg} was higher than 5E[147]; higher than 1E[148], and higher than HC[149].

In DG, one-way ANOVA showed a significant effect of condition on S_{avg}[150] and paired-sample T-tests confirmed higher INF sizes in 5E versus 1E[151] and also larger sizes in 5E versus HC[152]. There was no difference between INF sizes in HC and 1E[153]. Another one-way ANOVA test that excluded MECS sizes also yielded significance across INF sizes between HC, 1E, and 5E INF sizes[154]. MECS S_{avg} for DG appeared over-inflated as verified by manual verification but still included for analysis. MECS S_{avg} was higher than 5E[155]; higher than 1E[156]; and higher than HC[157].

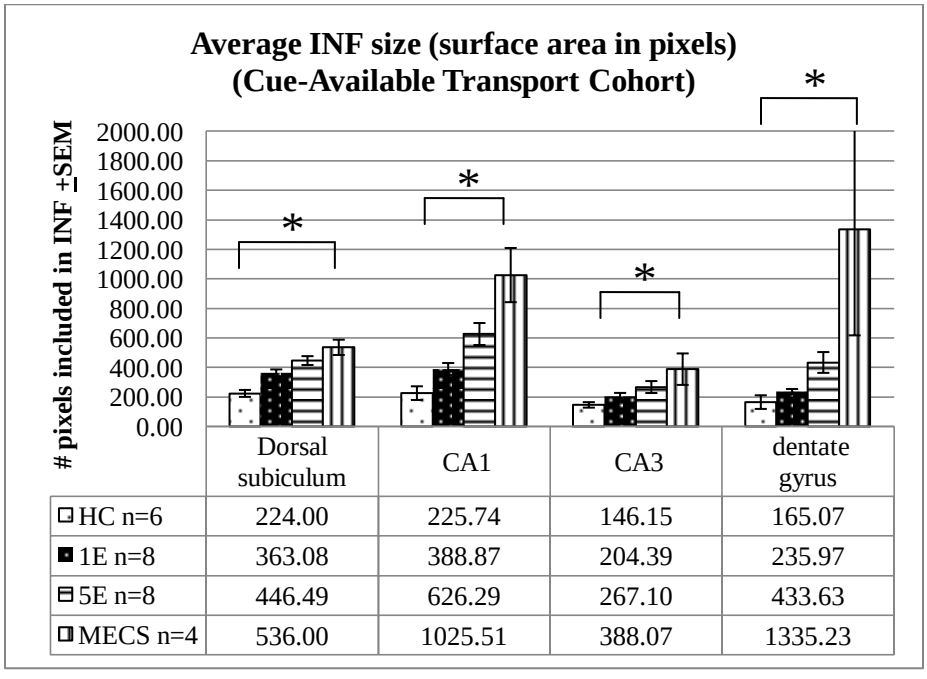

	Dorsal subiculum	CA1	CA3	dentate gyrus
HC n=6	224.00	225.74	146.15	165.07
1E n=8	363.08	388.87	204.39	235.97
5E n=8	446.49	626.29	267.10	433.63
MECS n=4	536.00	1025.51	388.07	1335.23

Figure II.6 Average size of INFs (S_{avg}), expressed as area in pixels, across behavioural conditions within sub-regions, in CA (cue-available) transport cohort. Overall significant effect of cumulative environmental exposure on S_{avg} across all regions.

Table II.9 Statistical data showing significant effect of cumulative environmental exposure on S_{avg} in CA cohort.

[126] [F(3,22)=15.88, p<0.0001]	[127] [F(2,19)=16.62, p<0.0001]	[128] (t(7)=-4.249, p=0.004)
[129] (t(7)=7.021, p=0.0002)	[130] (t(7)=-2.385, p=0.049)	[131] (t(7)=-3.948, p=0.006)
[132] (t(7)=4.366, p=0.003)	[133] (t(7)=18.236, p<0.0001)	[134][F(3,22) = 14.878, p<0.0001]
[135] (t(7)=-3.175, p=0.016)	[136] (t(7)=-4.287, p=0.004)	[137] (t(7)=-4.848, p=0.002)
[138] [F(2,19)=11.61, p=0.0005]	[139] (t(7)=7.393, p=0.0002)	[140] (t(7)=9.726, p<0.0001)
[141] (t(7)=7.96, p<0.0001)	[142] [F(3,22)=25.4, p<0.0001]	[143](t(7)=-2.878, p=0.024)
[144] (t(7)=-2.27, p=0.057)	[145] (t(7)=-1.364, p=0.215)	[146] [F(2,19)=3.668, p=0.045]
[147] (t(7)=6.068, p=0.0004)	[148] (t(7)=-11.25, p<0.0001)	[149] (t(7)=-15.554, p<0.0001)
[150] [F(3,22)=24.07, p<0.0001]	[151] (t(7)=-3.145, p=0.016)	[152] (t(7)=-3.114, p=0.017)
[153] (t(7)=-2.02, p=0.08)	[154] [F(2,19)=7.449, p=0.004]	[155] (t(7)=7.318, p=0.00016)
[156] (t(7)=-7.825, p=0.0001)	[157] (t(7)=-7.908, p=<0.0001)	

2c. No difference in INF sizes between CA and CD counterparts

Paired-sample t-tests were conducted to investigate whether the use of cue-available or cue-deprived transportation affected average INF size (S_{avg}) within the same conditions sub-regions. Refer to Table II.10 for statistical data regarding the effect of cued-transport on S_{avg}. The only significant effect of cue-available transport was observed in region DS in MECS condition across cohorts[158]. In the HC condition, there were no differences between CA and CD cohorts in DS[159], CA1[160], CA3[161] and DG[162], which was to be expected in this control group. In the 1E condition, there were no significant effects of cued-transport on S_{avg} between CA and CD cohorts in DS[163], CA1[164], CA3[165] or DG[166]. Within the 5E condition, there were no significant differences in INF sizes in any region of interest: DS[167]; CA1[168]; CA3[169], or DG[170]. MECS S_{avg} were most likely inflated in DG but then did not show significance between CR and CA cohorts[171]; same non-significance applied for CA1[172] and CA3[173].

Table II.10 Statistical data showing non-significant effect of cued-transport on S_{avg}.

[158] (t(3)=-4.13, p=0.026)	[159] (t(5)=0.909, p=0.405)	[160] (t(5)=0.961, p=0.381)
[161] (t(5)=1.529, p=0.187)	[162] (t(5)=0.184, p=0.861)	[163] (t(7)=-1.621, p=0.149)
[164] (t(7)=1.566, p=0.161)	[165] (t(7)=1.507, p=0.176)	[166] (t(7)=2.02, p=0.083)
[167] (t(7)=-1.395, p=0.206)	[168] (t(7)=0.226, p=0.828)	[169] (t(7)=0.541, p=0.606)
[170] (t(7)=-0.895, p=0.400)	[171] (t(3)=1.117, p=0.346)	[172] (t(3)=-2.784, p=0.069)
[173] (t(3)=-2.874, p=0.064)		

2d. Differences across sub-regions in INF size (S_{avg})

One-way ANOVA and paired-sample t-tests were conducted to analyze whether INF size (S_{avg}) was inherently different depending on the region in which INFs were expressed. That is, these tests investigated whether there were regional effects within matched-conditions on average INF size. All statistical tests employed an alpha level of 0.05 where appropriate.

In the CD transport cohort, the effect of region on S_{avg} within individual conditions was analyzed (HC, 1E, 5E, or MECS). One-way ANOVA only reported significant differences between conditions in 5E[174]. Refer to Table II.11 for statistical data regarding effect of cued-transport on S_{avg}.

In CD-HC condition, one-way ANOVA did not show a significant regional effect on S_{avg} [175] and paired-sample t-tests confirmed no difference of S_{avg} in DS versus CA3[176], between DS and CA1[177]; DS and DG[178]; CA1 and CA3[179] , CA3 and DG[180] and between DG and CA1[181].

In CD-1E, one-way ANOVA did not show significant regional effect on S_{avg} [182] and paired-sample t-tests confirmed no difference between CA1 and CA3[183], DS and CA1[184]; DS and CA3[185]; DS and DG[186], CA1 and DG[187], CA1 and CA3[188].

In CD-5E, one-way ANOVA showed significant differences between regions[189] and paired-sample t-tests confirmed larger S_{avg} in CA1 than DS[190]; larger in CA1 than

CA3[191]; larger in DS than CA3[192]; CA1 larger than DG[193]. There were no significant differences between DS and DG[194]; or between CA3 and DG[195].In CD-MECS, there was no effect of region in S_{avg} values[196].

Table II.11 Statistical data showing mild effect of region on S_{avg} in CD cohort. Lowest values observed in CA3.

[174] [F(3,16)=24.17, p<0.0001]	[175] [F(3,12)=1.133, p=0.375]	[176] (t(3)=2.393, p=0.096)
[177] (t(3)=-1.217, p=0.155)	[178] (t(3)=1.550, p=0.219)	[179] (t(3)=1.843, p=0.162)
[180] (t(3)=0.233, p=0.831)	[181] (t(3)=-1.637, p=0.201)	[182][F(3,15)=2.069, p=0.145]
[183] (t(4)=2.120, p=0.101)	[184] (t(4)=-2.522, p=0.065)	[185] (t(4)=0.724, p=0.509)
[186] (t(4)=0.335, p=0.755)	[187] (t(4)=2.351, p=0.078)	[188] (t(4)=2.12, p=0.101)
[189] [F(3,16)=24.17, p<0.0001]	[190] (t(4)=-6.796, p=0.002)	[191] (t(4)=8.352, p=0.001)
[192] (t(4)=3.415, p=0.0269)	[193] (t(4)=4.863, p=0.008)	[194] (t(4)=1.111, p=0.329)
[195] (t(4)=-2.754, p=0.051)	[196] [F(3,8)=3.341, p=0.077]	

In the CA transport cohort, the effect of region on S_{avg} within individual conditions (HC, 1E, 5E, or MECS) was analyzed. Refer to Table II.12 for statistical data.

In CA-HC, one-way ANOVA did not show a significant effect of region on S_{avg}[197] and paired-sample t-tests confirmed that there were no differences between DS and CA1[198]; CA1 and CA3[199], DS and CA3[200], CA3 and DG[201], DS and DG[202] ; and CA1 and DG[203].

In CA-1E, one-way ANOVA reported regional differences in S_{avg} [204] and paired-sample t-tests confirmed larger S_{avg} in DS than CA3[205]; larger in DS than DG[206]; larger in CA1 than CA3[207]; and larger in CA1 than DG[208]. There were no differences between DS and CA1[209], CA3 and DG[210].

In CA-5E, there was a significant effect of region on S_{avg} [211] and paired-sample t-tests confirmed larger INF in CA1 than DS[212]; larger in DS than CA3[213]; larger in CA1 than CA3[214]; larger in DG than CA3[215]; and larger in CA1 than DG[216]. There were no differences in S_{avg} between DS and DG[217].

In CA-MECS, one-way ANOVA reported regional differences in S_{avg} [218] and paired-sample t-tests failed to confirmed any statistically significance differences between regions: DS and CA1[219]; DS and CA3[220]; DS and DG[221]; CA1 and CA3[222]; CA3 and DG[223]; and CA1 and DG[224].

Table II.12 Statistical data showing mild effect of region on S_{avg} in CA cohort. Lowest values observed in CA3.

[197][F(3,20)=1.283, p=0.3074]	[198] (t(5)=-0.0257, p=0.98)	[199] (t(5)=2.312, p=0.069)
[200] (t(5)=2.261, p=0.073)	[201] (t(5)=-0.386, p=0.715)	[202] (t(5)=1.474, p=0.2)
[203] (t(5)=0.774, p=0.474)	[204][F(3,28)=10.918, p <0.0001]	[205] (t(7)=7.611, p<0.0001)
[206] (t(7)=6.277, p=0.0004)	[207] (t(7)=5.151, p=0.001)	[208] (t(7)=3.537, p=0.0095)
[209] (t(7)=-0.735, p=0.486)	[210] (t(7)=-1.294, p<0.237)	[211][F(3,28)=6.613, p=0.0016]
[212] (t(7)=-2.791, p=0.0268)	[213] (t(7)=4.492, p=0.0028)	[214] (t(7)=7.67, p=0.0001)
[215] (t(7)=-3.315, p=0.013)	[216] (t(7)=3.673, p=0.008)	[217] (t(7)=0.2644, p=0.799)
[218] [F(3,12)=7.668, p =0.004]	[219] (t(3)=-3.026, p=0.056)	[220] (t(3)=-0.986, p=0.397)
[221] (t(3)=-3.011, p=0.057)	[222] (t(3)=1.503, p=0.23)	[223] (t(3)=-3.07, p=0.054)
[224] (t(3)=-2.489, p=0.089)		

2e. Post-hoc test results of grouped data (S_{avg})

Table II.13 Bonferroni post-hoc tests to determine which conditions differed in S_{avg} (average size) values when both cohorts were combined and grouped according to HC, 1E, 5E, or MECS.

Region	Condition	Condition	Critical value	Bonferroni p-value	Significant?
DS	HC n=10	5E n=13	0.008333	2.07E-06	**Yes**
DS	HC n=10	1E n=13	0.01	0.000705	**Yes**
DS	1E n=13	5E n=13	0.0125	0.002845	**Yes**
DS	HC n=10	MECS n=7	0.016667	0.005741	**Yes**
DS	1E n=13	MECS n=7	0.025	0.121491	No
DS	5E n=13	MECS n=7	0.05	0.959703	No
CA1	HC n=10	5E n=13	0.008333	1.08E-05	**Yes**
CA1	1E n=13	5E n=13	0.01	0.000391	**Yes**
CA1	HC n=10	MECS n=7	0.0125	0.000843	**Yes**
CA1	1E n=13	MECS n=7	0.016667	0.001709	**Yes**
CA1	HC n=10	1E n=13	0.025	0.009565	**Yes**
CA1	5E n=13	MECS n=7	0.05	0.097955	No
CA3	HC n=10	MECS n=7	0.008333	0.000333	**Yes**
CA3	1E n=13	MECS n=7	0.01	0.001302	**Yes**
CA3	HC n=10	5E n=13	0.0125	0.001709	**Yes**
CA3	5E n=13	MECS n=7	0.016667	0.004652	**Yes**
CA3	HC n=10	1E n=13	0.025	0.086027	No
CA3	1E n=13	5E n=13	0.05	0.197085	No
DG	HC n=10	5E n=13	0.016667	0.000417	**Yes**
DG	1E n=13	5E n=13	0.025	0.005925	**Yes**
DG	HC n=10	1E n=13	0.05	0.019183	**Yes**

3. Average green intensity of all INF pixels (I_{avg})

In addition to analyzing the average peak intensity values (I_{max}) reflecting the brightest pixel (the "origin") in all identified INFs, the average intensity of all green pixels (I_{avg}) in INFs per ROI sub-image was also calculated. Comparison of I_{avg} across conditions and across regions followed a similar trend as in the I_{max} measurements, although the peak intensity values were lower since all pixels included in all INFs were considered. Following magnified image analysis, it was determined that all INFs followed an approximately circular Gaussian shape such that the brightest pixel at the centre of the INF (the "origin") started declining chains such that adjacent pixels emanating from the centre of the INF declined in intensity value. Since most green pixels

fall below the maximum intensity value outside the origin, lower average green channel intensities were observed but still generally increased with behavioural exposure. The sum of all INF pixel intensities was divided by the sum of all INF pixels to derive the average green intensity I_{avg} per sub-image. Sub-images were averaged across regions, and then across subjects. One-way ANOVA and paired-sample t-tests were conducted to determine whether region or condition affected the average green intensity in all identified INF pixels, and an alpha level of 0.05 was where appropriate.

3a. Cue-Deprived (CD) Transport Cohort

Refer to Figure II.7. There was a general trend of increase in I_{avg} as behavioural conditions increased in exposure. The highest I_{avg} values belonged to INFs in MECS sub-images, and the lowest I_{avg} values were seen in the HC INF averages. Among regions, the greatest increases were observed in DG. Refer to Table II.14 for statistical data referenced regarding effect of behaviour on I_{avg}.

In dorsal subiculum (DS), one-way ANOVA reported a significant effect of condition on I_{avg} [225] and paired-sample t-tests confirmed higher I_{avg} in 1E versus HC[226]; higher 5E than 1E[227]; and higher 5E than HC[228]. MECS I_{avg} was significantly higher than 5E[229]; higher than 1E[230]; and higher than HC[231].

In CA1, there was a significant effect of condition on I_{avg} [232] and paired-sample t-tests confirmed higher I_{avg} in 1E compared to HC[233]; higher in 5E than 1E[234]; and higher in 5E than HC[235]. MECS was significantly higher than 5E[236]; higher than 1E[237]; and higher than HC[238].

In CA3, one-way ANOVA showed significant differences in I_{avg} across conditions[239] and paired-sample T-tests confirmed I_{avg} in 1E versus HC[240]; higher in 5E versus HC[241]; and higher 5E versus 1E[242]. MECS I_{avg} was significantly higher than 5E[243]; higher than 1E[244]; and higher than HC[245].

In DG, there was a significant effect of condition in I_{avg} [246] while paired-sample t-tests also confirmed higher I_{avg} in 1E versus HC[247]; higher in 5E versus 1E[248]; and higher in 5E versus HC[249]. MECS I_{avg} was significantly higher than 5E[250]; higher than 1E[251]; and higher than HC[252].

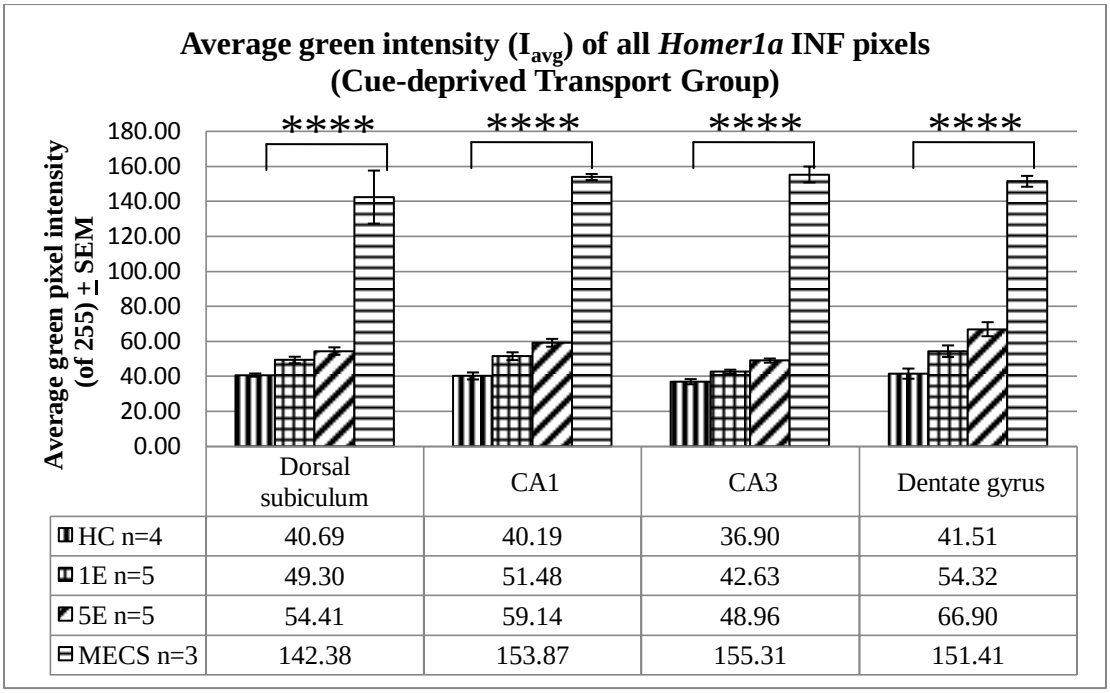

	Dorsal subiculum	CA1	CA3	Dentate gyrus
HC n=4	40.69	40.19	36.90	41.51
1E n=5	49.30	51.48	42.63	54.32
5E n=5	54.41	59.14	48.96	66.90
MECS n=3	142.38	153.87	155.31	151.41

Figure II.7 Average green intensity (I_{avg}) of all pixels included in all INFs in sub-images of ROIs in CD (Cue-Deprived Transport cohort). Significant increases in I_{avg} in cumulative environmental exposure in all regions.

Table II.14 Statistical data showing significant effect of condition on I_{avg} in CD cohort.

[225] [F(3,13)=61.8, p<0.0001]	[226] (t(4)=-5.547, p=0.005)	[227] (t(4)=-4.697, p=0.009)
[228] (t(4)=-7.542, p=0.0017)	[229] (t(4)=-10.123; p=0.001)	[230] (t(4)=-11.48, p=0.0003)
[231] (t(4)=-11.71, p=0.0003)	[232][F(3,13)=261.47, p<0.0001]	[233] (t(4)=-5.67, p=0.005)
[234] (t(4)=-4.739, p=0.009)	[235] (t(4)=-6.454, p=0.003)	[236] (t(4) =30.62, p<0.0001)
[237] (t(4)=43.01, p<0.0001)	[238] (t(4)=109.40, p<0.0001)	[239][F(3,13)=661.93, p <0.0001]
[240] (t(4)=-4.197, p=0.014)	[241] (t(4)=-9.139, p=0.0008)	[242] (t(4)=-8.303, p=0.001)
[243] (t(4)=34.82, p<0.0001)	[244] (t(4)=36.62, p<0.0001)	[245] (t(4)=56.20, p<0.0001)
[246][F(3,13)=150.21, p<0.0001]	[247] (t(4)=-3.381, p=0.028)	[248] (t(4)=-5.063, p=0.007)
[249] (t(4)=-5.889, p=0.004)	[250] (t(4)=18.215, p<0.0001)	[251] (t(4)=24.395, p<0.0001)
[252] (t(4)=121.26, p<0.0001)		

3b. Cue-available (CA) Transport Cohort

Refer to Figure II.8. There was a general trend of increase in I_{avg} as behavioural conditions increased in exposure. The highest I_{avg} values belonged to INFs in MECS sub-images, where the lowest intensities were seen in the HC INF averages. Refer to Table II.15 for statistical data referenced regarding the effect of condition on $I_{avg.}$

In dorsal subiculum (DS), one-way ANOVA showed a significant effect of condition on I_{avg}[253] and paired-sample t-tests showed significantly higher I_{avg} in 1E versus HC[254]; higher in 5E than 1E[255]; and higher in 5E than HC[256]. MECS I_{avg} was significantly higher than in 5E[257]; higher than in 1E[258] and also higher than in HC[259].

In CA1, one-way ANOVA reported a significant effect of condition on I_{avg}[260] and paired-sample t-tests confirmed higher I_{avg} in 1E compared to HC[261]; higher in 5E versus 1E[262]; and higher in 5E than HC[263]. MECS I_{avg} was significantly higher than 5E[264]; higher than 1E [265], and higher than HC[266].

In CA3, there was a significant effect of condition on I_{avg} [267] while paired-sample t-tests confirmed higher I_{avg} in 1E versus HC[268] and higher in 5E versus HC[269]. There was no significant difference between I_{avg} in 1E and 5E[270]. MECS I_{avg} was significantly higher than 5E[271]; higher than 1E[272]; and higher than HC[273].

In DG, there was a significant effect of condition on I_{avg} [274] while paired-sample t-tests confirmed higher I_{avg} in 1E versus HC[275]; higher in 5E versus[276], and higher in 5E compared to HC[277]. MECS values were significantly higher than 5E[278]; higher than 1E[279]; and higher than HC[280].

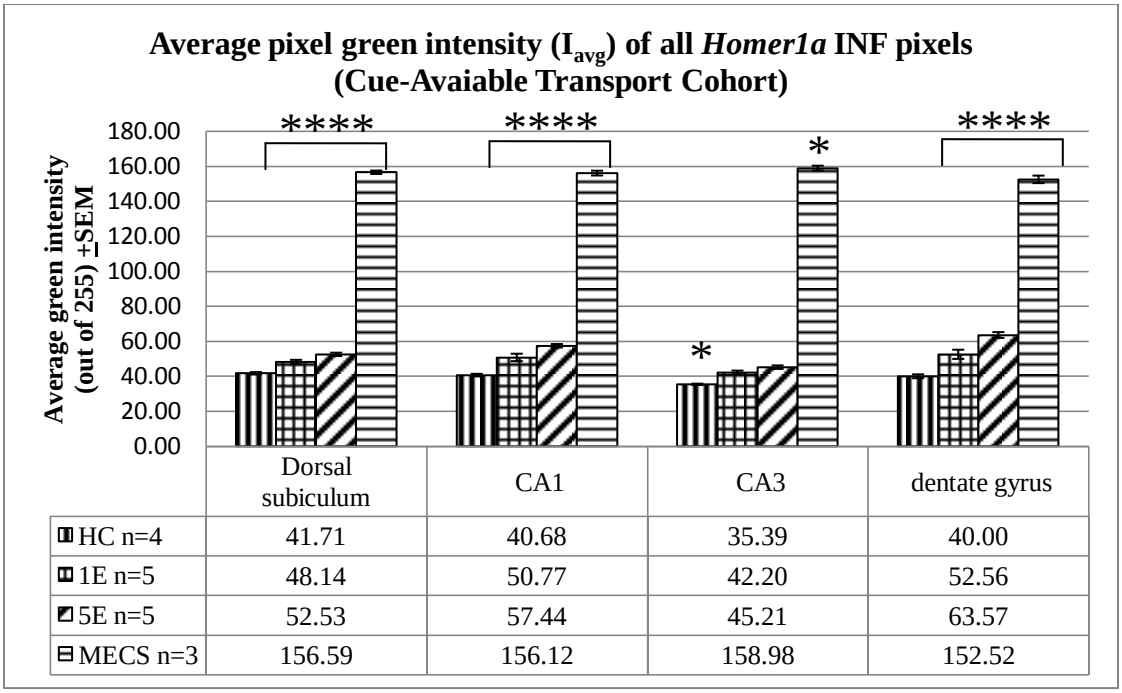

	Dorsal subiculum	CA1	CA3	dentate gyrus
HC n=4	41.71	40.68	35.39	40.00
1E n=5	48.14	50.77	42.20	52.56
5E n=5	52.53	57.44	45.21	63.57
MECS n=3	156.59	156.12	158.98	152.52

Figure II.8 Average green channel intensity (I_{avg}) of all pixels included in all INFs in sub-images of ROIs in CA (cue-available transport cohort). Significant effect of cumulative environmental exposure on I_{avg}, in all regions except for CA3.

Table II.15 Statistical data showing significant effect of condition on I_{avg} in CA cohort, except in CA3.

[253][F(3,22)=1777.49, p<0.0001]	[254] (t(7)=-5.3, p=0.001)	[255] (t(7)=-2.851, p=0.025)
[256] (t(7)=-8.479, p<0.0001)	[257] (t(7)=136.44, p<0.0001)	[258] (t(7)=78.71, p<0.0001)
[259] (t(7)=125.93, p<0.0001)	[260][F(3,22)=813.94, p<0.0001]	[261] (t(7)=-4.806, p=0.002)
[262] (t(7)=-3.1, p=0.017)	[263] (t(7)=-18.85, p<0.0001)	[264] (t(7)=129.67, p<0.0001)
[265] (t(7)=43.48, p<0.0001)	[266] (t(7)=153.84, p<0.0001)	[267][F(3,22)=2354.22, p<0.00001]
[268] (t(7)=-6.075, p=0.0005)	[269] (t(7)=-10.66, p<0.0001)	[270] (t(7)=-2.244, p=0.06)
[271] (t(7)=141.19, p<0.0001)	[272] (t(7)=89.30, p<0.0001)	[273] (t(7)=224.01, p<0.0001)
[274][F(3,22)=409.53, p<0.0001]	[275] (t(7)=-4.11, p=0.004)	[276] (t(7)=-4.06, p=0.005)
[277] (t(7)=-14.26, p<0.0001)	[278] (t(7)=87.79, p<0.0001)	[279] (t(7)=33.77, p<0.0001)
[280] (t(7)=114.13, p<0.0001)		

3c. Raw differences in average green intensity between conditions across sub-regions

The raw differences in I_{avg} were calculated to analyze whether there were a) robust increases across conditions within sub-regions and b) whether there was a significant effect of cue-information availability during transport on I_{avg}. i.e. whether there were significant differences between average intensities between specific counterparts in CD and CA cohorts.

Refer to Table II.16. The highest increase in I_{avg} was observed between 5E and HC conditions across all regions. The lowest increase was observed in CA3 in the CA cohort between 5E and 1E conditions.

For statistical data, refer to Table II.17. The effect of cue-deprived transportation versus cue-available transportation on I_{avg} was then analyzed. The only group in which there was a significant effect was in CA3 in 5E condition[281]. All other regions and conditions showed non-significant effect of cue-information availability during transport to the various environments on I_{avg}. In the HC condition, as expected, DS-CD and DS-CA

showed no difference in I_{avg} [282]; same for CA1-CD and CA1-CA[283]; CA3-CD and CA3-CA[284]; and DG-CD versus DG-CA[285]. In 1E, CD/CA did not show a significant effect on DS[286], CA1[287], CA3[288] and DG[289]. In 5E, there were no differences between DS-CD and DS-CA in I_{avg}[290], CA1-CD and CA1-CA[291]; DG-CD and DG-CA[292]. In MECS, as expected, there were no significant effects of cue-information available transport on I_{avg}: DS[293], CA1[294], CA3[295], and DG[296].

Table II.16 Difference in average green pixel intensity (I_{avg}) of all pixels included in detected INFs in CD and CA cohorts.

Difference in I_{avg}	**Dorsal subiculum**		**CA1**		**CA3**		**Dentate gyrus**	
	CD	CA	CD	CA	CD	CA	CD	CA
$1E_{Iavg}$-HC_{Iavg}	8.61	6.43	11.84	10.09	5.73	6.81	12.81	12.56
$5E_{Iavg}$-$1E_{Iavg}$	5.11	4.39	7.66	6.67	6.32	3.02	12.58	11.01
$5E_{Iavg}$-HC_{Iavg}	13.72	10.81	19.50	16.76	12.06	9.82	25.39	23.57
$MECS_{Iavg}$-$5E_{Iavg}$	87.97	104.06	94.73	98.68	106.35	113.77	84.51	88.95
$MECS_{Iavg}$-$1E_{Iavg}$	93.08	108.45	102.39	105.35	112.68	116.78	97.09	99.96
$MECS_{Iavg}$-HC_{Iavg}	101.69	114.88	113.68	115.44	118.41	123.59	109.9	112.52

Table II.17 Statistical data showing non-significant effect of cued-transport on I_{avg}.

[281] (t(7)=4.811, p=0.002)	[282](t(5)=-0.951, p=0.385)	[283] (t(5)=-0.303, p=0.774)
[284] (t(5)=1.506, p=0.192)	[285] (t(7)=0.776, p=0.473)	[286] (t(7)=0.661, p=0.530)
[287] (t(7)=0.249, p=0.810)	[288] (t(7)=0.341, p=0.743)	[289] (t(7)=0.488, p=0.64)
[290](t(7)=1.895, p=0.10)	[291] (t(7)=0.803, p=0.448)	[292] (t(7)=1.535, p=0.169)
[293] (t(3)=-1.424, p=0.250)	[294] (t(3)=-0.746, p=0.510)	[295] (t(3)=-0.816, p=0.474)
[296] (t(3)=-0.3, p=0.784)		

3d. Analysis of average INF intensity (I_{avg}) by sub-region

Regional effects on I_{avg} were analyzed with statistical tests of one-way ANOVA across regions and paired-sample t-tests between regions. All statistical tests employed the alpha level of 0.05 where appropriate.

Refer to Figure II.9 and Table II.18. Within the CD (cue-deprived transport) cohort, there was no significant difference in I_{avg} in HC condition between regions[297].

However, paired-sample t-tests in the CD-HC group reported significantly higher I_{avg} in DS versus CA3[298] and CA1 versus CA3[299].

In CD-1E condition, there were significant differences in I_{avg} between sub-regions[300]; CA1 values were higher than DS[301]; DS was higher than CA3[302]; while CA1 was higher than CA3[303], and DG was higher than CA3[304]. Thus in CD-1E, lowest I_{avg} values were observed in CA3.

Within the CD-5E condition, there was a significant effect of region on I_{avg} [305] while paired-sample t-tests confirmed higher values in CA1 versus DS[306]; DS higher than CA3[307]; DG higher than DS[308], DG higher than CA1[309]; CA1 higher than CA3[310], and DG was significantly higher than CA3[311]. In CD-5E condition, CA3 contained lowest I_{avg}.

In the CD-MECS condition, there was no significant effect of region in I_{avg} [312].

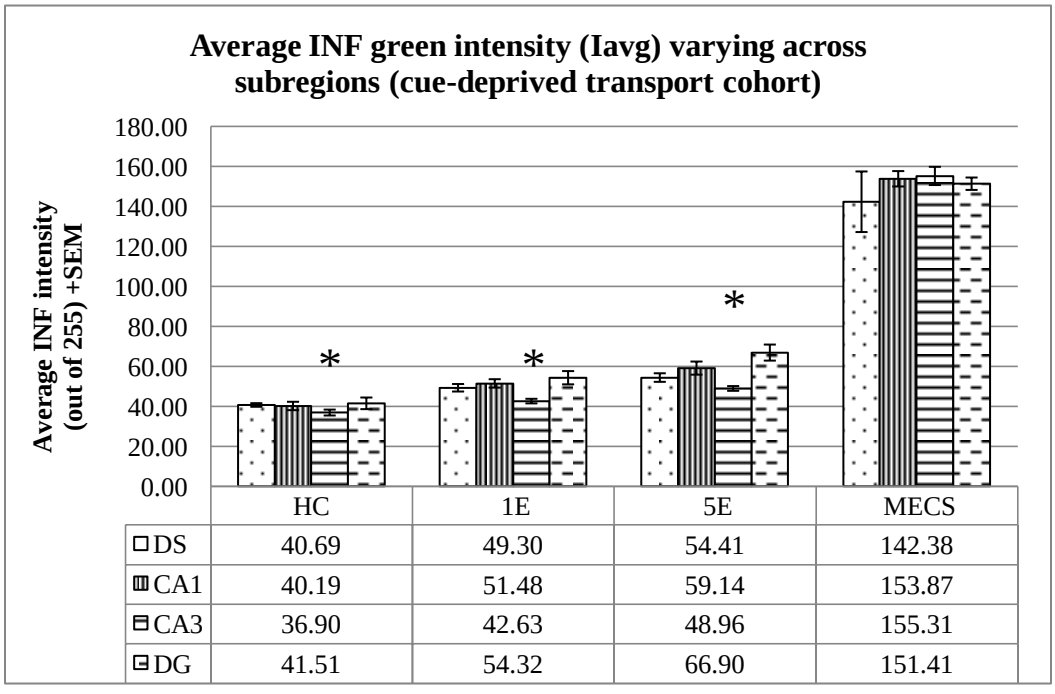

	HC	1E	5E	MECS
DS	40.69	49.30	54.41	142.38
CA1	40.19	51.48	59.14	153.87
CA3	36.90	42.63	48.96	155.31
DG	41.51	54.32	66.90	151.41

Figure II.9 Average INF green intensities (I_{avg}) (out of possible 255) across sub-regions in CD (cue-deprived) transport cohort. Lowest values observed in CA3.

Table II.18 Statistical data showing minor effect of region on I_{avg} in CD cohort. Lowest values observed in CA3.

[297] [F(3,12)=1.033, p=0.412]	[298] (t(3)=3.887, p=0.030)	[299] (t(3)=5.22, p=0.014)
[300] [F(3,16)=4.882, p=0.013]	[301] (t(4)=-2.9, p=0.044)	[302] (t(4)=3.921, p=0.017)
[303] (t(4)=4.99, p=0.008)	[304] (t(4)=-4.91, p=0.008)	[305][F(3,16)=7.03, p=0.003]
[306] (t(4)=0.021, p=0.02)	[307] (t(4)=5.53, p=0.005)	[308] (t(4)=-5.03, p=0.007)
[309] (t(4)=-3.58, p=0.02)	[310] (t(4)=4.815, p=0.009)	[311] (t(4)=-5.87, p=0.004)
[312] [F(3,8)=0.490, p=0.699]		

Refer to Figure II.10 and Table II.19. Within the CA (cue-available transport) cohort, one-way ANOVA reported significant differences between regions in I_{avg} [313] in HC-CA condition. Paired-sample t-tests confirmed that DS was higher than CA3 in I_{avg} [314], CA1 was higher than CA3[315], and DG was higher than CA3[316]. In the HC condition, CA3 contained the lowest I_{avg}.

In the CA-1E condition, one-way ANOVA reported significant differences between regions in I_{avg} [317] and paired-sample t-tests confirmed that DS was higher than CA3[318], CA1 was higher than CA3[319], and DG was higher than CA3[320]. Thus, CA3 contained the lowest I_{avg}.

In CA-5E condition, one-way ANOVA showed a significant effect of region on I_{avg} [321]. Paired-sample t-tests confirmed significantly higher I_{avg} in CA1 than DS[322]; higher in DS than CA3[323], higher in DG than DS[324], higher in DG than CA1[325], higher in DG than CA3[326] and higher in CA1 than CA3[327]. In the CR-5E group, the lowest I_{avg} values were observed in CA3.

In the CA-MECS group, one-way ANOVA reported no significant effect of region on I_{avg} [328] but paired-sample t-tests reported significantly higher I_{avg} in CA3 than CA1[329], higher in DS than DG[330], higher in CA3 than DG[331] and higher in CA1 than DG [332] which were reverse trends compared to other conditions.

Table II.19 Statistical data showing minor effect of region on I_{avg} in CA cohort. Lowest values observed in CA3.

[313][F(3,20)=12.93, p<0.0001]	[314](t(5)=7.04, p=0.0009)	[315] (t(5)=6.53, p=0.0013)
[316] (t(5)=-5.86, p=0.002)	[317][F(3,28)=5.78, p=0.003]	[318] (t(5)=5.769, p=0.0007)
[319] (t(7)=5.96, p=0.0006)	[320] (t(7)=-5.23, p=0.001)	[321] [F(3,28)=42.78, p<0.0001]
[322] (t(7)=-4.66, p=0.002)	[323] (t(7)=7.626, p=0.0001)	[324] (t(7)=-7.02, p=0.0002)
[325] (t(7)=-6.52, p=0.0003)	[326] (t(7)=-12.35, p<0.0001)	[327] (t(7)=15.64, p<0.0001)
[328][F(3,12)=3.022, p=0.072]	[329] (t(3)=-5, p=0.015)	[330] (t(3)=2.76, p=0.07)
[331] (t(3)=6.36, p=0.008)	[332](t(3)=4.46, p=0.02)	

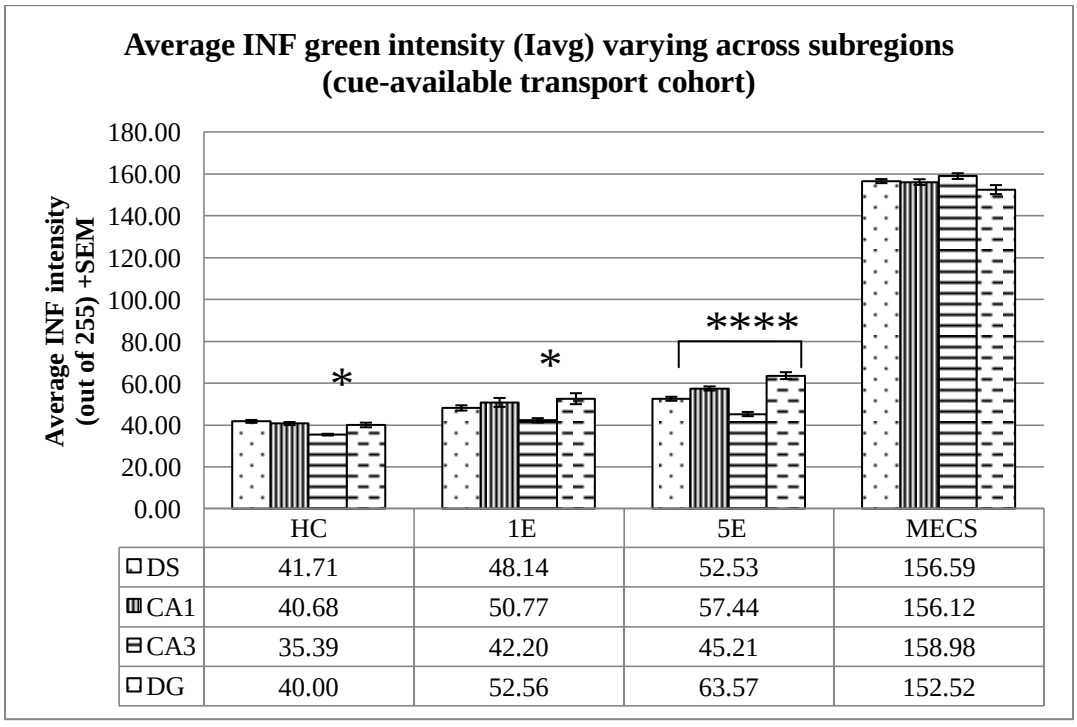

Figure II.10 Average INF green intensities (I_{avg}) across sub-regions in CAA (cue-available) transport cohort. Lowest values observed in CA3.

3e. Post-hoc test results of pooled cohort data (I_{avg})

Table II.20 Bonferroni post-hoc tests to determine which conditions differed in I_{avg} (average INF-pixel intensity) values when both cohorts were combined and grouped according to HC, 1E, 5E, or MECS.

Region	Condition	Condition	Critical Value	Bonferroni p-value	Significant?
DS	1E n=13	MECS n=7	0.008333	3.63E-14	**Yes**
DS	5E n=13	MECS n=7	0.01	7.84E-14	**Yes**
DS	HC n=10	MECS n=7	0.0125	2.3E-12	**Yes**
DS	HC n=10	5E n=13	0.016667	3.47E-09	**Yes**
DS	HC n=10	1E n=13	0.025	1.04E-05	**Yes**
DS	1E n=13	5E n=13	0.05	0.003259	**Yes**
DS	1E n=13	MECS n=7	0.008333	3.63E-14	**Yes**
CA1	HC n=10	MECS n=7	0.008333	7.58E-20	**Yes**
CA1	5E n=13	MECS n=7	0.01	9.06E-20	**Yes**
CA1	1E n=13	MECS n=7	0.0125	1.04E-19	**Yes**
CA1	HC n=10	5E n=13	0.016667	1.2E-09	**Yes**
CA1	HC n=10	1E n=13	0.025	1.34E-05	**Yes**
CA1	1E n=13	5E n=13	0.05	0.001754	**Yes**
CA3	1E n=13	MECS n=7	0.008333	9.26E-23	**Yes**
CA3	5E n=13	MECS n=7	0.01	6.29E-22	**Yes**
CA3	HC n=10	MECS n=7	0.0125	6.25E-20	**Yes**
CA3	HC n=10	5E n=13	0.016667	1.06E-08	**Yes**
CA3	HC n=10	1E n=13	0.025	3.9E-06	**Yes**
CA3	1E n=13	5E n=13	0.05	0.001314	**Yes**
DG	HC n=10	MECS n=7	0.008333	1.21E-18	**Yes**
DG	1E n=13	MECS n=7	0.01	1.45E-17	**Yes**
DG	5E n=13	MECS n=7	0.0125	3.3E-17	**Yes**
DG	HC n=10	5E n=13	0.016667	1.08E-09	**Yes**
DG	HC n=10	1E n=13	0.025	6.1E-05	**Yes**
DG	1E n=13	5E n=13	0.05	0.000232	**Yes**

4. Average blue intensity (I_b) of pixels in *Homer1a* INFs

Due to the overlapping emission spectra of DAPI (blue, 461nm peak) and FITC (green, 519nm peak) wavelengths, there are presumably overlapping portions of INF signal in the blue and green intensity channels, although most of the signal would belong to the green intensity spectrum. Also, the DAPI counter-stain may contribute to the overall green INF signal. Thus, the effect of increased behavioural condition on average blue intensity (I_b) was also analyzed. The automated INF quantification program calculated the sum of all blue intensity values in all pixels included in detected INF within each ROI sub-image. The sums were then divided by total pixels included in all counted INFs per image and averaged over sub-regions and then across subjects per behavioural condition. One-way ANOVA tests and paired-sample t-tests were carried out to determine whether behavioural manipulations or cue-availability during transport affected blue intensity averages in the same linear manner as observed in the green intensity channel (I_{max} and I_{avg}). For all statistical tests, an alpha level of 0.05 was employed where appropriate.

In both CD and CA cohorts, there was minimal change across conditions, and there was a fairly flat gradient from HC to 1E to 5E. High average blue intensity (I_b) values were observed in all MECS groups across regions and cohorts, probably as a result of green overlap from the fluorescent marker for *Homer1a* foci. The highest increases in I_b were observed between conditions in DG. The lowest increases were observed in CA3 and were higher in 5E than 1E, and higher than HC in 1E in the CD cohort. In DS-CA group, HC was higher than 1E, 1E was higher than 5E, and HC was higher than 5E. In

CA3-CA group, HC was higher in blue intensity than 5E, and 1E was higher than 5E in blue intensity.

4a. Average blue intensity (I_b) in cue-deprived (CD) transport cohort

Refer to Figure II.11. There were non-significant effects of condition on I_b in INF pixels except for dentate gyrus. In all regions, MECS groups showed the highest blue average intensity. Refer to Table II.21 for statistical data referenced.

In DS, there was a non-significant effect of condition on I_b [333] while paired-sample t-tests confirmed no difference in I_b between 1E versus HC[334]; 1E and 5E[335]; HC and 5E[336], and even MECS and 5E did not differ significantly[337]. MECS and 1E were also the same[338], as were MECS and HC[339].

In CA1, there was a significant effect of condition on I_b [340] while paired-sample t-tests reported non-significant differences of I_b between HC and 1E[341]; between 1E and 5E[342]; and also between HC and 5E[343]. There was a significant difference between MECS and 5E[344] I_b values, 1E[345] and HC[346].

In CA3, there was a significant effect of condition on I_b[347] and paired-sample t-tests confirmed higher I_b in MECS than 5E[348], 1E[349] and HC[350]. There were no significant differences between HC and 1E[351]; 1E and 5E[352]; HC and 5E[353].

In DG, there was a significant effect of condition on I_b [354] and paired-sample t-tests confirmed that MECS was higher than 5E[355]; higher than 1E[356]; and higher than HC[357]. There were no significant differences between HC and 1E[358] or 1E and 5E[359]. I_b values were significantly higher in 5E than HC[360].

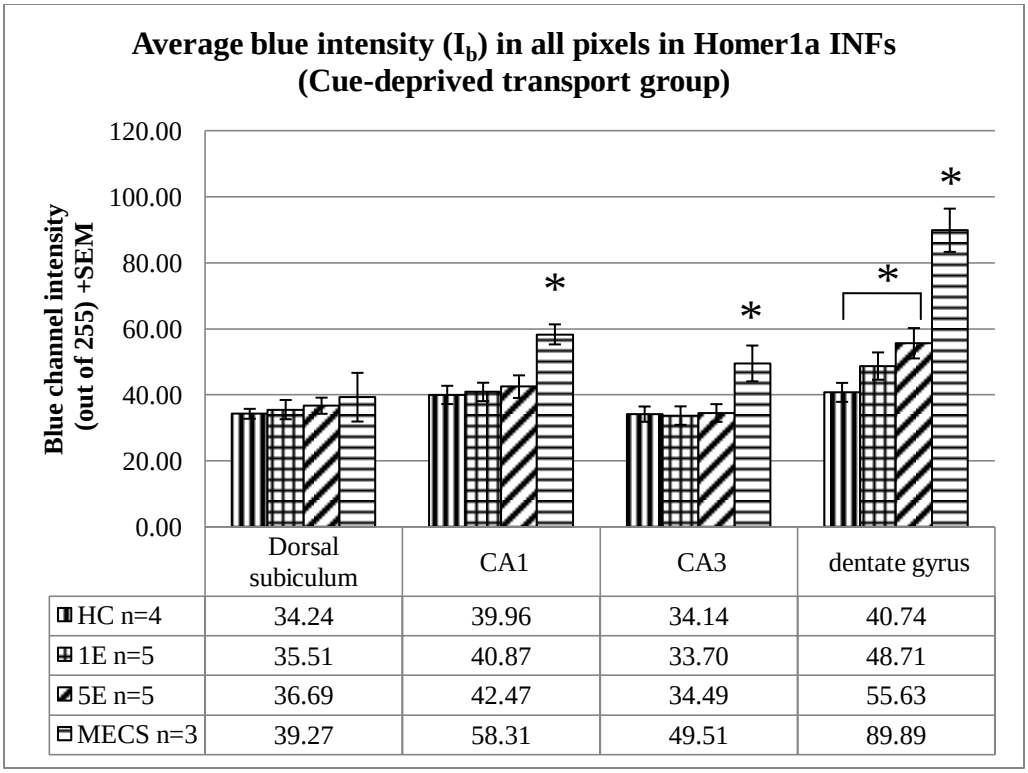

	Dorsal subiculum	CA1	CA3	dentate gyrus
HC n=4	34.24	39.96	34.14	40.74
1E n=5	35.51	40.87	33.70	48.71
5E n=5	36.69	42.47	34.49	55.63
MECS n=3	39.27	58.31	49.51	89.89

Figure II.11 Average blue intensity (I_b) in all pixels of *Homer1a* INFs in CD (cue-deprived transport cohort). Highest values in MECS conditions, but no significant effect of condition on I_b.

Table II.21 Statistical data showing non -significant effect of condition on I_b in CD cohort.

[333][F(3,13)=0.318, p=0.812]	[334] (t(4)=-0.426, p=0.6992)	[335] (t(4)=-0.795, p=0.471)
[336] (t(4)=-1.01, p=0.371)	[337] (t(4)=-0.517, p=0.633)	[338] (t(4)=0.772, p=0.483)
[339] (t(4)=0.972, p=0.386)	[340][F(3,13)=5.96, p=0.009]	[341] (t(4)=-0.28, p=0.793)
[342] (t(4)=-0.94, p=0.399)	[343] (t(4)=-0.678, p=0.535)	[344] (t(4)=-4.267, p=0.01)
[345] (t(4)=-6.10, p=0.004)	[346] (t(4)=-4.99, p=0.008)	[347][F(3,13)=4.693, p=0.02]
[348] (t(4)=-3.69, p= 0.02)	[349] (t(4)=4.11, p=0.014)	[350] (t(4)=3.243, p=0.03)
[351] (t(4)=0.139, p=0.896)	[352] (t(4)=-0.457, p=0.671)	[353] (t(4)=-0.12, p=0.91)
[354][F(3,13)=17.912, p<0.0001]	[355] (t(4)=-6.32, p=0.003)	[356] (t(4)=8.21, p=0.001)
[357] (t(4)=8.67, p=0.001)	[358] (t(4)=-1.87, p=0.135)	[359] (t(4)=-2.237, p=0.09)
[360] (t(4)=-3.32, p=0.029)		

4b. Average blue intensity (I_b) in cue-available (CA) transport cohort

Refer to Figure II.12. There were no significant increases in average blue intensity (I_b) as a result of increased environmental exposure. Refer to Table II.22 for statistical data referenced. In DS, one-way ANOVA reported significant effect of condition on I_b[361] and paired-sample t-tests confirmed that MECs was significantly higher than HC[362]; higher than 1E[363]; and higher than 5E[364]. There were no differences of I_b between HC and 1E[365]; 1E and 5E[366], and between 5E and HC[367].

In CA1, there was a significant effect of condition on I_b [368] and MECS was significantly higher than 5E[369]; higher than 1E[370] and higher than HC[371]. There were no differences in I_b between HC and 1E[372], 1E and 5E[373], and between HC and 5E[374].

In CA3, there were no significant effect of condition on I_b[375] and paired-sample t-tests confirmed MECS values were significantly higher than 5E[376]; and higher than HC[377]. There were no significant differences of 1_b between MECS and 1E[378], HC and 1E[379], 1E and 5E[380], and HC and 5E[381].

In DG, there was a significant effect of condition on I_b [382]. Paired-sample t-tests showed significantly higher I_b in 1E than in HC[383], higher in 5E than 1E[384], and higher in 5E than HC[385]. MECS I_b values were higher than 5E[386], higher than 1E[387]; and higher than HC[388].

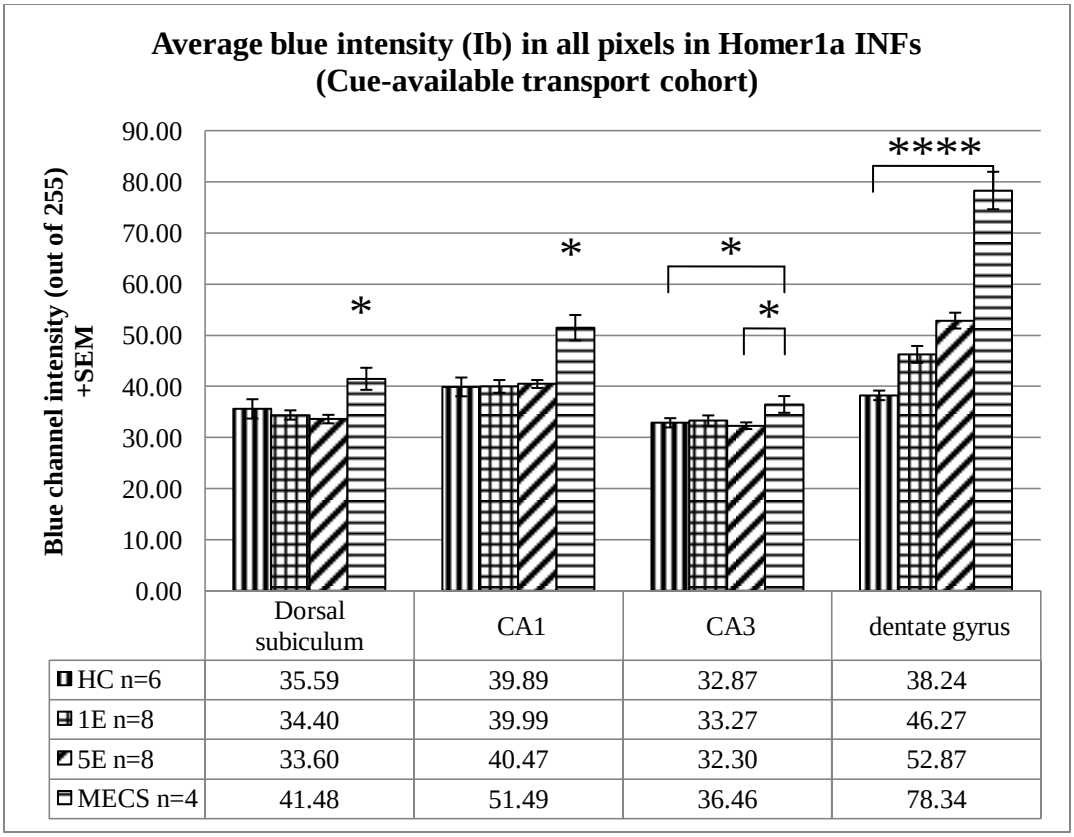

	Dorsal subiculum	CA1	CA3	dentate gyrus
HC n=6	35.59	39.89	32.87	38.24
1E n=8	34.40	39.99	33.27	46.27
5E n=8	33.60	40.47	32.30	52.87
MECS n=4	41.48	51.49	36.46	78.34

Figure II.12 Average blue intensity (I_b) in all pixels of quantified *Homer1a* INFs in CA (cue-available transport cohort). MECS conditions showed highest I_b but no overall significant effect of condition on I_b.

Table II.22 Statistical data showing non-significant effect of condition on I_b in CA cohort.

[361][F(3,22)=5.358, p=0.006]	[362] (t(7)=-2.99, p=0.02)	[363] (t(7)=-4.678, p=0.002)
[364] (t(7)=-17.46, p<0.0001)	[365] (t(7)=0.628, p=0.55)	[366] (t(7)=0.573, p=0.584)
[367] (t(7)=1.07, p=0.32)	[368][F(3,22)=10.769, p=0.0001]	[369] (t(7)=-12.11, p<0.0001)
[370] (t(7)=-6.18, p=0.0005)	[371] (t(7)=-12.21, p<0.0001)	[372] (t(7)=-0.05, p=0.964)
[373] (t(7)=-0.285, p=0.784)	[374] (t(7)=-0.47, p=0.65)	[375][F(3,22)=2.529, p=0.0836]
[376] (t(7)=-4.77, p=0.002)	[377] (t(7)=-5.857, p=0.0006)	[378] (t(7)=1.94, p=0.09)
[379] (t(7)=-0.295, p=0.78)	[380] (t(7)=0.605, p=0.564)	[381] (t(7)=0.582, p=0.579)
[382][F(3,22)=64.452, p<0.0001]	[383] (t(7)=-3.77, p=0.007)	[384] (t(7)=-3.21, p=0.015)
[385] (t(7)=-9.35, p<0.0001)	[386] (t(7)=-24.8, p<0.0001)	[387] (t(7)=-18.55, p<0.0001)
[388] (t(7)=-20.75, p<0.0001)		

4c. Raw differences in I_b between conditions

The raw differences in average blue intensity (I_b) were calculated to analyze whether there were a) robust increases across conditions within sub-regions and b) whether there was a significant effect of cue-information availability during transport i.e. whether there were significant differences between average intensities between specific counterparts in CD and CA cohorts.

Refer to Table II.23. The highest increase in I_b was observed between conditions in DG. The lowest increases were observed in CA3-CD (higher in 5E than 1E, and higher than HC in 1E in the CD cohort). In DS-CA group, HC was higher than 1E, 1E was higher than 5E, and HC was higher than 5E. There were no increases of I_b across increasing behavioural exposures, such that greater behavioural conditions sometimes yielded lower blue intensity averages.

Cue-deprived or cue-available transport was analyzed for significant effects on I_b within matched sub-region and conditions. Refer to Table II.24 for statistical data referenced. The only significant differences in I_b between cohorts was observed in MECS condition in CA3[389]; and also in DG[390].

In HC condition, cued-transport did not affect blue intensity values significantly in DS[391], CA1[392], CA3[393], or DG[394]. In 1E condition, cued-transport did not affect blue intensity values significantly in DS[395], CA1[396], CA3[397], or DG[398]. In 5E condition, cued-transport did not affect blue intensity values significantly in DS[399], CA1[400], CA3[401], or DG[402]. In MECS condition, there was no significant effect of cued-transport on DS[403] or in CA1[404].

Table II.23 Difference in average blue pixel intensity (I_b) of all pixels included in detected INFs in CD and CA cohorts. Increased behavioural condition did not yield robust increases in I_b.

Difference in average blue intensity (I_b)	**Dorsal subiculum**		**CA1**		**CA3**		**Dentate gyrus**	
	CD	CA	CD	CA	CD	cA	CD	CA
$1E_{Ib}$ -HC_{Ib}	1.27	-1.19	0.91	0.09	-0.44	0.40	7.97	8.03
$5E_{Ib}$-$1E_{Ib}$	1.18	-0.80	1.60	0.49	0.79	-0.97	6.92	6.61
$5E_{Ib}$-HC_{Ib}	2.45	-2.00	2.51	0.58	0.35	-0.57	14.89	14.63
$MECS_{Ib}$-$5E_{Ib}$	2.59	7.88	15.84	11.02	15.02	4.16	34.26	25.47
$MECS_{Ib}$-HC_{Ib}	5.03	5.89	18.35	11.6	15.37	3.59	49.15	40.1
$MECS_{Ib}$-$1E_{Ib}$	3.76	7.08	17.44	11.5	15.81	3.19	41.18	32.07

Table II.24 Statistical data showing no significant effect of cued-transport on I_b.

[389] (t(3)=4.38, p=0.02)	[390] (t(3)=3.89, p=0.03)	[391] (t(5)=-0.57, p=0.59)
[392] (t(5)=0.02, p=0.98)	[393] (t(5)=0.603, p=0.573)	[394] (t(5)=1.32, p=0.244)
[395] (t(7)=0.61, p=0.564)	[396] (t(7)=0.40, p=0.702)	[397] (t(7)=0.255, p=0.806)
[398] (t(7)=0.78, p=0.463)	[399] (t(7)=2.14, p=0.07)	[400] (t(7)=0.861, p=0.418)
[401] (t(7)=1.32, p=0.229)	[402] (t(7)=0.93, p=0.381)	[403] (t(3)=-0.603, p=0.589)
[404] (t(3)=2.76, p=0.07)		

4d. Blue intensity (I_b) variation by sub-region

Refer to Figure II.13. In the CD transport cohort, there were a few significant differences between sub-regions within conditions, as the lowest values were observed in CA3. Refer to Table II.25 for statistical data referenced regarding effect of region on I_b in CD cohort. In CD-HC condition, there was no significant effect of region on I_b[405] while paired-sample t-tests showed significantly higher I_b in CA1 than DS[406], higher in DG than DS[407], higher in CA1 than CA3[408], and higher in DG than CA3[409].

In CD-1E, there was a significant effect of region on I_b[410] and paired-sample t-tests confirmed significantly higher values in CA1 versus DS[411], higher in DS than CA3[412]; and higher in DG than DS[413]; higher values in DG than CA1[414]; and higher in

CA1 versus CA3[415], and higher in DG than CA3[416]. In CD-1E, the lowest blue intensity values were observed in CA3.

In CD-5E, there was a significant effect of region on I_b[417] and paired-sample t-tests reported significantly higher values in DG than DS[418], higher in CA1 than DS[419]; higher in CA1 versus CA3[420]; higher in DG versus CA3[421]; and higher in DG than CA1[422]. There was no significant difference between DS and CA3 I_b [423].

In CD-MECS, there was a significant effect of region on I_b[424] and paired-sample t-tests confirmed higher blue values in DG than DS[425]; higher in DG than CA3[426], and higher in DG than CA1[427]. There were no significant differences in I_b between DS and CA1[428]; DS and CA3[429]; or between CA1 and CA3[430].

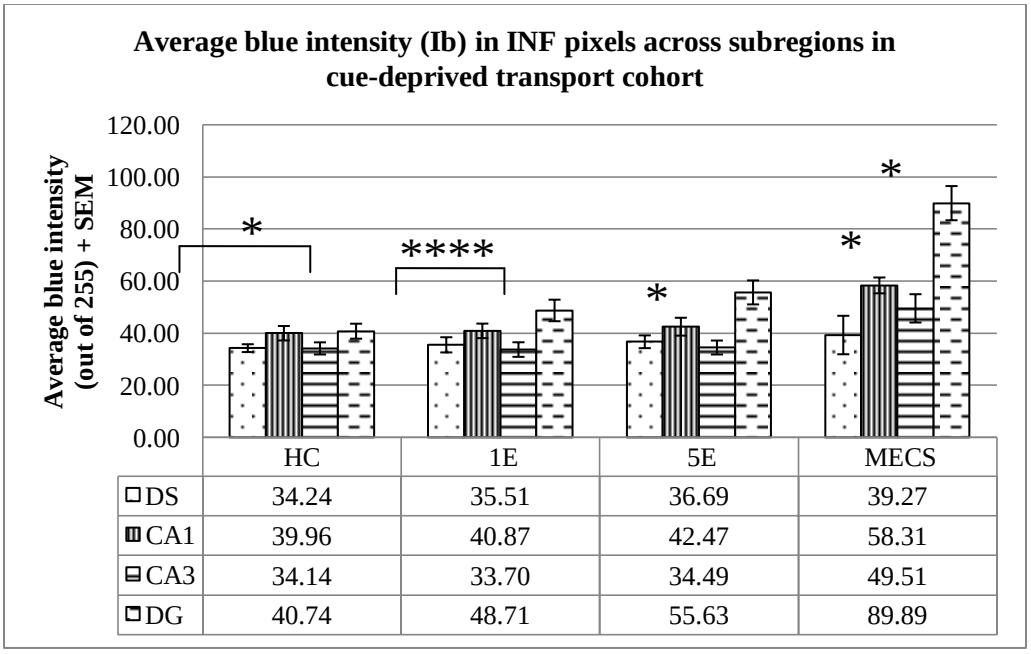

	HC	1E	5E	MECS
DS	34.24	35.51	36.69	39.27
CA1	39.96	40.87	42.47	58.31
CA3	34.14	33.70	34.49	49.51
DG	40.74	48.71	55.63	89.89

Figure II.13 Average blue intensity (I_b) across sub-regions within CD (cue-deprived transport) cohort, and within conditions. Lowest values observed in CA3.

Table II.25 Statistical data showing minor effect of region on I_b in CD cohort. Lowest values observed in CA3.

[405][F(3,12)=2.160, p=0.146]	[406] (t(3)=-4.38, p=0.02)	[407] (t(3)=-4.61, p=0.02)
[408] (t(3)=7.02, p=0.006)	[409] (t(3)=-6.60, p=0.007)	[410] [F(3,16)=4.4, p=0.019]
[411] (t(4)=-11.15, p=0.0004)	[412] (t(4)=2.17, p=0.096)	[413] (t(4)=-9.81, p=0.0006)
[414] (t(4)=-5.56, p=0.005)	[415] (t(4)=15.07, p<0.0001)	[416] (t(4)=-10.33, p=0.0005)
[417][F(3,16)=7.817, p=0.002]	[418] (t(4)=-5.17, p=0.007)	[419] (t(4)=5.81, p=0.004)
[420] (t(4)=3.81, p=0.019)	[421] (t(4)=-9.81, p=0.0006)	[422] (t(4)=-3.82, p=0.019)
[423](t(4)=1.19, p=0.30)	[424][F(3,8)=14.028, p=0.001]	[425] (t(2)=-22.21, p=0.002)
[426] (t(2)=-26.80, p=0.001)	[427] (t(3)=-8.66, p= 0.013)	[428] (t(2)=-3.81, p=0.06)
[429](t(2)=-2.87, p=0.10)	[430] (t(2)=3.67, p=0.067)	

Refer to Figure II.14 and Table II.26 for statistical data referenced in regard to effect of region on I_b in CA cohort. Within the CA-transport cohort, there were significant effects of region on I_b within some but not all conditions. In the CA-HC condition, there was a significant effect of region on I_b [431] and paired-sample t-tests confirmed higher values in CA1 than DS[432], higher in DG than CA3[433]; higher in CA1 than CA3[434]. There were no significant differences in I_b between DS and CA3[435]; between DS and DG[436]; or between CA1 and DG[437].

In CA-1E condition, there was a significant effect of region on I_b[438] and paired-sample t-tests showed significantly higher values in CA1 than DS[439]; higher in DG versus DS[440]; and higher in CA1 than in CA3[441]; and higher in DG versus CA3[442]; and higher in DG than CA3[443]; and higher in DG than CA1[444]. There was no significant difference in I_b between DS and CA3[445].

In CA-5E, there was a significant effect of region on I_b[446] and paired-sample t-tests confirmed higher I_b values in DG higher than DS[447]; significantly higher I_b in CA1

than DS[448]; and higher in DS than CA3[449]; and higher in DG than in CA1[450]; and higher in CA1 than CA3[451]; and higher in DG than CA3[452]. Thus, in CR-5E, lowest I_b values were observed in CA3.

In CA-MECS condition, there was a significant effect of region on I_b[453] while paired-sample t-tests confirmed significantly higher values in DS versus DG[454]; higher in CA1 than CA3[455]; higher in DG than CA3[456]; and higher in DG than CA3[457]. There were no significant differences between I_b values in DS versus CA1[458] or between DS and CA3[459].

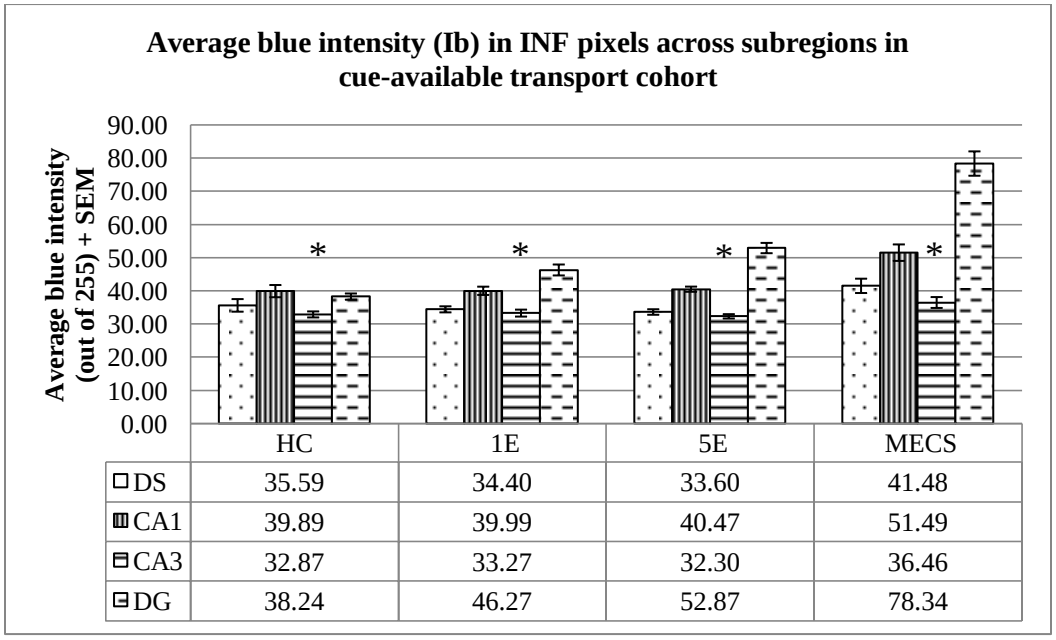

	HC	1E	5E	MECS
DS	35.59	34.40	33.60	41.48
CA1	39.89	39.99	40.47	51.49
CA3	32.87	33.27	32.30	36.46
DG	38.24	46.27	52.87	78.34

Figure II.14 Average blue intensity (I_b) across sub-regions within CA (cue-available transport) cohort, and within conditions. Lowest values observed in CA3.

Table II.26 Statistical data showing minor effect of region on I_b in CA cohort. Lowest values observed in CA3.

[431][F(3,20)=4.369, p=0.016]	[432] (t(5)=-5.18, p=0.004)	[433] (t(5)=-3.42, p=0.02)
[434] (t(5)=6.71, p=0.001)	[435] (t(5)=2.03, p=0.098)	[436] (t(5)=-1.04, p=0.345)
[437] (t(5)=0.694, p=0.518)	[438][F(3,28)=22.903, p <0.001]	[439] (t(7)=-6.74, p=0.0003)
[440] (t(7)=-7.44, p=0.0001)	[441] (t(7)=6.25, p=0.0004)	[442](t(7)=-6.42, p=0.0004)
[443] (t(7)=-6.42, p=0.0004)	[444] (t(7)=-3.89, p=0.006)	[445] (t(7)=1.67, p=0.14)
[446][F(3,28)=85.965, p<0.0001]	[447] (t(7)=-17.21, p=0.0001)	[448] (t(7)=-8.38, p<0.0001)
[449](t(7)=2.63, p=0.03)	[450] (t(7)=-12.22, p<0.0001)	[451] (t(7)=9.82, p<0.0001)
[452] (t(7)=-14.07, p<0.0001)	[453] [F(3,12)=51.69, p<0.0001]	[454] (t(3)=-11.16, p=0.002)
[455] (t(3)=-12.89, p=0.001)	[456] (t(3)=-17.28, p=0.0004)	[457] (t(3) =-13.42, p=0.0009)
[458] (t(3)=-3.1, p=0.05)	[459] (t(3)=2.28, p=0.11)	

5. Correlation between INF intensity and INF size

5a. Correlation of INF maximum intensity (I_{max}) and INF size (S_{avg})

Correlation tests (single regression and Pearson correlation tests) were performed between INF maximum intensity (I_{max}) and size (S_{avg}) across conditions and combined CD/CA cohorts. Without including MECS values (sizes may reflect inaccurate INF border detection by current version of analysis software), it was observed that as mean I_{max} increases, mean S_{avg} also increased when all regions, conditions, and CD and CA cohorts were combined ($r=0.85$, $r^2=0.72$) (see Results, Figure 7). With inclusion of current MECS values, linearity decreased when all regions and conditions are analyzed ($r=0.53$, $r^2=0.28$) (Figure II.15).

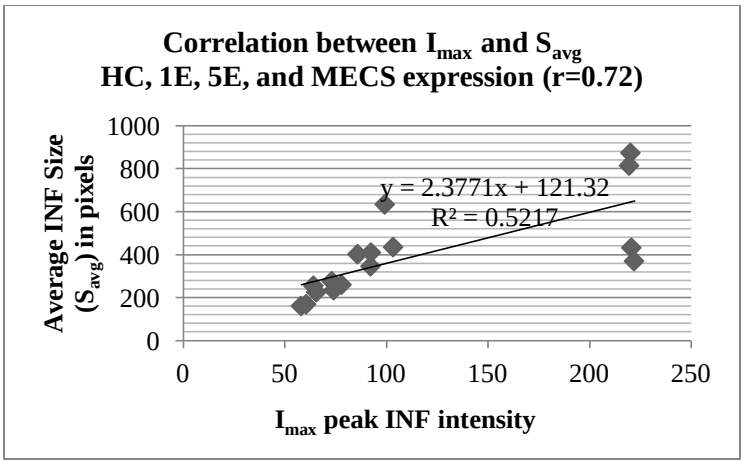

Figure II.15 Strong correlation (r=0.72, r^2=0.52) between maximum intensity (I_{max}) versus size (S_{avg}) in HC, 1E, 5E and including current MECS with pooled cohort data across all regions.

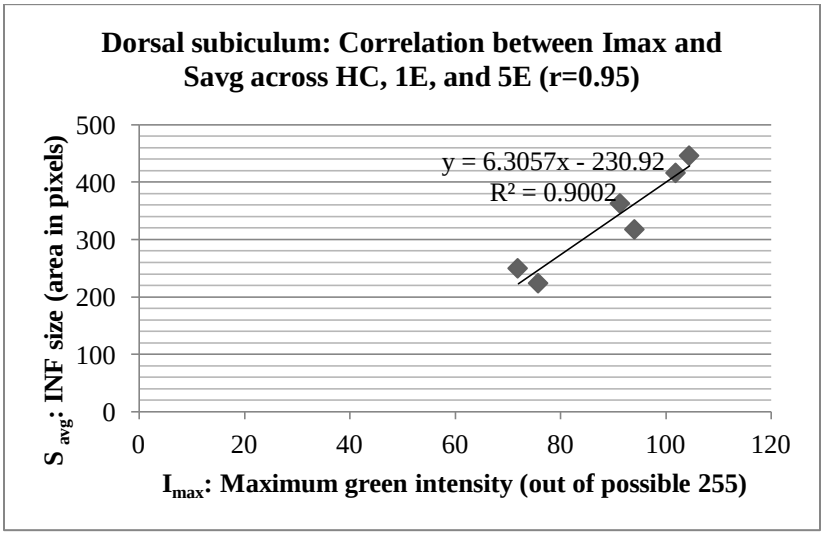

Figure II.16 Dorsal subiculum: Strong correlation (r=0.95, r^2=0.90) between peak intensity I_{max} and average size S_{avg} across HC, 1E, 5E, with pooled cohort averages. Weaker correlation with inclusion of MECS (r=0.45, r^2=0.20) (not shown).

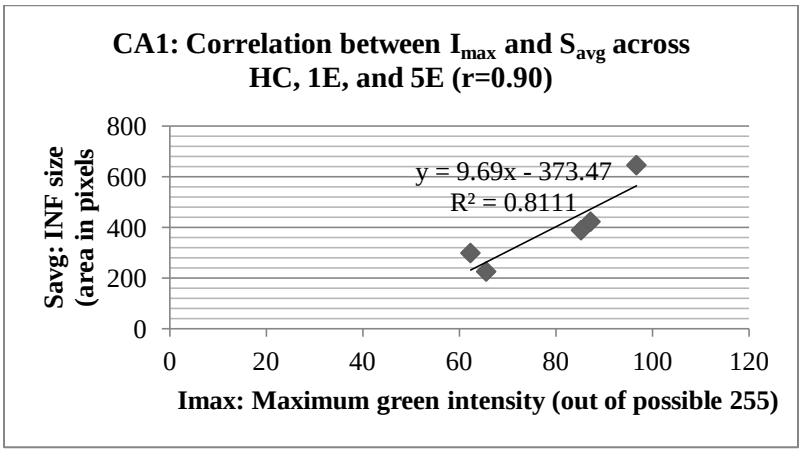

Figure II.17 CA1: Strong correlation (r=0.90, r^2=0.81) between peak intensity I_{max} and average size S_{avg} with pooled data in HC, 1E, and 5E conditions, but weaker correlation with inclusion of MECS values (r=0.86, r^2=0.74) (not shown).

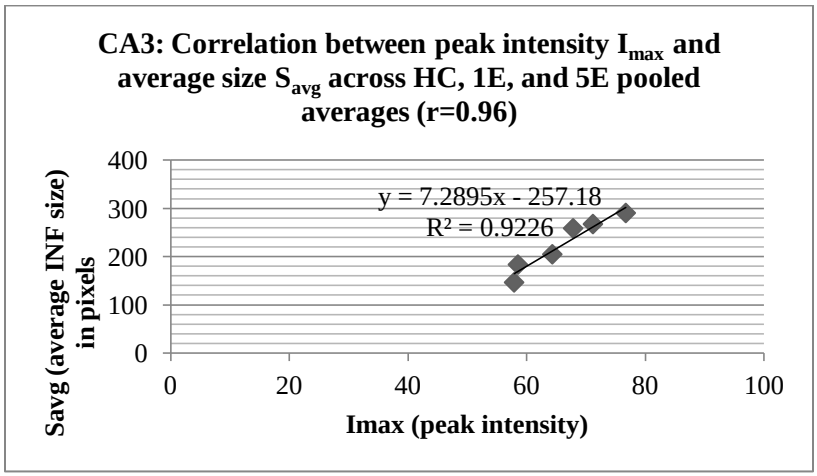

Figure II.18 CA3: Strong correlation (r=0.96, r^2=0.92) between peak intensity (I_{max}) and average size (S_{avg}) without MECS group but weaker correlation with MECS (r=0.810, r^2=0.656).

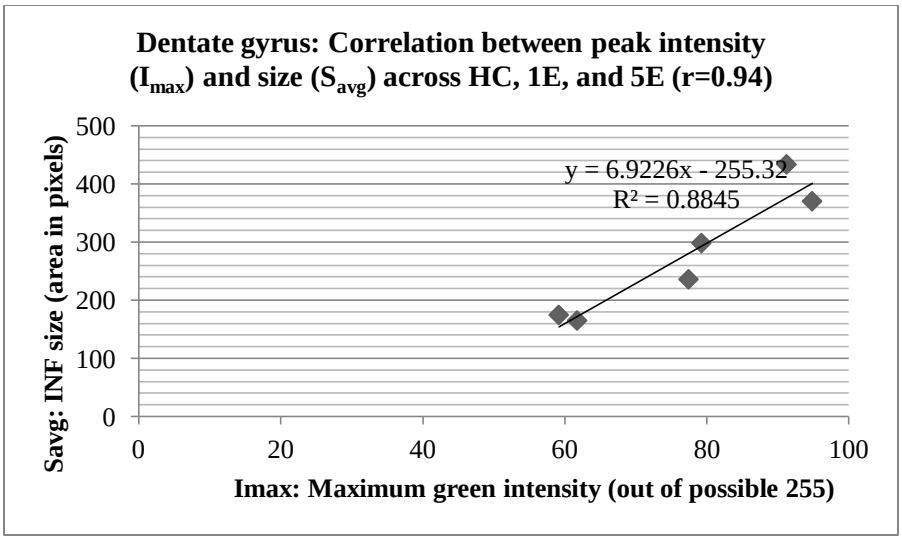

Figure II.19 Dentate gyrus: Strong correlation (r=0.94, r^2=0.88) between peak intensity I_{max} and average size S_{avg} without MECS) and stronger correlation with MECS considered (r=0.99, r^2=0.97) (not shown).

5b. Correlation between INF average green intensity (I_{avg}) and INF size (S_{avg})

Correlation tests (single regression, Pearson correlation tests) were performed between INF average green intensity (I_{avg}) and size (S_{avg}) across conditions and combined CD/CA cohorts. There were strong correlations between I_{avg} and S_{avg} but weaker than relationships observed in I_{max} versus S_{avg}.

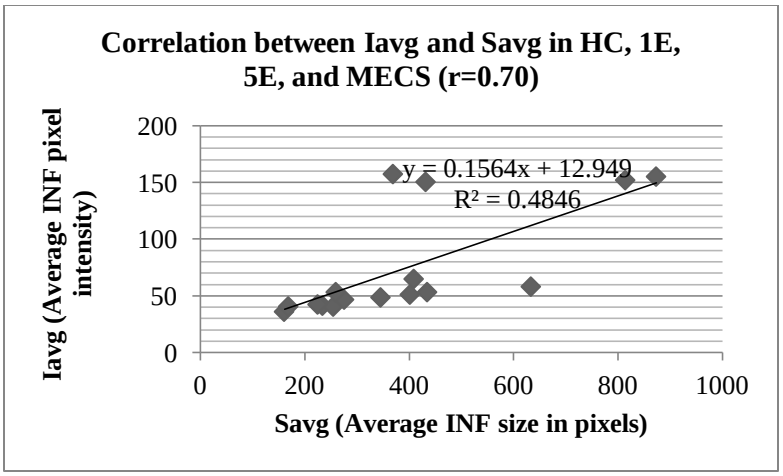

Figure II.20 Across all regions and conditions, with all averages pooled, I_{avg} and S_{avg} were strongly correlated (r=0.70, r^2 =0.48).When MECS values were excluded, the correlation between I_{avg} and S_{avg} increased slightly (r=0.79, r^2=0.62) (not shown).

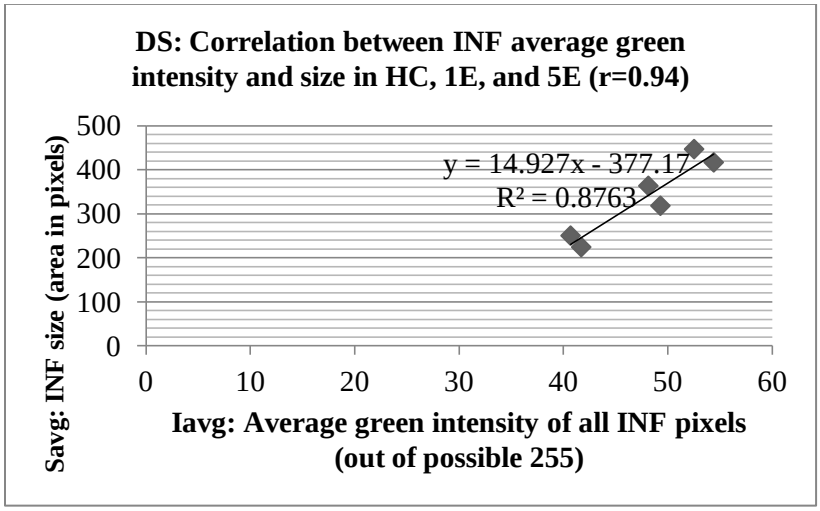

Figure II.21 Dorsal subiculum: Strong correlation (r=0.94, r^2=0.88) between average INF intensity (I_{avg}) and size (S_{avg}). Correlation weakened when MECS values were included (r=0.46, r^2=0.208) (not shown).

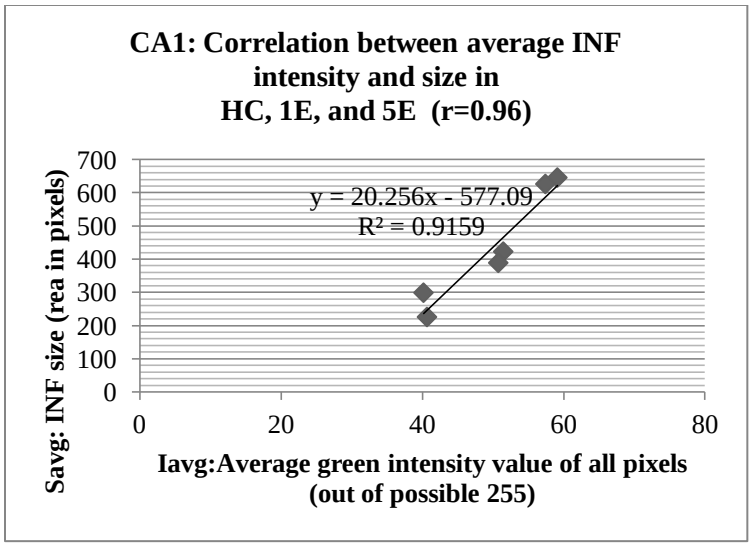

Figure II.22 CA1: Strong correlation (r=0.96, r^2=0.92) between INF average intensity (I_{avg}) and size (S_{avg}) with MECS values excluded. Correlation weakened (r=0.81, r^2=0.66) when MECS values were included (not shown).

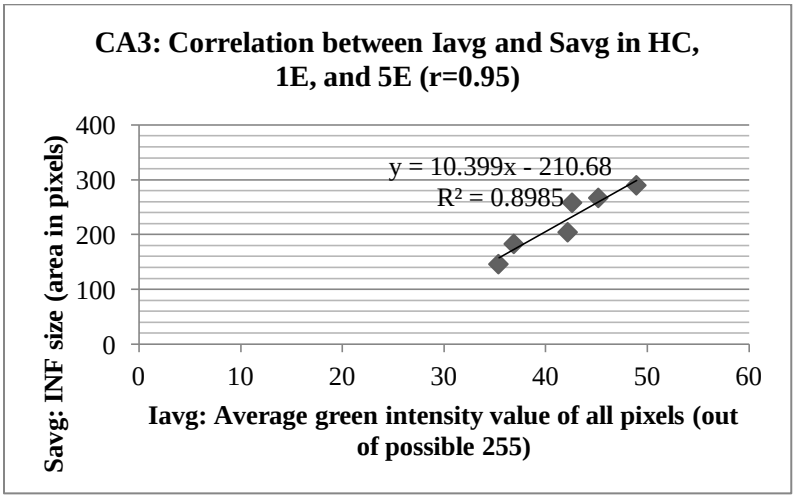

Figure II.23 CA3: Strong correlation (r=0.95, r^2=0.90) between INF average green intensity (I_{avg}) and size (S_{avg}). Correlation weakened (r=0.81 r^2=0.66) when MECS values were included (not shown).

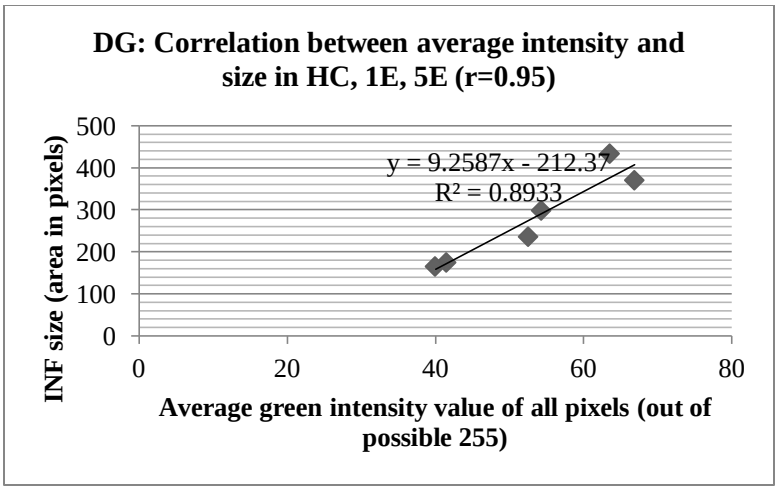

Figure II.24 DG: Strong correlation (r=0.95, r^2=0.89) between average INF intensity (I_{avg}) and size (S_{avg}) across HC, 1E, and 5E conditions, but weaker correlation with MECS values included (r=0.55, r^2=0.30) (not shown).

6. Correlations between peak and average intensity, and average blue intensity

6a. I_{max} versus I_{avg} (Green intensity values)

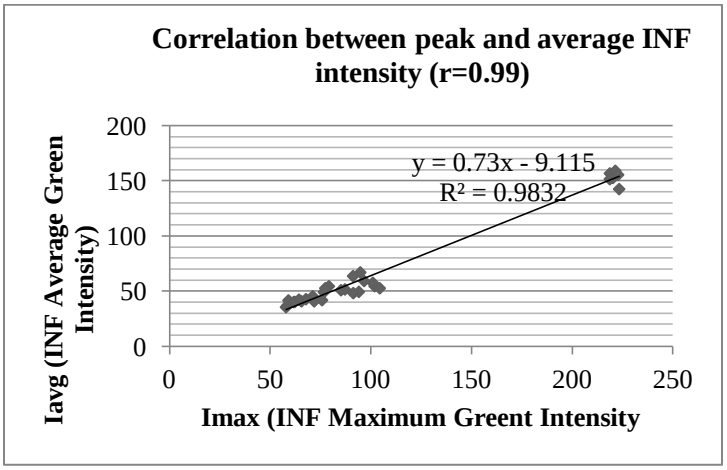

Figure II.25 Strong correlation (r=0.99, r^2=0.98) between INF maximum intensity (I_{max}) and INF average intensity (I_{avg}) in the green channel. All data points pooled, including HC, 1E, 5E, and MECS values across all regions. I_{max} was a reliable predictor of I_{avg} as the two distributions were highly correlated

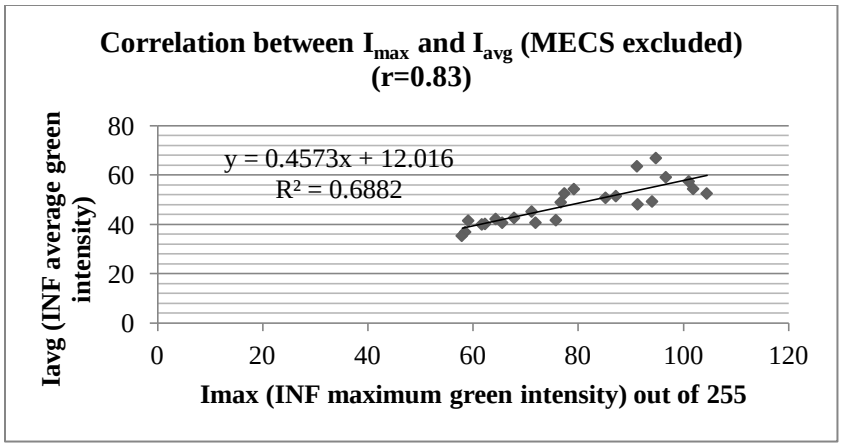

Figure II.26 Correlation between I_{max} and I_{avg} decreased (r= 0.83, r^2=0.69) when MECS values were excluded, due to potential INF border detection faults with software, this analysis was performed to ensure unbiased statistical investigation. All data points pooled, excluding MECS values across all regions.

6b. I_{avg} versus I_b (Average green versus average blue intensity in all INF pixels)

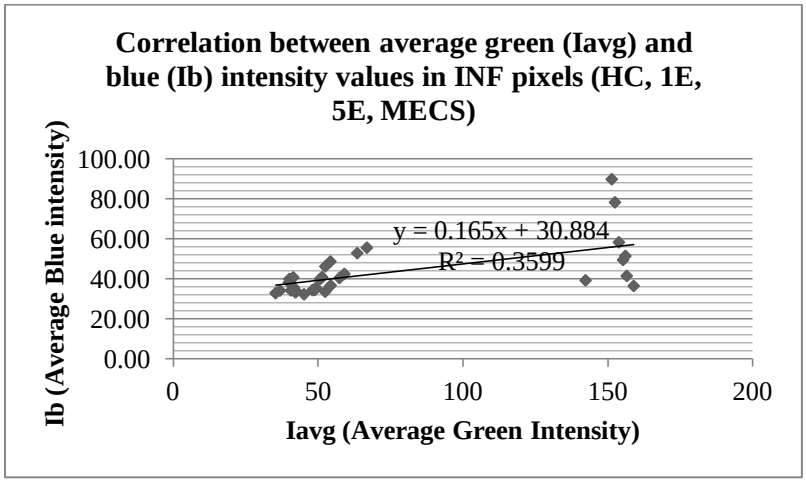

Figure II.27 I_{avg} was weakly correlated with I_b (r=0.60, r^2=0.36) so each parameter was an unreliable predictor of the other. All data points pooled, across HC, 1E, 5E, and MECS conditions in all regions.

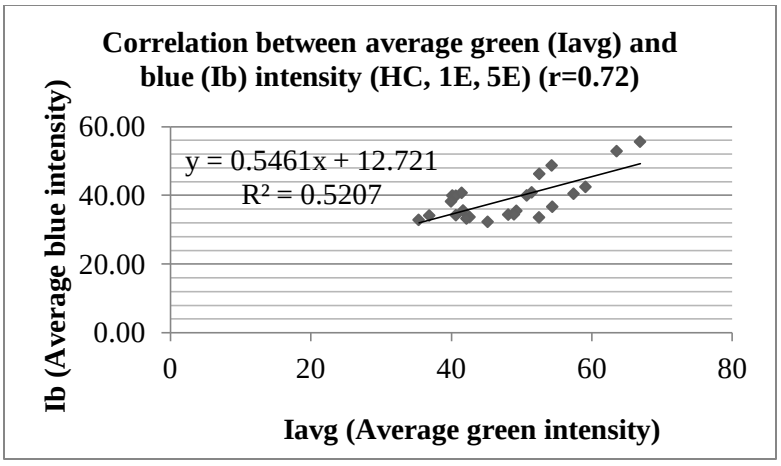

Figure II.28 The correlation between I_{avg} and I_b increased (r= 0.72, r^2=0.52) when MECS values were excluded, due to potential INF border detection issues with software.

All data points combined, across HC, 1E, and 5E conditions in all regions.

6c. I_{max} versus I_b (INF maximum intensity versus average blue intensity)

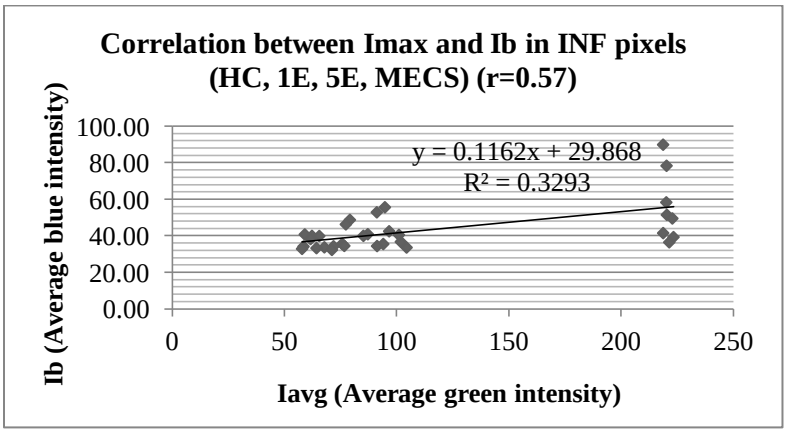

Figure II.29 I_{max} was weakly correlated with I_b (r=0.574, r^2=0.33). Parameters were not reliable predictors of the other. All data points pooled, across HC, 1E, 5E, and MECS conditions, in all regions.

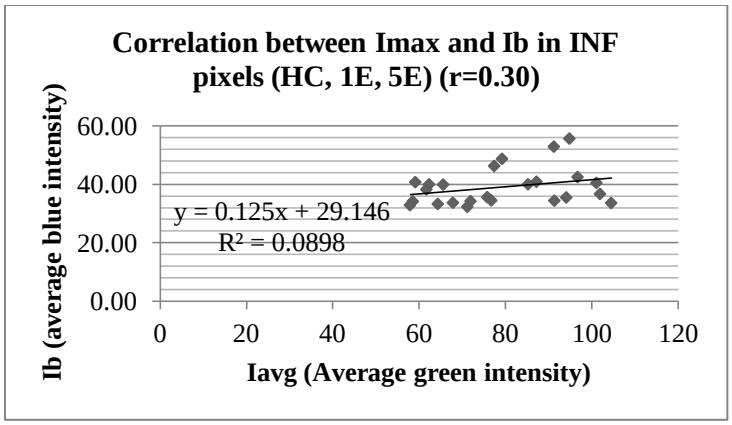

Figure II.30 The correlation between I_{max} and I_b weakened (r= 0.30, r^2=0.09) when MECS values were excluded, due to potential INF border detection issues in the analysis software. This measure was performed to ensure unbiased statistical investigation.

APPENDIX III
SYSTEMATIC SURVEY OF NEURONAL AND GLIAL CHARACTERISTICS

The software employed to perform automated intranuclear quantification and characterization required user-determined thresholds. The derivation of appropriate thresholds required systematic surveys of average neuronal versus glial nuclear intensity and circumferential area in pixels. This detection required the mass random sampling of neuronal and glial nuclei from ROI images from many FISH batches to control for inter-batch variability (e.g. variation in reagent samples and processing conditions). Neuronal nuclei were cropped from pre-processed bitmap images and the size and average blue DAPI intensity were averaged across samples and hippocampal regions.

Image acquisition

Following tissue processing as previously described in methodology of Chapters 1, 2, and 3 of this thesis, images were scanned as .NDPI extension files with a Nanozoomer digital scanner (Olympus) under consistent parameters (40X objective focus, 4.4.4 RGB scale). ROIs of CA1, CA3, dentate gyrus, and dorsal subiculum from coordinates -4.92mm to -6.96mm from bregma were manually cropped with reference to the rat brain atlas (Paxinos & Watson, 2007, 6th Ed.) Images were then converted to bitmap images via an in-house software (NDPConvert by V. Trivedi). Each bitmap image was then re-cropped such that nuclei were cropped along their intimate circumferences in Microsoft Paint. Behavioural conditions were ignored but included in the analysis to ensure a pure cross-section of all nuclear types.

Derivation of average nuclei size

Whole, non-segmented neuronal nuclei were isolated from ROI bitmap images by manually cropping with Microsoft Paint such that the intimate circumferences of neuronal nuclei were saved as individual images. These nuclei-only images were then processed with the GreenDot.exe software (used in other analyses in this thesis), to derive the average size. The total pixel number in each image was outputting in a comma separated values file and then averaged. These images were only 2D so there were angular variations depending on how the nucleus was sliced during cryosectioning and also their situation in space prior to flash-freezing. A total of 200 neuronal nuclei selected at random, cropped, and generated 200 individual files for quantification of pixel area. The files were divided into 50 batches so there were 4 nuclei in each, one from each of CA1, CA3, DG, and dorsal subiculum to create a true average. All total area values in pixels were then averaged in each batch, and then the mean of all batch averages were then derived, and the value of 3013.58 was derived as the average surface area estimation from this analysis.

Table III.1 Average nuclear area in pixels (in a 2D plane) from 200 randomly-selected nuclei from sub-images containing ROIs of CA1, CA3, dentate gyrus, and dorsal subiculum.

Nuclei file batch	Average pixels in nucleus	Nuclei File Batch	Average pixels in nucleus
1	1997	**26**	3335
2	3900	**27**	3658
3	2164	**28**	1982
4	1974	**29**	3593
5	3420	**30**	2498
6	2562	**31**	3481
7	3089	**32**	2638

8	2297	**33**	3659
9	3803	**34**	2663
10	3410	**35**	3081
11	3139	**36**	2991
12	3167	**37**	2724
13	3414	**38**	2713
14	2937	**39**	3106
15	2553	**40**	3145
16	2632	**41**	2597
17	2313	**42**	2842
18	4779	**43**	2806
19	2305	**44**	3338
20	3125	**45**	3128
21	3616	**46**	4619
22	1925	**47**	4043
23	2724	**48**	3664
24	2993	**49**	1966
25	3100	**50**	3071
		Average	3013.58

Following the compilation of ROI data (batch-processing with GreenDot.exe software), another in-depth study of neuronal nuclear size was conducted to verify the accuracy of this average neuronal area. This post-hoc analysis was conducted to increase the sample-size and also to employ the histogram reporting function of Adobe Photoshop Image Editor, which was discovered as a useful tool after the first set of automated INF quantification was conducted.

For this post-hoc analysis, 620 randomized experimental ROI images (single-labeled with FITC for H1a and counterstained with DAPI) were selected (155 each of HC, 5E, MECS, and 1E conditions were selected, distributed such that there were also 155 each of DS, CA1, and CA3 regions). A single neuronal nucleus was selected, cropped manually such that cropping adhered to the perimeter of the circular/elliptical border in Adobe Photoshop. A histogram of information was produced which analyzed the area selected, circularity, and number of pixels per blue intensity value (from 1 to

255). Each neuronal nucleus from each image was compiled in an Excel spreadsheet. It was observed this average was 2975.59 (versus previously measured 3013.58). These same ROI images were then processed by the same automation software as used in all chapters of this thesis for INF detection. Automated verification of neuronal nuclei derived an average of 2971.60 pixels, and an average of 1583.86 pixels for glial nuclei.

Derivation of average nuclei intensity

In the automated INF quantification analyses, a set range of nuclei blue pixels were quantified. The parameters of minimum blue and maximum blue intensity values of this range were 15 and 80, respectively. These values were derived from a systematic random sampling of pixel values from inspecting individual pixels of neuronal and glial nuclei. ImageJ Freeware was used to zoom and crop 200 neuronal and 100 nuclei. The arrow-pointer tool detected the blue channel intensity of all pixels and this was tabulated across all nuclear files. Experimenters survey the entire 2D area of nuclei and averaged intensities across all pixels. It was detected that 80 was the most convenient and suitable blue intensity division between neuronal nuclei (generally dimmer) and glial nuclei (generally very bright and saturated) and 15 was set as the minimal blue threshold to eliminate diffuse background pixels. Due to the biological nature of overlapping in space and colouration, there were pixels in each which cross this boundary but it was found as a suitable compromise for the sake of estimation of neuronal nuclei counts.

Blue pixel intensity distributions of glial versus neuronal nuclei

From the experimental images, 620 ROI images (single-labeled with FITC for H1a and counterstained with DAPI) were randomly selected (155 each of HC, 5E,

MECS, and 1E conditions were selected, distributed such that there were also 155 each of DS, CA1, and CA3 regions) to determine average neuronal nuclei intensity and area. Also randomly selected were 80 ROI images (20 each of HC,5E, MECS and 1E, distributed such that included were also 20 each of DS, CA1, and CA3 images) to crop out glial nuclei.

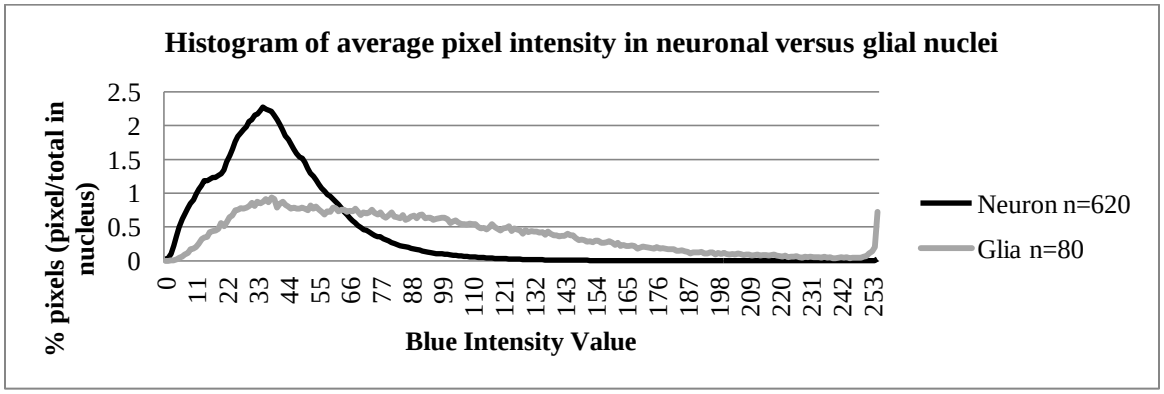

Figure III.1 Histogram of average intensity distribution of pixels within nuclei (neuronal or glial) across blue intensity values (0-255). Most neuronal nuclear pixels could be detected below intensity values of 80. Glial neurons showed greater spread of intensity distributions, with a sharp increase at highest intensities (around 250).